Design and Analysis of Magnetorheological Dampers for Train Suspension

LAU YIU KEE

A Thesis Submitted in Partial Fulfillment

of the Requirements for the Degree of

Master of Philosophy

in

Department of Automation and Computer-Aided Engineering

August 2004

用於火車懸掛系統的磁流變阻尼器的設計與分析

摘要

因爲高速火車已經被肯定爲一個既經濟同時又可以減少對環境污染的交通公具，所以很多不同國家對高速火車的發展都十分感興趣。 不過，高速行駛中的火車會對車身造成極大震盪。 爲了改善乘坐舒適及行車安全，因此必需有效地控制車身的振動。 不同的火車懸掛系統，包括被動，主動及半主動系統都可以減緩震盪對乘客的影響。在這些系統中，半主動系統不但可以達到高性能同時又可以維持系統穩定性及提供失效保護[1]。 本論文旨在設計一個適合半主動火車懸掛系統的磁流變阻尼器以改善行車質素。 本研究設計，製造及測試了雙頭出入磁流變阻尼器。 之後一個描述磁流變阻尼器數學模型與一個完全火車模型的次懸掛系統互相結合。 另外採用了一個根據量度車身絕對速度的半主動開/關控制策略。 受控系統的性能與不同的懸掛系統作出了比較。 結果顯示結合磁流變阻尼器的了半主動火車懸掛系統的可行性與效能。

[1] 旨在當設備發生故障時，仍可繼續發揮作用

ABSTRACT

The development of high-speed railway vehicles has been a great interest of many countries because high-speed trains have been proven as an efficient and economical transportation means while minimizing air pollution. However, the high speed of the train would cause significant car body vibrations. Thus effective vibration control of the car body is needed to improve the ride comfort and safety of the railway vehicle. Various kinds of railway vehicle suspensions such as passive, active, and semi-active systems could be used to cushion passengers from vibrations. Among them, semi-active suspensions are believed to achieve high performance while maintaining system stable and fail-safe. In this thesis, it is aimed to design a magnetorheological (MR) fluid damper that is suitable for semi-active train suspension system in order to improve the ride quality. Double-ended MR dampers are designed, fabricated, and tested. Then a model for the double-ended MR damper is integrated in the secondary suspension of a full-scale railway vehicle model. A semi-active on-off control strategy based on the absolute velocity measurement of the car body is adopted. The controlled performances are compared with other types of suspension systems. The results show the feasibility and effectiveness of the semi-active train suspension system with the developed MR dampers.

ACKNOWLEDGMENTS

I would like to express my sincere appreciation to my advisor, Professor Liao Wei-Hsin, for providing me with the opportunity to work in the project of magnetorheological damper technology, for his guidance and mentorship, and for his encouragement and support at all levels over the past two years.

I would like to thank Mr. Allan Mok and Mr. Philip Lee for their technical advices on this project; their insights and advices enabled me to break through some technical problems. Also, I wish to acknowledge Mr. Andrew Li for his assistance during the experiments.

Besides, I want to thank all my close colleagues who have helped and supported me during the project and been there with me in many lonely times. Finally, I would like to thank my family for their life-long love and support.

TABLE OF CONTENTS

LIST OF TABLES

LIST OF FIGURES

CHAPTER 1

INTRODUCTION

1.1 Motivation

Under competition with other means of transportation, railway operators are seeking to offer their passengers with shorter journey time and better ride comfort to make the railways more competitive with air transport while providing better safety. Increasing the speed of a railway vehicle can shorten the journey time but the ride quality would be deteriorated since the high speed of the train will cause significant car body vibrations due to the limited performances of conventional suspension systems [1]. When the rail vehicle is bending a curve, the running speed of the rail vehicle can be increased by tilting the car bodies of the train inwards during curving, consequently reducing the lateral forces and lateral accelerations perceived by the passengers [2]. The suspension system, however, has to cope with both high speed and high centrifugal force to be able to produce a smooth ride during curving. Improper suspension system will make the passengers feel substantial ride discomfort caused by the lateral accelerations. Therefore, an effective suspension system is necessary to increase the traveling speed of rail vehicle while maintaining

(or even improving) the passenger's ride comfort.

1.2 Railway Vehicle Suspension

In general, the suspension systems used in railway vehicles can be categorized as passive, active, and semi-active types, to cushion riders from vibrations. A passive railway vehicle suspension employing springs and hydraulic dampers has some advantages such as design simplicity and cost effectiveness. However, since the design of the passive system is fixed, the performance could be limited when the system or the operating condition changes such as variation of number of passengers or excitations induced by the rail track irregularities. On the other hand, several researchers have proposed and investigated active suspension technologies for railway vehicles [2-6]. The active suspension utilizing hydraulic or pneumatic actuators can provide high control performance, but it requires high power and sophisticated control implementation. The active system could also be destabilized as the mechanical power could be imported into the system. Therefore, semi-active suspensions are proposed to overcome those shortcomings as aforementioned in order to achieve high performance while the systems are stable and fail-safe. The main semi-active devices that have been considered for railway vehicles are variable orifice dampers [7-10], which are composed of hydraulic cylinders and mechanical valves, so the system reliability may be reduced and the maintenance may be costly due to the use of

valves. Besides, the time delays of the valves would degrade the performance of the suspension system [8]. In view of these problems, semi-active dampers using controllable magnetorheological (MR) fluids will be considered in this study.

1.3 Semi-Active Magnetorheological Fluid Damper

Semi-active vibration control devices are receiving significant attention because they can offer combined advantages of both passive and active control systems. Method for creating a damper with variable damping include changing the size of orifice through which the hydraulic fluid passes, changing the stiffness of the devices, controlling the friction of the isolators, and changing the field of ER/MR fluid dampers.

In the past decade, the idea of applying smart materials to structural systems has been studied in various disciplines [11]. Continuing developments in materials science have provided a number of promising materials with adaptive properties that can be used as intelligent elements for smart structures. In particular, it has been found that magneto-rheological (MR) fluids can be outperforms its ER fluid counterparts [12] and they are quite promising for vibration reduction applications [13].

Controllable fluids are materials that respond to applied magnetic or electric

fields with dramatic changes in rheological behaviors. The essential feature of the MR fluid is its ability for reversible change from free flowing, viscous liquid to semi-solid with controllable yield strength in milliseconds when exposed to a magnetic field. Comparing with the valve based semi-active dampers, MR fluid devices have the advantages such that they are fast responding, having no moving parts, which make them simple and reliable, and requiring low power. These have been the primary factors for motivating the development of such devices [14]. For railway vehicle applications, Liao and Wang [15] showed the feasibility for applying MR fluid dampers to control the vertical vibrations of a railway vehicle; Wang and Liao [16] studied the controlled secondary suspension system with MR fluid dampers to attenuate the lateral and yaw motions of railway vehicle. Atray and Roschke [1] presented the procedures used for design, fabrication, testing, and modeling of an MR damper for the vibration control of a 70-ton railcar.

1.4 Research Objectives

In this research, it is aimed to design and fabricate magnetorheological (MR) fluid dampers, which are suitable for a semi-active train suspension system for improving the ride quality of the railway vehicle. First of all, the characteristics of MR fluid, MR damper design as well as the railway suspension system will be

studied. Secondly, double-ended MR dampers for railway application will be designed and fabricated. Then the fabricated MR dampers will be tested in order to find out their characteristics and performances. A mathematical model will be adopted to describe the MR damper behaviors. Furthermore, the validated MR damper model will be integrated in the secondary suspension of a full-scale railway vehicle model. Finally, simulation will be done to show the feasibility and effectiveness of the semi-active train suspension system with MR dampers.

1.5 Thesis Outline

The thesis consists of seven parts. Chapter 1 gives an introduction, which describes the motivation of this thesis as well as an overview of the MR damper and railway vehicle suspension system.

Chapter 2 provides the background information concerned in this thesis. It includes the essential behaviors of MR fluids; basic operation, advantages and applications of the MR devices; overview on the railway vehicle and suspension system; and reviews of the literature survey and achievements of previous related researches.

Chapter 3 is concerned with design and considerations of the MR dampers. Different designs and structures of current MR dampers are discussed, then the MR

damper geometry design is considered and the basic magnetic circuit is described.

Chapter 4 presents the development and fabrication of the MR damper. Additional practical considerations of MR damper design and fabrication process is described.

Chapter 5 shows the experimental setup and results for testing the MR damper. The force-displacement and force-velocity results are investigated. In addition, the force-lag phenomenon, the MR fluid filling setup and the effect of the internal pressure of MR damper is discussed.

Chapter 6 gives the simulation results of the semi-active train suspension using MR dampers. The MR damper tested in Chapter 5 is modeled by a mathematical model in SIMULINK and then integrated with the railway vehicle model developed in the railway dynamic software VAMPIRE©. Four different test tracks including the lower sway mode, upper sway mode, mixed sway mode and BR high speed assault course is used to test the performance of the semi-active suspension system. Then the comparison between different suspension systems is provided and then human ride comfort is discussed.

Chapter 7 summarizes the results and conclusions of this thesis.

CHAPTER 2

BACKGROUND

In this chapter, the essential behaviors and basic operation modes of MR fluids is introduced. Besides, the advantages and applications of the MR devices is also discussed. Then, an overview on railway vehicles and railway vehicle suspension systems is presented. The literatures and achievements of previous related research and projects are also reviewed.

2.1 MR Fluids

2.1.1 Composition of MR fluids

Common MR fluids consist of three major components: dispersed ferromagnetic particles, a carrier liquid and a stabilizer [17]. About 20 to 40 percent of the MR fluids are composed of the soft iron dispersed ferromagnetic particles (e.g. carbonyl iron particles or iron base alloys) that are just 3 to 5 micrometers in diameter. The carrier liquid serves as a continuous isolating medium. This can be any medium conventionally employed in a fluid responsive to a magnetic field. The third component of a MR fluid is a stabilizer, which serves to keep the particles suspended evenly in the fluid. Stability of MR fluid is one of the most important properties of the fluid. Some additives are put in to inhibit gravitational settling of the iron particles, promote particle suspension, enhance lubricity, modify viscosity and inhibit

wear.

2.1.2 Properties and characteristics of MR fluids

The initial discovery and development of MR fluids and devices can be credited to Jacob Rainbow at the US National Bureau of standards in the late 1940s [18]. These fluids are materials that respond to an applied magnetic field with a dramatic change in rheological behavior.

When no magnetic field is applied (off-state), MR fluids flow freely as like as a liquid with plastic viscosity in the range of 0.10 to 0.70 *Pa/sec* [12]. When an external magnetic field is applied (on-state), the particles become magnetized and behave like tiny magnets. Then this particles line up along the direction of the magnetic field and forms a particle chain (see Fig. 2.1). A shear force is needed to break this particle chain, which contributes to the considerable increase of the MR fluid static yield stress. The strength of the fluid increases as the applied magnetic field increases. The essential characteristic of these fluids is their ability to reversibly change from free-flowing, linear viscous liquids to semi-solids having controllable yield strength in milliseconds when exposed to a magnetic field.

The ultimate strength of an MR fluid depends on the square of the saturation magnetization of the suspended particles. The key to be a strong MR fluid is to choose a particle with a large saturation magnetization [18]. The best available particles are alloys of iron and cobalt that have saturation magnetization of about 2.4 Tesla. However, alloys of iron and cobalt are expensive for most practical applications. So, simply pure iron will be the best particles for practical applications

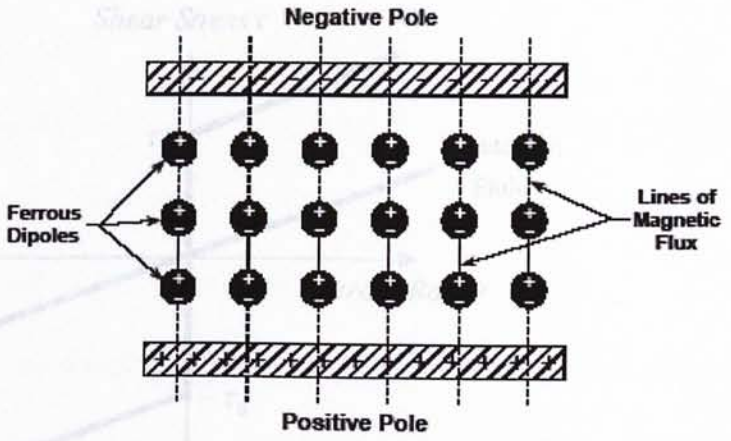

Figure 2.1: Particle chain of MR fluid [35].

TABLE 1: PROPERTIES OF THREE DIFFERENT TYPES OF MR FLUIDS [W1].

MR Fluid	MRF-132 AD	MRF-240BS	MRF-336AG
Base Fluid	Hydrocarbon	Water	Silicone
Operating Temperature (°C)	-40 to 130	-10 to 70	-40 to 150
Response Time	Milliseconds.	Milliseconds.	Milliseconds.
Density (g/cc)	3.09	3.86	3.45
Weight Percent Solids	81.64 %	85 %	82.02 %
Coefficient of Thermal Expansion (Volume, 1/°C)	$\sim 0.55 \times 10^{-3}$ (0 – 50 °C)	0.223×10^{-3}	0.58×10^{-3}
Specific Heat @ 25°C (J/g °C)	0.80	0.94	0.65
Viscosity @ 10s-1/50s-1 (Pa·sec)	0.09 Pa-s ± 0.02 Pa/s	13.6 Pa-s @ 10 sec^{-1} shear rate	0.09 Pa-s ± 0.02 Pa/s
Applications	Multi purpose, dampers, Brakes, Mounts	Mounts, Demo devices, Toys	Mounts, Dampers

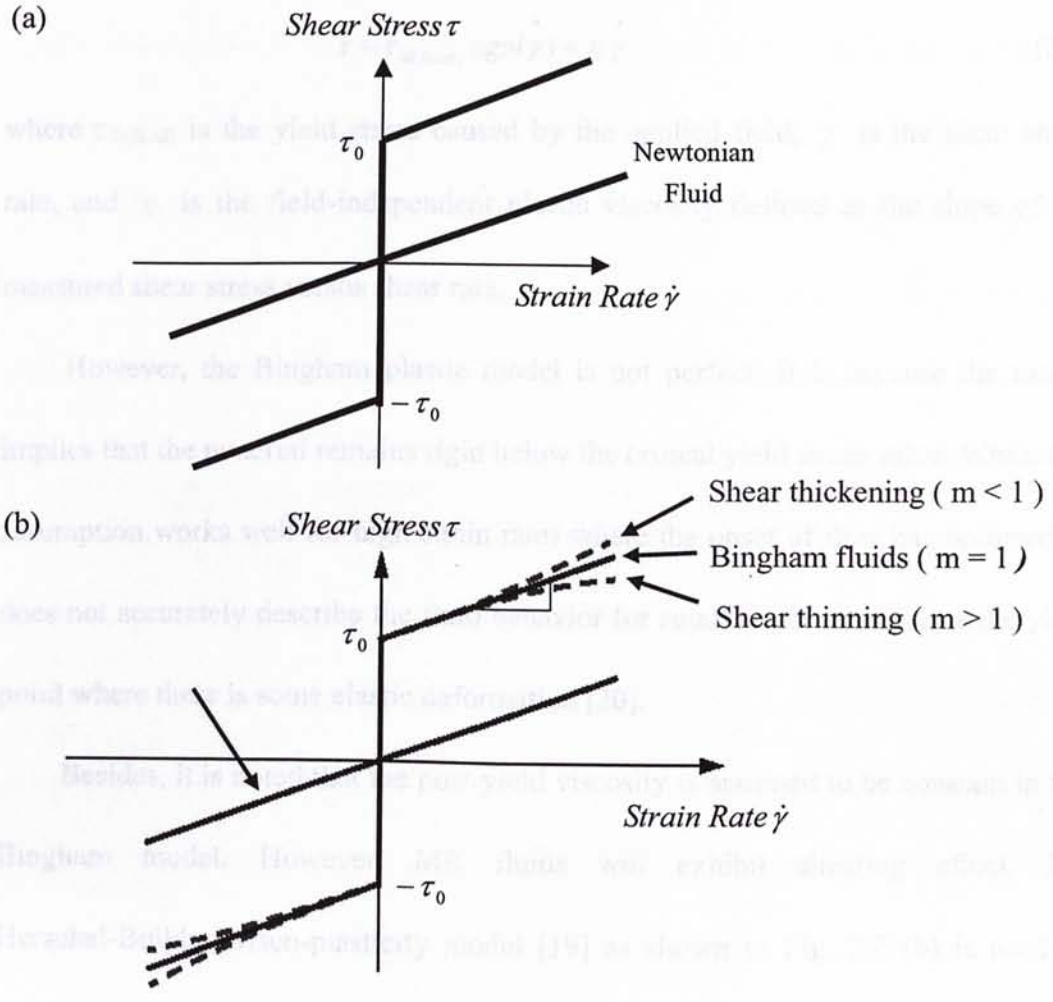

Figure.2.2: (a) Bingham model (b) Visco-plasticity models of MR fluids [19].

as they have magnetization of 2.15 Tesla.

The Lord Company has manufactured five types of MR fluids, which are commercially available. They are MRF-122-2ED (hydrocarbon-based), MRF-132AD (hydrocarbon-based), MRF-241ES (water-based), MRF-240BS (water-based), and MRF-336AG (silicone-based). Table 1 gives the main properties of three of them.

A simple Bingham plasticity model [19] is shown in Fig. 2.2 (a). This model is convenient in describing the essential field dependent fluid characteristics. In this model, the total shear stress τ is given by

$$\tau = \tau_{0(field)} \operatorname{sgn}(\dot{\gamma}) + \eta \dot{\gamma} \tag{2.1}$$

where $\tau_{0(field)}$ is the yield stress caused by the applied field, $\dot{\gamma}$ is the shear strain rate, and η is the field-independent plastic viscosity defined as the slope of the measured shear stress versus shear rate.

However, the Bingham plastic model is not perfect. It is because the model implies that the material remains rigid below the critical yield stress value. While this assumption works well for high strain rates where the onset of flow has occurred, it does not accurately describe the fluid behavior for small strain rates below the yield point where there is some elastic deformation [20].

Besides, it is noted that the post-yield viscosity is assumed to be constant in the Bingham model. However, MR fluids will exhibit shearing effect. So, Herschel-Bulkley visco-plasticity model [19] as shown in Fig. 2.2 (b) is used to accommodate this effect. In this model, the constant post-yield plastic viscosity in the Bingham model is replaced with a power law model dependent on shear strain rate. Therefore,

$$\tau = \left(\tau_0(H) + K \left| \dot{\gamma} \right|^{\frac{1}{m}} \right) \operatorname{sgn}(\dot{\gamma}) \tag{2.2}$$

where m and K are fluid parameters , which are positive. Comparing Eqn. (2.1) with eqn. (2.2), the equivalent plastic viscosity of the Herschel-Bulkley model is

$$k = K \left| \dot{\gamma} \right|^{\frac{1}{m}-1} \tag{2.3}$$

Eqn. (2.3) indicates that the equivalent plastic viscosity η_e decreases as the shear strain $\dot{\gamma}$ increases when $m > 1$ (shear thinning). Besides, this model can also be

used to describe the fluid shear thickening effect when $M < 1$. The Herschel-Bulkley model is reduced to the Bingham model when $m = 1$, therefore $\eta = K$ [19]

Besides, the other characteristic of MR fluid is the stiction phenomenon. The illustration of stiction phenomenon is shown in Fig. 2.3, which is similar to Coulomb friction. When the MR damper force is below the yield level, it is operated mainly in the pre-yield region, which means that the MR fluid is not flowing and having very small elastic deformation. On the contrary, when the damper force exceeds the yield level, the MR damper is operated in the post-yield region.

At the moment when damper force exceeds the yield level, the damper force loss occurs because of the transition from the pre-yield to post-yield region and this is the stiction phenomenon. It can be seen from Fig. 2.3 that when the MR fluid stress increases in the pre-yield region when strain increases. As the strain exceeds the critical strain, the MR fluid changes from pre-yield to post-yield region and begins to flow, so the elastic stress is released, and stress loss is resulted [19].

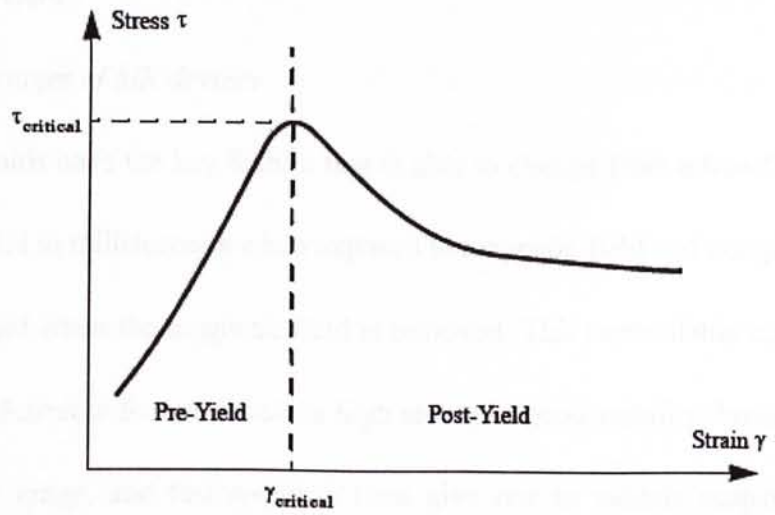

Figure 2.3: Illustration of stiction phenomenon of MR fluids [19].

2.1.3 Literature review

There are quite a lot of studies concerned about MR fluid; some of them are quoted below. Carlson and Weiss [12] explained why MR fluids can outperform the ER fluids and discussed the advantages and possibilities of exploiting the controllable properties of MR fluids. Sims et al. [13] have defined smart fluids and shown how those can be used as the basis for constructing controllable vibration damping devices. They also outlined major advances in the field before 1999. Ashour et al. [17] have conducted characterization and manufacturing studies on MR fluids. They have conducted several experiments to optimize the composition of MR fluid, which was found to minimize the initial viscosity of the fluid and maximize its stability. Carlson [27] discussed about the IUT (In-Use-Thickening) phenomenon of MR fluid and concluded that MR fluid durability and life have been found to be more significant barriers to commercial success than yield strength or stability.

2.2 MR Devices

2.2.1 Advantages of MR devices

MR fluids have the key feature that is able to change from a free-flowing liquid to a semisolid in milliseconds when exposed to magnetic field and completely reverts back to liquid when the magnetic field is removed. This controllable change of state with some desirable features such as high strength, good stability, broad operational temperature range, and fast response time give rise to vehicle suspension system applications and other commercial applications. Besides, in a conventional adjustable

shock absorber, the design and mechanism of the main piston head and the pneumatic reservoir independently control the yield force and damping. Therefore, the devices need to be disassembled for manual adjustment, which is time-consuming and inconvenient. On the contrary, MR fluid devices can vary the amount of damping force without disassembling the devices by means of controlling the magnetic field dependent yield stress of the MR fluids. Furthermore, MR devices contain no moving parts other than the pistons in the dampers, which make them simple, reliable and low-cost. Therefore, MR fluid dampers are considered as promising semi-active devices for the semi-active suspension systems.

2.2.2 Common device geometries

Most devices that use MR fluids can be classified as operating in valve mode (pressure driven flow mode), direct-shear mode, squeeze mode or a combination of these modes [18]. Valve mode is the most widely used mode in MR fluid devices. It has a fixed pole as shown in Fig. 2.4 (a) and then the MR fluid flow from one reservoir to another between the two poles. Examples of pressure driven flow mode devices include servo-valves, dampers and shock absorbers. Shear mode have one or two relatively moveable poles, which sandwiched the MR fluids as shown in Fig. 2.4 (b). The shear mode is suitable for applications that are not required to produce large force. Examples of direct-shear mode devices include clutches, brakes, chucking and locking devices. A third mode of operation is known as squeeze mode as shown in Fig. 2.4 (c). It has been used in low motion and high force applications.

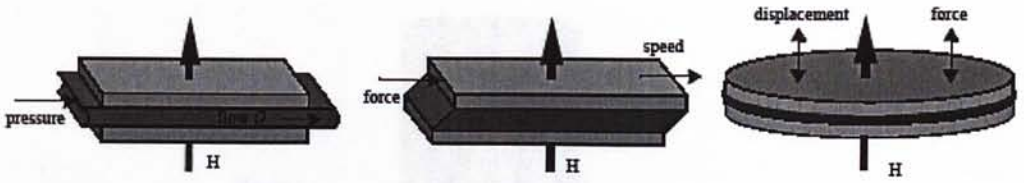

(a) Valve Mode (b) Direct Shear Mode (c) Squeeze Mode

Figure 2.4: Basic operational modes for controllable fluid devices [19].

However, for some damper designs, the operational mode could be a combination of the valve and shear modes. For example, in a double-ended damper, the MR-fluid is driven through the gap between the piston and cylinder by pressure flow. Since one wall in the gap has relative motion with respect to the other so that it is a combination of flow and parallel modes. This kind of combination of flow is known as Couette flow [22].

2.2.3 MR fluid based applications

There are many applications with the use of MR fluids; some of them are mentioned here. Lord Company has manufactured a MR rotary brake (MRB-2107-3) [23] which can be used for exercise equipment, pneumatic actuators, steer-by-wire systems, and other similar applications. This MR brake is a compact proportional brake unsurpassed in its combination of controllability, responsiveness, and functionality. The advantage of this brake is it requires substantially less power to operate than eddy current or magnetic hysteresis brakes. It has other benefits such as precise and instantaneous control, easy integration, high torque at low speed, rugged design and construction.

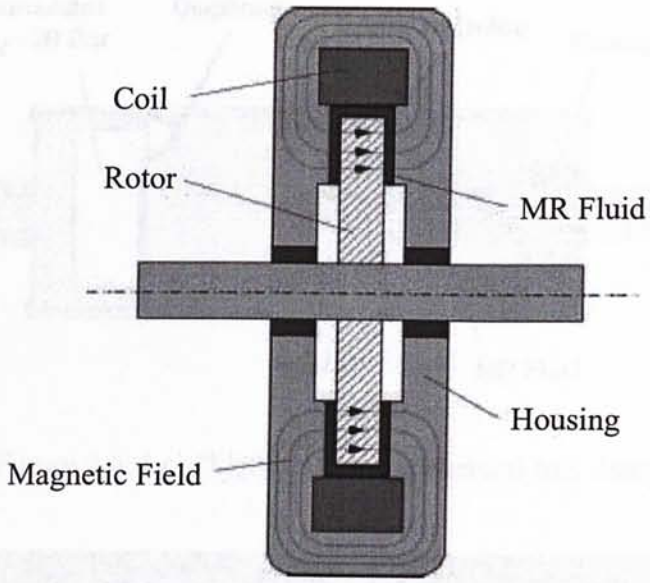

Fig 2.5: Lord Corporation's MRB-2107-3 MR brake [23].

Another well-known commercial product of MR fluid is the Lord Corporation's RD-1005-3 MR damper. It is a small, monotube damper designed for use in a semi-active suspension system in a large on- and off- highway vehicle seat as shown in Fig. 2.6. This suspension system is called "Motion Master" ride management system [24], which consists of the sensor arm; a controller and a ride mode switch as shown in Fig. 2.7. This semi-active suspension system overcomes the limitations of passive suspension systems by sensing the vibration and position of the truck seat and then adjusting the damping force of the MR damper in order to provide effective vibration of the truck seat across a wider range of road conditions and driver weight than the original passive system. This product has introduced to the truck market in 1998. Besides, the Lord Corporation has also applied the MR damper to washing machines, tactile feedback devices, and prosthetics (artificial knee damper as shown in Fig. 2.8).

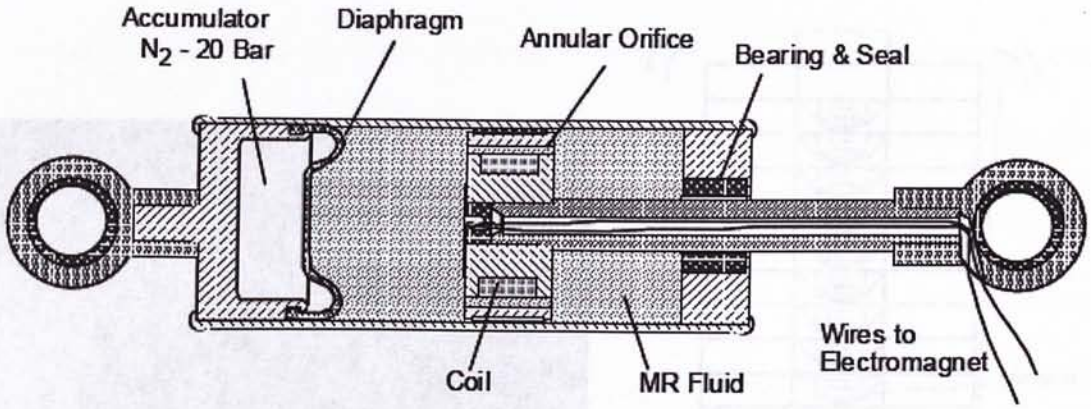

Figure 2.6: Lord Corporation commercial MR damper [21].

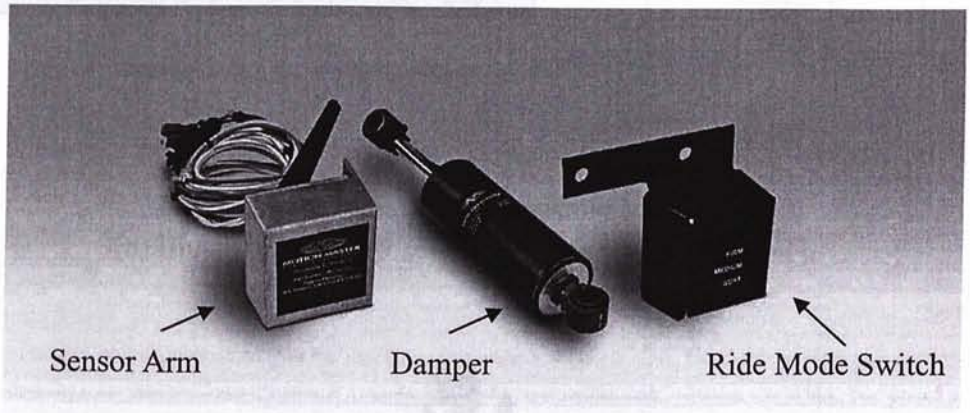

Figure 2.7: Lord Corporation's Motion-Master kit [W1].

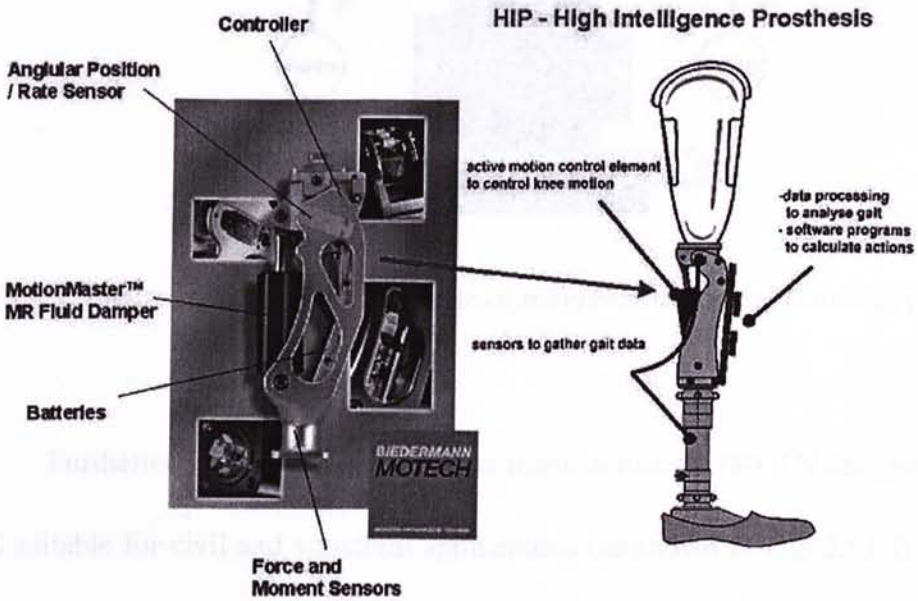

Figure 2.8: Motech above the knee prosthesis featuring Lord Corporation rheonetic MR fluid damper [W1].

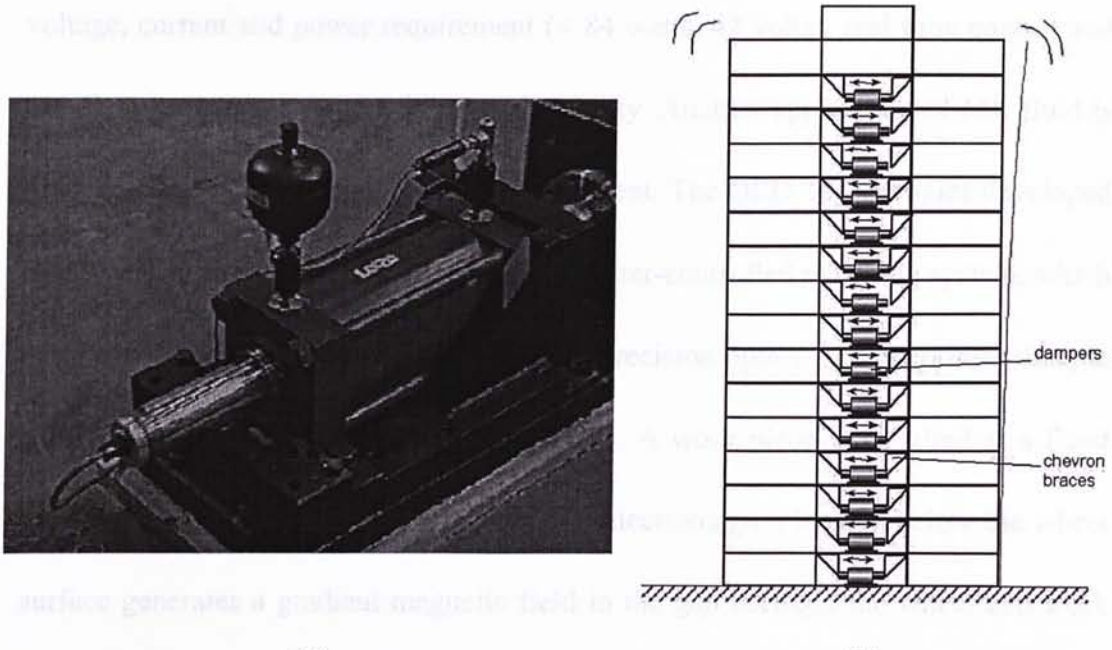

(a) (b)

Figure 2.9: (a) The 180 KN seismic MR damper
(b) Illustration of how seismic MR damper work [W1].

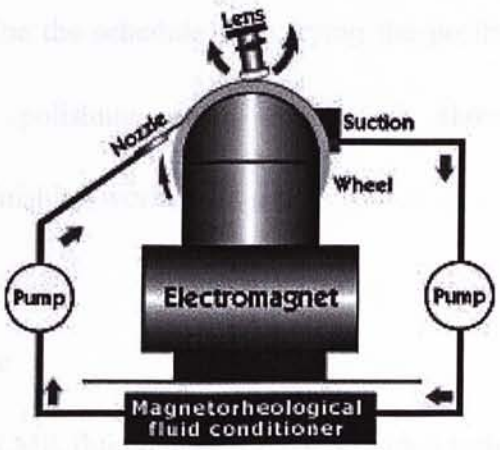

Figure 2.10: Working principle of magnetorheological finishing [W2].

Furthermore, Lord Corporation has manufactured a 180 KN damper [25], which is suitable for civil and structural applications (as shown in Fig. 2.9). It has benefits such as precise and instantaneous control, continuously variable damping, low

voltage, current and power requirement (< 84 watts, 42 volts), real time control and excellent long term reproducibility and stability. Another application of MR fluid is used in automated precision polishing equipment. The QED Technologies developed a Magnetorheological Finishing (MRF) computer-controlled polishing system, which can produce better, faster, and cheaper high-precision optics. The working principle of this polishing system is briefed here [W2]. A work piece is installed at a fixed distance from a moving spherical wheel. An electromagnet located below the wheel surface generates a gradient magnetic field in the gap between the wheel and work piece. When the MR fluid is delivered to the wheel, it is pulled against the wheel surface by the magnetic field gradient. The fluid acquires the wheel velocity, develops high stresses, and becomes a subaperture polishing tool. Then a computer program will determine the schedule for varying the position of the rotating work piece through the polishing zone. Fig. 2.10 shows the diagram how magnetorheological finishing works.

2.2.4 Literature review

It is believed that MR fluid dampers have provided technology that has enabled effective semi-active control in a number of real world applications. The following studies explored the performances and applications of MR dampers. Dyke et al. [28] have studied the application of MR damper to reduce structural response of a three-story scaled building model due to seismic loads by using a clipped-optimal control strategy based on acceleration feedback. Pang et al. [29] have characterized

the linearized MR damper behavior using equivalent viscous damping and complex stiffness and discussed four different nonlinear modeling perspectives including nonlinear Bingham plastic model, nonlinear biviscous model, nonlinear hysteretic biviscous model and nonlinear viscoelastic-plastic model. Jolly et al. [21] discussed the reheological and magnetic properties of some commercial MR fluids and discussed different applications of MR fluids including heavy duty vehicles seat suspension, seismic vibration control and seal-less vibration damper. Spencer et al. [30] examined the scalability of MR damper for civil engineering applications by designed and built a 20-ton full scale MR damper. They also compared the analytical and experimental results of the 20-ton MR damper. Sunakoda et al. [31] have designed and manufactured a 20 ton bypass type MR damper and clarified the effectiveness of MR fluid damper in real building structures. Yang et al. [32] studied the overall dynamic model of MR damper system and subsequent MR damper response analysis was performed by using the mechanical model with the Bouc-Wen model to predict the MR damper behavior under dynamic loading.

Other researchers were concerned with the designs of MR dampers. Muriuki and Clark [22] have studied the effects of magnetic field orientation on damper performance by using the same damper geometry to test for the differences between (i) magnetic field parallel to the axis of the cylinder and (ii) perpendicular field-flow orientation. Kelso [33] made a prototype MR damper including a description of the device technology and characterization test results. He developed an MR damper that is composed of simple, commercial-off-the-shelf (COTS) components and cost

effective components to present an attractive and practical MR damper. Gavin et al. [34] studied the minimization of the electrical power consumption and the inductive time constant when the nonlinear magnetic behavior of the steel alloy is coupled with the non-Newtonian MR fluid. Poynor [35] has presented the results of evaluating several different MR damper designs and also made recommendations for the design of new MR dampers.

For the MR damper mathematical model, Spencer et al. [36] proposed a mechanical model based on the Bouc-Wen model. This model can well capture the force roll-off in the low velocity region due to bleed or blow-by of fluid between the piston and cylinder. However, this Bouc-Wen model has not considered the fluid inertia effects especially in the low velocity region. Yang et al. [37] has proposed mechanical model of MR damper that has considered the shear thinning and inertial effects. Sims et al. [38] proposed the two degrees of freedom of model, which can describe the dynamic non-sinusoidal excitation conditions, and compatible with the numerical simulation of complex dynamic structures.

2.3 Overview of Railway Vehicles

2.3.1 Passive, active and semi-active suspensions

In general, various kinds of railway vehicle suspensions, which can be categorized as passive, active, and semi-active types, have been designed to cushion riders from vibrations. Their key differences are discussed as follows.

Passive – It will use uncontrolled dampers, which requires no input power to

operate in the suspension system. A passive railway vehicle suspension employing springs and hydraulic dampers has some advantages such as design simplicity and cost effectiveness. However, since the design of the passive system is fixed, it is unable to adapt to the system or the operating condition changes such as variation of number of passengers or excitations induced by the rail track irregularities.

Active – It will use active actuators, which are force generators that actively push on the structure to counteract disturbances in the suspension system. Utilizing hydraulic or pneumatic actuators can provide high control performance, but it requires high power and sophisticated control implementation. The active system could also be destabilized as the mechanical power could be imported into the system.

Semi-Active – Semi-active controlled dampers will be used in this suspension system. The main semi-active devices that have been considered for railway vehicles are variable orifice dampers. Semi-active suspensions are proposed to overcome those shortcomings of passive and active suspensions in order to achieve high performance while the systems are stable and fail-safe. It combines features of passive and active controls, rather than push on the structure they counteract motion with a controlled resistive force to reduce motion. They are controllable yet require little input power. Besides, unlike active devices, they do not have the potential to go out of control and destabilize the structure.

2.3.2 Basic railway vehicle structure

A train can be viewed as a collection of rigid bodies representing the car body, the bogie frames and the wheelsets. These rigid bodies are connected by kinematic joints, which constrain their relative motion.

Almost all railway vehicles use bogies (trucks in US parlance) to carry and guide the body along the track. The suspension system between the wheelsets and the bogie is called primary suspension system and the suspension system between the car body and the bogie is called secondary suspension system. It is a very important issue for the railway vehicle that the interface between vehicle body and wheel needs some sort of cushion system to reduce the vibration perceived by the passengers as the train moved along the track. The primary suspensions (the suspension from the bogie to the wheelsets) are responsible for the guidance and stability of the vehicle while the secondary suspensions (the suspension from the bogie to vehicle body) are responsible for damping the vibrations and noise in the passenger compartments. Therefore, the dynamic behaviours and the vibration control are strongly dependent on the primary and secondary suspension characteristics and influenced by the wheel rail interaction.

A railway vehicle can be described as shown in Fig. 2.11. The car body directly rests on the secondary suspension and its weight is transmitted downward to the track through the bogie frames, primary suspension, axle-boxes, wheelsets and wheel-rail interface. Conversely, forces arising from the track nominal geometry and irregularities are transmitted upwards through the same components. Basically, the

suspension system will cope with the longitudinal, lateral, vertical, roll, pitch and yaw motions of the car body as shown in Fig. 2.12. The resulting vehicle performances and car body accelerations, ultimately responsible for the ride quality, are affected by the characteristics of the mechanical elements used in the vehicle.

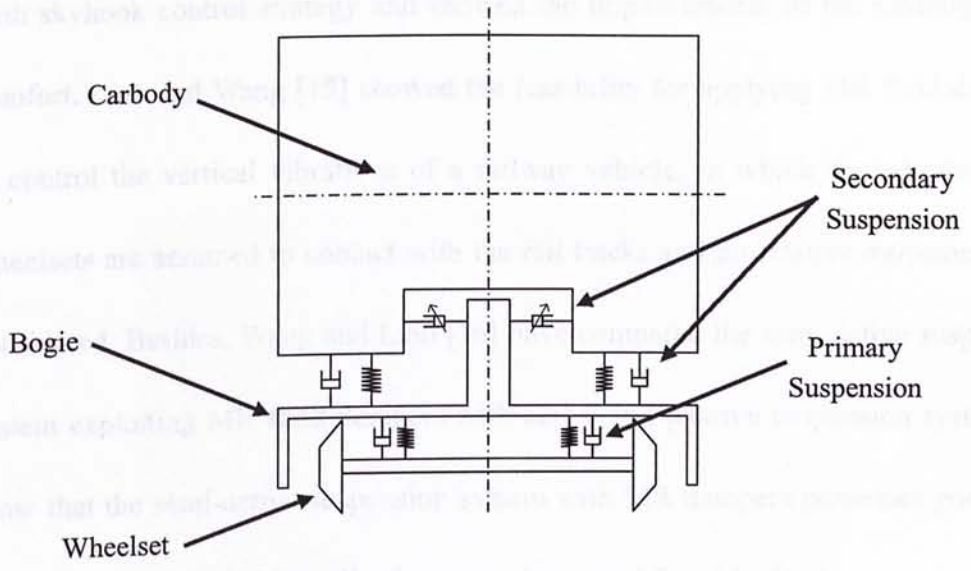

Figure 2.11: Schematic representation of a railway vehicle model.

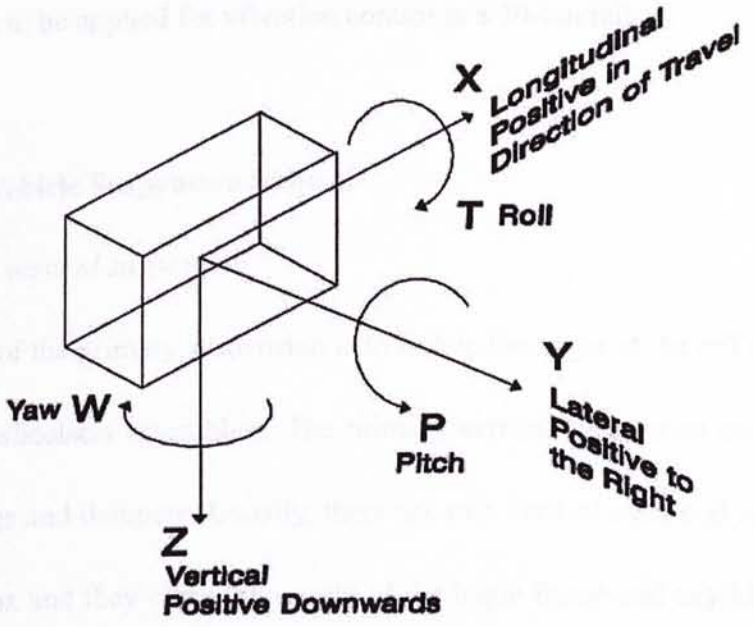

Figure 2.12: The basic axis system of railway vehicle.

2.3.3 Literature review

O'Neill and Wale [8] have outlined a computer simulation using a non-linear program on a semi-active railway suspension system with a controllable damper. Stribersky et al. [10] developed a semi-active damping system used on rail vehicle with skyhook control strategy and showed the improvements of the passenger ride comfort. Liao and Wang [15] showed the feasibility for applying MR fluid dampers to control the vertical vibrations of a railway vehicle, in which the wheels of the wheelsets are assumed to contact with the rail tracks and no relative movements are considered. Besides, Wang and Liao [16] have compared the semi-active suspension system exploiting MR fluid dampers with active and passive suspension systems to show that the semi-active suspension system with MR dampers possesses good ride quality improvement ability. Furthermore, Atray and Roschke [1] have presented the procedure used for design, fabrication, testing and numerical modeling of an MR damper that is to be applied for vibration control in a 70-ton railcar.

2.4 Railway Vehicle Suspension Systems

2.4.1 Primary vertical suspension

The role of the primary suspension is to isolate the bogie of the rail vehicle from the axle and wheelsets assemblies. The primary vertical suspension consists of the vertical springs and dampers. Usually, there are two vertical steel coil springs fitted to each axlebox and they carry the weight of the bogie frame and anything attached. Then the vertical dampers are to dissipate vibrational energy and control the

movements between axle box and bogie frame. The movements include the bogie bouncing and pitching in relation to the axles, which are induced by irregularities in the track, rail joints points and crossing. A serious wheel unloading with danger of derailment would occur if these motions are out of control. Fig. 2.13 shows the picture of a primary vertical spring and Fig. 2.14 shows the diagram of the suspension system.

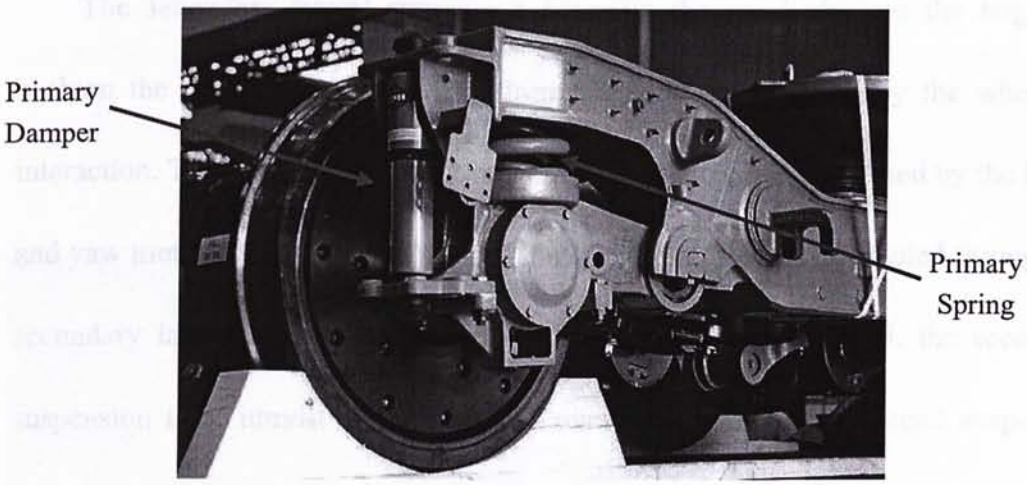

Figure 2.13: Vertical spring and shock absorber. [W3].

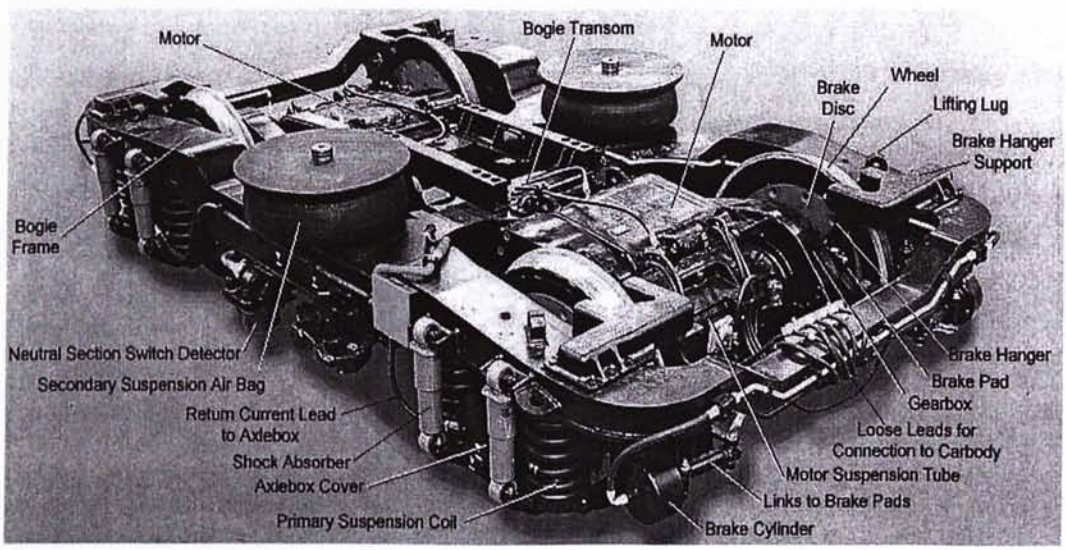

Figure 2.14 Picture of bogie with primary coil spring and damper [W4].

2.4.2 Secondary vertical suspension

The secondary vertical suspension, on the other hand, is used to isolate the rail vehicle's car body from the bogie. It controls the vertical movements and pitching of the car body relative to the bogie. Besides, it assists the secondary lateral suspension secondary to control rolling oscillations of the car body (see Fig. 2.15).

2.4.3 Secondary lateral suspension

The secondary lateral suspension connects the car body and the bogies to cushion the passenger compartment from the vibration induced by the wheel-rail interaction. The lateral vibration of the railway vehicle could be caused by the lateral and yaw motions coupled with the roll motion, which will be attenuated through the secondary lateral suspension. When the ride quality is concerned, the secondary suspension is of utmost importance. An overdamped secondary lateral suspension can induce excessive sway to the car body, which reduces the passenger's ride comfort greatly. Fig. 2.15 shows the bogie with the secondary lateral damper.

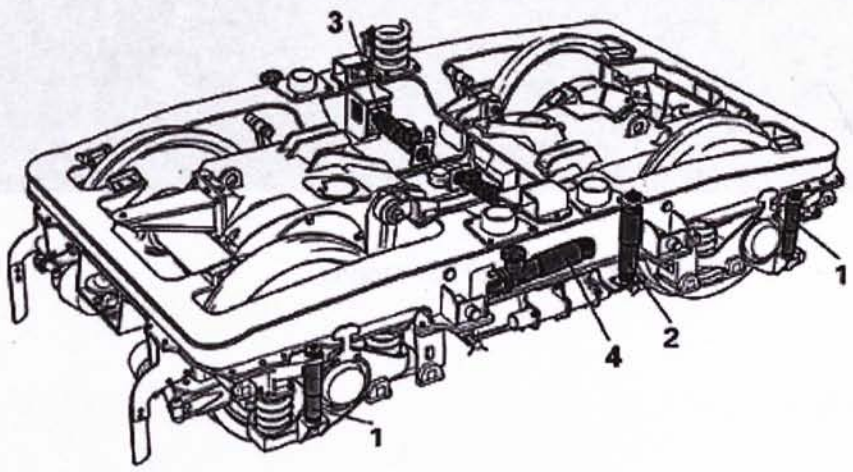

1. Primary Vertical Damper
2. Secondary Vertical Damper
3. Secondary Lateral Damper
4. Yaw Damper

Figure 2.15: The bogie [W5].

2.4.4 Yaw suspension

Yaw dampers are dampers designed to control the rotation of the bogie around the centre pivot of the bogie, which can increase wear and tear between the rails and train wheels as well as noise. A fundamental characteristic of the bogie is that it must rotate relative to the body on curves, while retaining high rotational resistance during high-speed running on straight sections in order to prevent wheelset hunting that reduces ride comfort [26] and would be in risk of derailment in case of high-speed trains. As shown in Fig. 2.16. Yaw dampers are usually positioned longitudinally to control rotation of the bogie without influencing lateral damping.

Figure 2.16: Yaw damper [W4].

CHAPTER 3

DESIGN CONSIDERATIONS FOR MR DAMPERS

Chapter 3 is concerned with the design considerations of MR dampers. First of all, there are an overview of different designs and structures of existing MR dampers. Then the issues for the MR damper magnetic circuits are discussed. Finally, the design on the geometry of the MR damper concerning the controllable force, active fluid volume and the magnetic circuit is considered.

3.1 Overview of Existing MR Dampers

3.1.1 Monotube MR fluid damper

A schematic of an MR damper shown in Fig. 3.1 is a prototype of an MR damper with linear stroke, which is manufactured by Lord Corporation. As shown in Fig. 3.1, the hydraulic cylinder houses the damper piston, in which is mounted a magnetic circuit. At the base inside the hydraulic cylinder, a nitrogen accumulator is used to pressurize the approximate 50 ml of MR fluid to above atmospheric pressure. This is a standard technique used to prevent cavitations on the low pressure side of the piston while it is in motion. Besides, the MR fluid flows through an annular

orifice in the piston head, where the MR fluid will be magnetized by the magnetic field developed by the electromagnetic coil when current is applied.

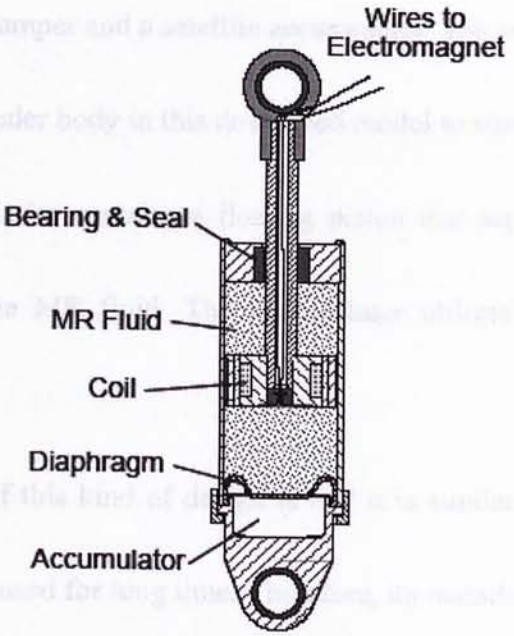

Figure 3.1: Schematic of an MR damper [28].

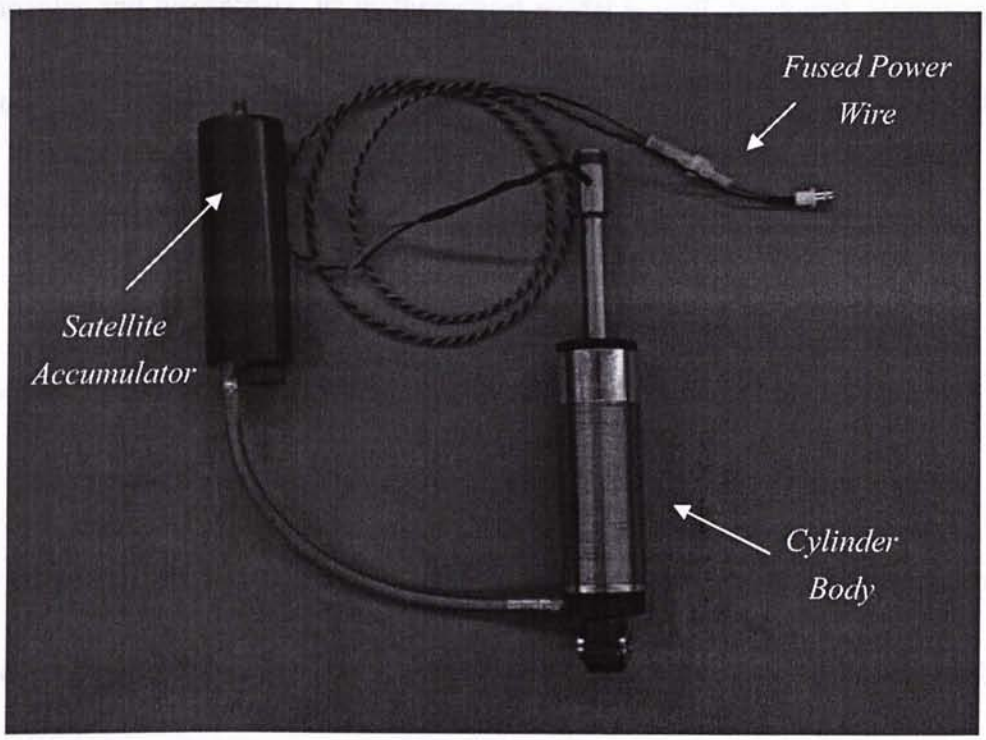

Figure 3.2: Monotube MR damper with satellite accumulator [33].

Another monotube MR damper with an external accumulator [33] (satellite accumulator) instead of an internal one is shown in Fig. 3.2. This MR device consists of a piston-cylinder damper and a satellite accumulator. The accumulator is separated from the damper cylinder body in this developed model to simplify frequent rebuilds. The accumulator cylinder contains a floating piston that separates the compressed nitrogen gas from the MR fluid. The accumulator utilizes a Schrader valve for pressurization.

The advantage of this kind of design is that it is similar to the current viscous damper that has been used for long time. Therefore, its manufacturing process is well known. Besides, since it is the most commonly used MR fluid damper used by companies and researchers, its mathematical model is well developed. However, the major disadvantage of this kind of design is the difficulty to make the accumulator and diaphragm.

3.1.2 Double-ended MR damper

The cross sectional view of a doubled-ended MR damper is shown in Fig. 3.3. The double-ended MR damper has piston rods of the same diameter to protrude through both ends of the damper. Therefore, the piston is supported by a shaft at both ends. Since there is no change in volume as the piston rod moves, this arrangement

has the advantage that a rod-volume compensator, accumulator or other similar devices are not needed to be incorporated into the damper [30]. However, a small pressurized accumulator may be used to accommodate the thermal expansion effect for a large scale MR fluid damper as shown in Fig. 3.4, which contains MR fluids up to 5 liters. Doubled-ended MR dampers have been used for bicycles, gun recoil applications, and for stabilizing buildings during earthquakes.

A full scale seismic doubled-ended MR-fluid damper has been designed and built [30, 32, 37]. For the nominal design, it has a maximum damping force of 200,000 N and a dynamic range (dynamic range concept will be discussed in Section 2.6.1) equal to ten. A schematic of the 20-ton MR damper is shown in Fig. 3.4. The damper uses a particularly simple geometry in which outer cylindrical housing is part of the magnetic circuit. The effective fluid orifice is the entire annular space between the piston outside diameter and the inside of the damper cylinder housing.

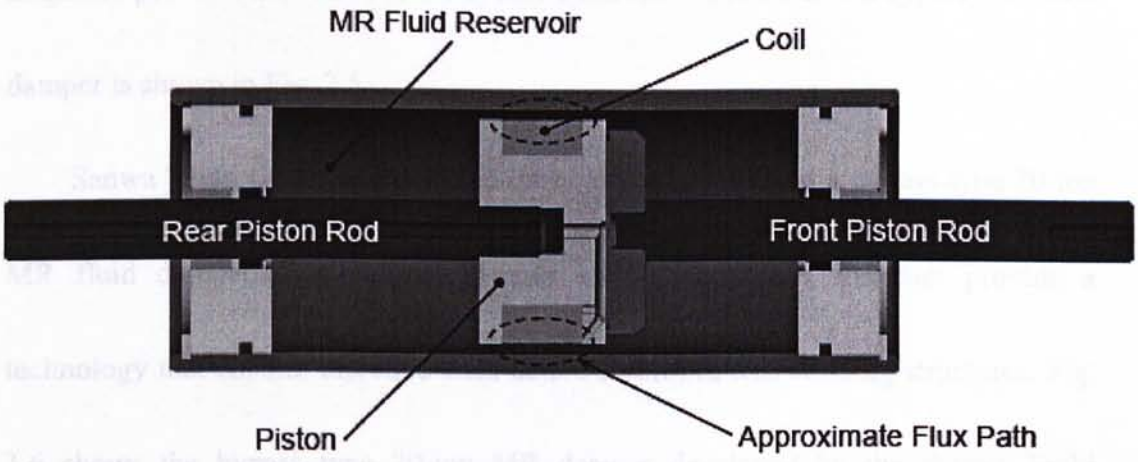

Figure 3.3: Double-ended MR damper [35].

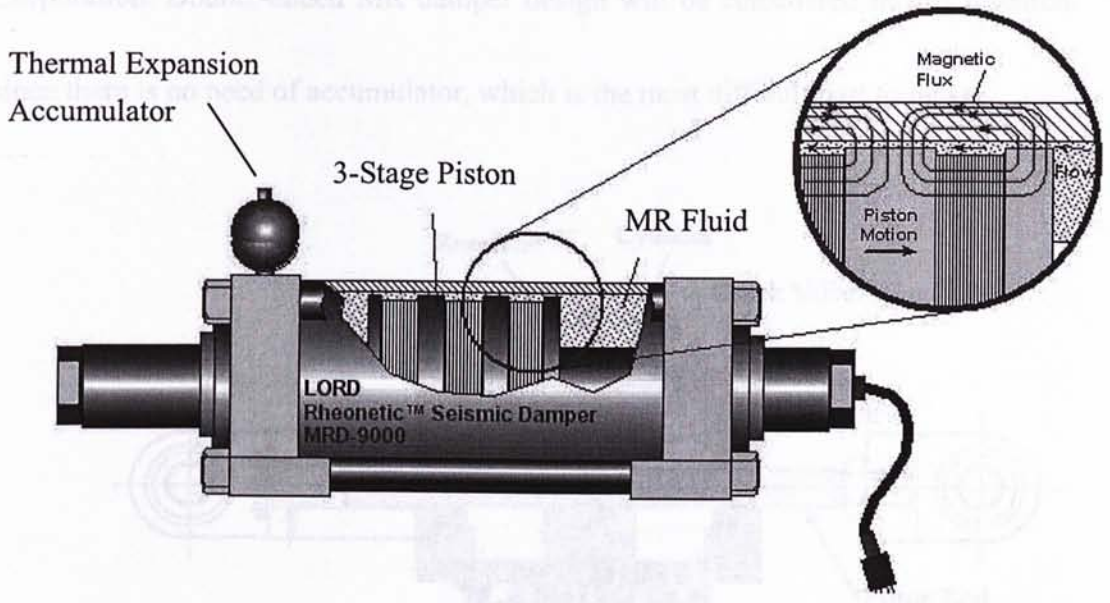

Figure 3.4: Schematic of 20-ton MR damper [W1].

Another kind of common double-ended MR damper is bypass type MR damper. Unlike the aforementioned configurations, MR fluid in bypass type flow from a high pressure chamber to a low pressure chamber in valve mode through a bypass outside the main cylinder. The bypass has an annular gap between the outside of the magnetic pole and the inside of the bypass cylinder. A double-ended bypass MR fluid damper is shown in Fig. 3.5.

Sanwa Tekki Corporation has designed and manufactured a bypass-type 20 ton MR fluid damper. This bypass damper clarified that MR dampers provide a technology that enables effective semi-active control in real building structures. Fig. 3.6 shows the bypass type 20-ton MR damper developed by the Sanwa Tekki

Corporation. Double-ended MR damper design will be considered in this research, since there is no need of accumulator, which is the most difficult part to make.

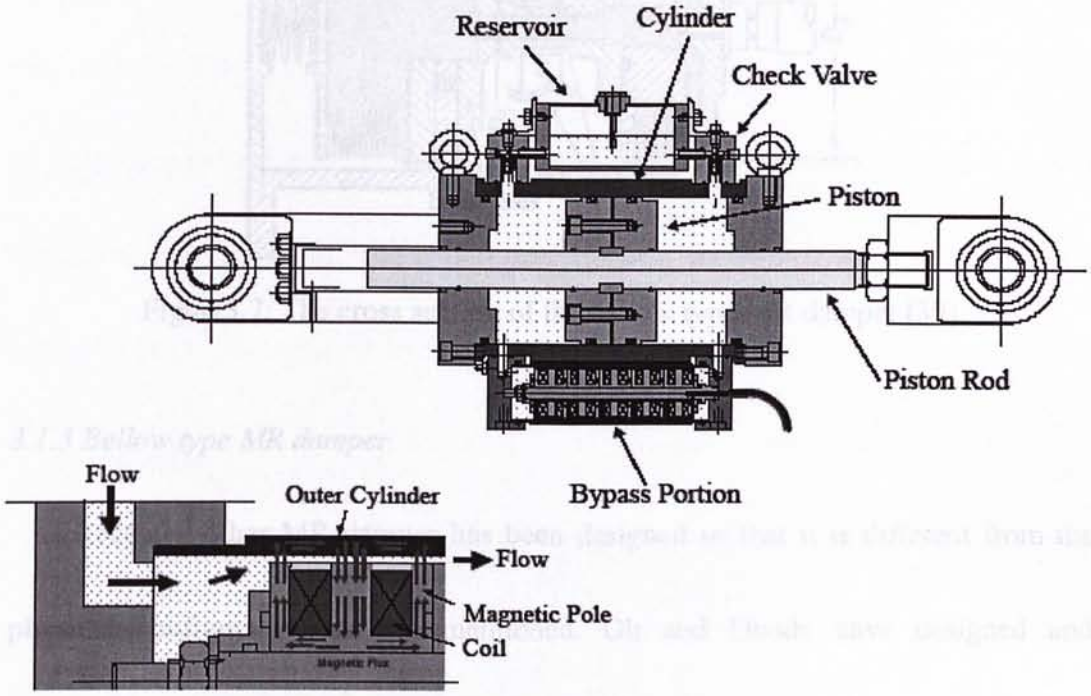

Figure 3.5: Hydraulic circuit of the bypass MR damper by Sanwa Tekki Corportation [19].

Figure 3.6: Bypass type 20-ton MR damper developed by the Sanwa Tekki Corporation [31].

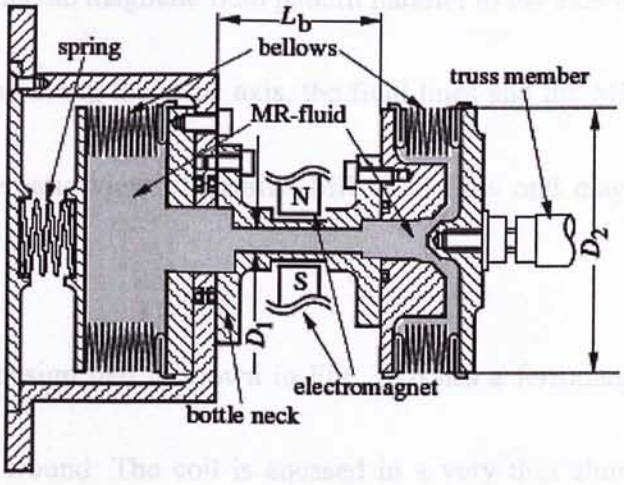

Figure3.7: The cross section of the bellow type MR damper [39].

3.1.3 Bellow type MR damper

Recently, other MR damper has been designed so that it is different from the physical configuration as aforementioned. Oh and Onoda have designed and fabricated a bellows type of MR fluid damper composed of two variable volume chambers filled with MR fluids [39]. Figure 3.7 shows the cross section of the bellow type MR fluid damper.

3.2 Optimal Design and Configuration of Magnetic Circuit

3.2.1 Magnetic circuit and magnetic field orientation

For the MR damper design, there are two kinds of magnetic field coil implementation commonly used. The first design is that the magnetic field coil is wrapped at the outer diameter of the damper (as shown in Fig. 3.8). This

configuration aligns the magnetic field pattern parallel to the axis of the cylinder [22]. Since piston is also along the same axis, the field lines and the MR fluid flow are in parallel. The schematic view of parallel MR fluid flow and magnetic flux lines is shown in Fig 3.9.

The second design that is shown in Fig. 3.10 has a ferromagnetic core around which the coil is wound. The coil is encased in a very thin aluminum sleeve to it from the fluid. The cylinder itself is made of iron and has aluminum end caps. The

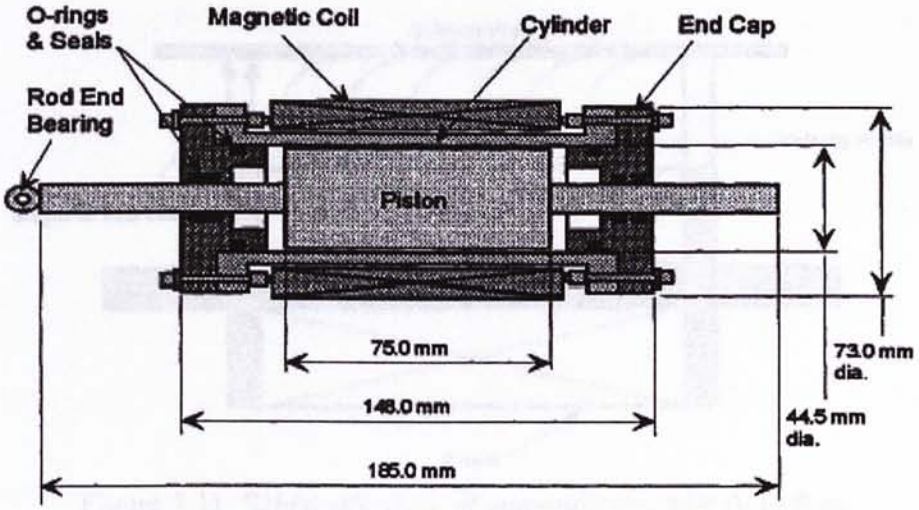

Figure 3.8: Piston-cylinder arrangement for the coil wrapped around the outer diameter [22].

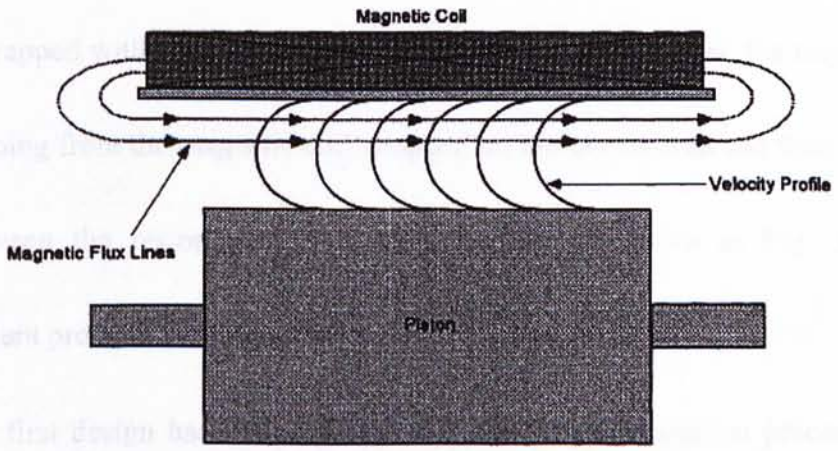

Figure 3.9: The schematic view of parallel MR fluid flow and magnetic flux [22].

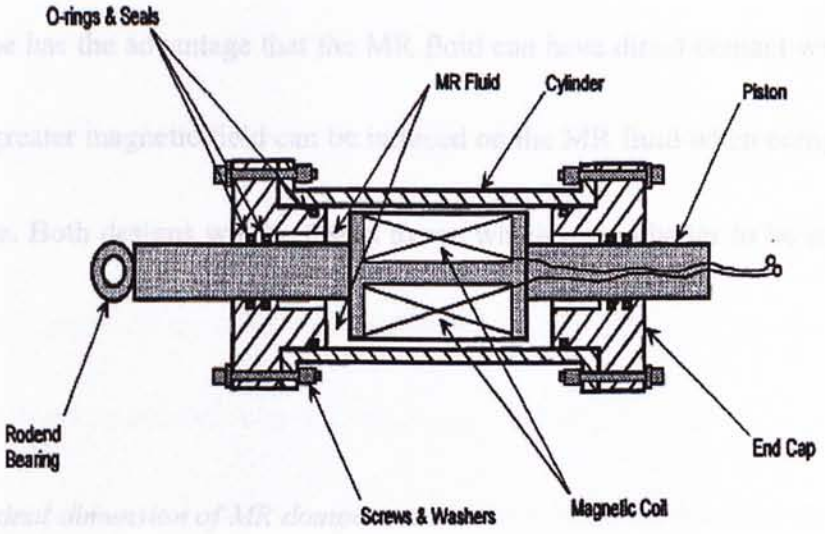

Figure 3.10: Piston-cylinder arrangement for perpendicular flux and MR fluid flow [22].

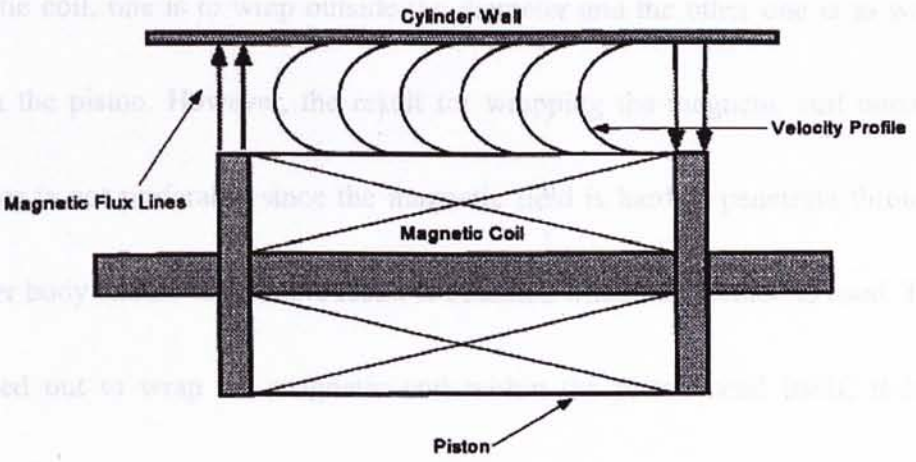

Figure 3.11: Schematic view of perpendicular MR fluid flow and magnetic flux lines [22].

coil is wrapped within the piston head itself. In this configuration, the magnetic flux path is going from the magnetic coil wrapped on the piston head and then across the gap between the piston and the cylinder, which is shown in Fig. 3.11. This arrangement provides the perpendicular field-flow orientation [22].

The first design has the advantage of simple implementation process and the

second one has the advantage that the MR fluid can have direct contact with the coil so that a greater magnetic field can be induced on the MR fluid when compared with design one. Both designs will be tested to see which one is better to be used in this research.

3.2.2 Physical dimension of MR damper

As mentioned in Section 3.3.1, there are two configurations of wrapping the magnetic coil, one is to wrap outside the diameter and the other one is to wrap the coil on the piston. However, the result for wrapping the magnetic coil outside the diameter is not preferable since the magnetic field is hard to penetrate through the cylinder body and no observable result is obtained when this method is used. Thus, it is turned out to wrap the magnetic coil within the piston head itself; it has the advantage that the MR fluid can have direct contact with the magnetic coil and greater magnetization effect can be developed.

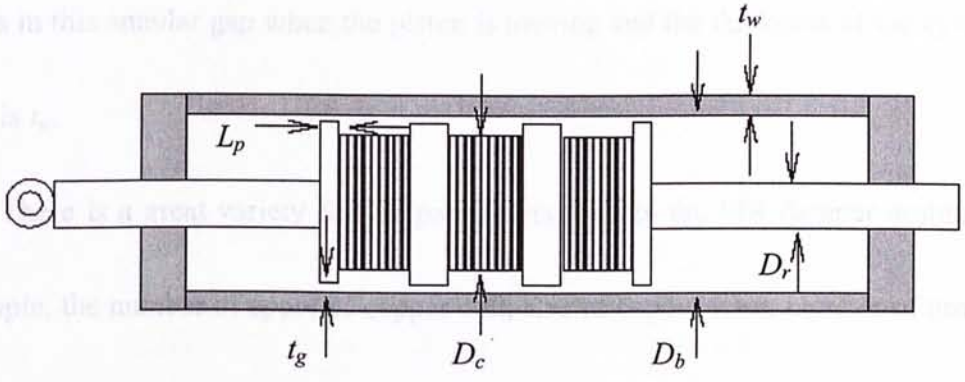

Figure 3.12: Physical dimension of the MR damper [34].

For this magnetic coil configuration, Kelso [33] has demonstrated how to use simple and commercial-off-the-shelf (COTS) components to make an MR damper. Gavin et al. [34] have a deep investigation on how to optimize the inductive time constant and minimize the electrical consumption. In this research, the magnetic coil design and configuration are based on their conclusions and results.

Having the magnetic coil wrapping outside the damper, there are six common physical dimension parameters involved, which are illustrated in Fig. 3.12. Those physical dimensions are the diameter of the casing bore, D_b, the diameter of the piston rod, D_r, the thickness of the casing wall, t_w, the diameter of the core, D_c, the pole length, Lp, and the thickness of the gap, t_g.

In Fig. 3.12, the vertical hash marks represent the spool of magnet wire that will generate magnetic flux within the steel piston. The flux in the magnetic circuit flows axially through the steel core diameter D_c, beneath the windings, radically through the piston poles of length Lp, through a gap of thickness t_g, in which the MR fluid flows in this annular gap when the piston is moving and the thickness of the cylinder wall is t_w.

There is a great variety for the parameters used in the MR damper design, for example, the number of spool of copper coil; size of copper wire; number of turns of coil, the orientation of wrapping the copper wire and length of the gap size t_g, etc.

Besides, the number of layers is limited by the maximum piston diameter and the gage of wire. The number of spools is limited by the maximum piston length. Therefore, those parameters are related interactively, and optimal range of parameters was investigated by Gavin et al. [34].

3.2.3 Connection polarity of electromagnetic circuit

Time response for an electromagnetic circuit can be modeled as a function of inductance and electrical resistance. This can be expressed as:

$$\tau = \frac{L}{R} \tag{3.1}$$

where τ is time response, L is inductance, and R is resistance. In order to have faster response time, we should minimize the L/R ratio so that the time constant of the electromagnetic circuit will be reduced. However, the total number of turns of coil is limited by the physical diameter of the piston head dimension so that the total

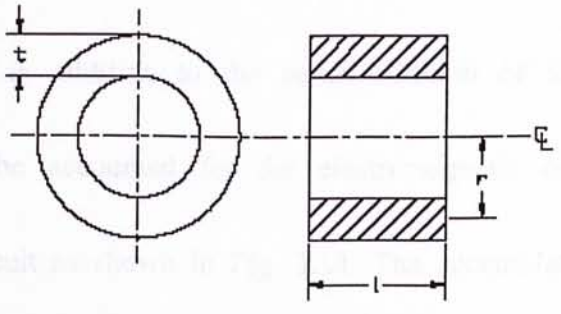

Figure 3.13: Cross-sectional view of solenoid coil [33].

resistance is fixed and cannot be manipulated. Therefore, only one parameter can be manipulated in order to reduce the time response: the inductance.

For the cross-sectional view of solenoid coil shown in Fig.3.13, the inductance of the coil, L_c, can be represented as [33]:

$$L_c = \frac{4\pi^2 N^2 r^2 K_n}{l} \cdot 10^{-6} \tag{3.2}$$

which units are in Henries, with radius in terms of inches. The geometry term, K_n, in Eq. (3.2) is defined as [33]:

$$K_n = \frac{1}{1 + 0.9\frac{r}{l} + 0.32\frac{t}{r} + 0.84\frac{t}{l}} \tag{3.3}$$

As shown in Fig. 3.13, r is the mean radius, t is the thickness, and l is the length of the coil along the centerline. Fig. 3.14 shows an arrangement of three smaller coils which sum of the cross-sectional area is equivalent to the area of the single coil shown in Fig. 3.13. It is assumed that the same number of turns of coil and the same gage of copper wire are used for both cases. The inductance of the electromagnetic circuit in Fig. 3.13 is calculated directly from Eqn. (3.2). However, the effects of mutual inductance in addition to the series addition of three individual coil inductances must be accounted for the electromagnetic circuit having series electromagnetic circuit as shown in Fig. 3.14. The accumulated inductance is as follows [33]:

$$L_s = L_1 + L_2 + L_3 \pm 2(M_{12} + M_{23} + M_{13}) \tag{3.4}$$

L_s is the summed inductance, L_1, L_2, L_3 are the inductances of the first, second and third coils respectively. M_{12} is the mutual inductance for the interaction between the first and second coil, M_{23} is mutual inductance for the interaction between the second and third coils, and M_{13} is mutual inductance of those two external coils. The plus/minus sign before the mutual inductance terms indicate that coupling is either additive or subtractive, depending on the connection polarity.

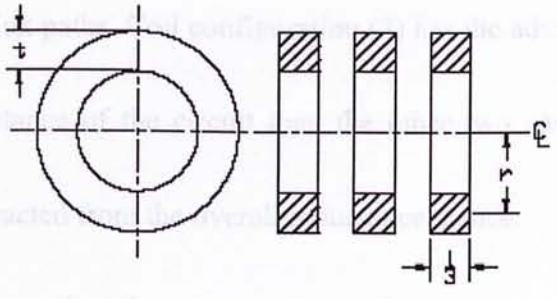

Figure.3.14: Cross-sectional view of 3 coils in series [33].

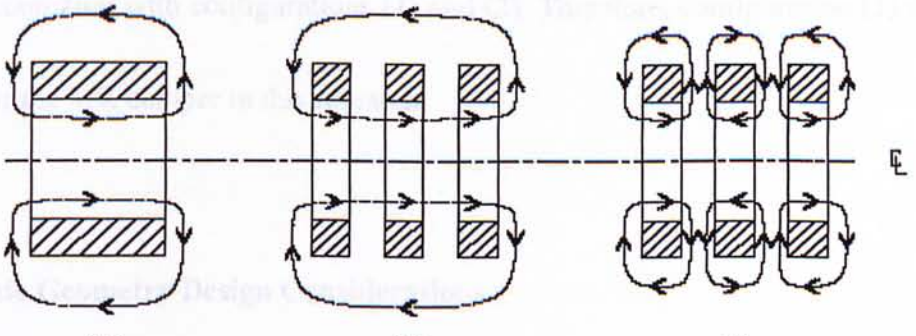

Figure 3.15: Flux path illustrations for three different coil configurations. The polarity (or direction of wind) of coils in configuration (3) is in alternative direction, while the polarity of coil in configuration (2) is in same direction [33].

Three different kinds of connection polarity are shown in Fig. 3.15. Coil configuration (1) has flux lines that flow around the single coil. Coil configuration (2) and (3) represent three spools of coils with the same number of turns of coils and resistance but have different polarity. Configuration (2) shows the flow of the flux around three coils with windings in one direction relative the centerline. Configuration (3) shows the flow of flux around three coils whose winding orientations alternate for each coil. The main difference between those configurations is the length of the flux paths. Coil configuration (3) has the advantage that it has the lowest overall inductance of the circuit than the other two cases [33]; the mutual inductances are subtracted from the overall inductance, hence:

$$L_3 << L_1 \quad \text{and} \quad L_3 << L_2 \tag{2.8}$$

When coil configuration (3) is adopted, there will have shorter time response when compared with configurations (1) and (2). Therefore, configuration (3) will be used for the MR damper in this research.

3.3 Basic Geometry Design Considerations

3.3.1 Controllable force and dynamic range

The controllable force and dynamic range are the two most important parameters to be considered when designing an MR damper. It is because these two

parameters can be used to evaluate the overall performance of the MR damper [19]. The total damper force F can be decomposed into a controllable force F_τ due to controllable yield stress τ_0 and an uncontrollable force F_{uc} as shown in Fig. 3.16. The uncontrollable force includes a plastic viscous force F_η and a friction force F_f. The dynamics range is defined as the ratio between the controllable force F_τ and the uncontrollable force F_{uc} as follows:

$$D = \frac{F_\tau}{F_{uc}} = \frac{F_\tau}{F_\eta + F_f} \tag{3.6}$$

Based on the parallel-plate Bingham model, F_η and F_τ are defined as:

$$F_\eta = \left(1 + \frac{whv_0}{2Q}\right)\frac{12\eta QLA_p}{wh^3} \tag{3.7}$$

$$F_\tau = c\frac{\tau_0 LA_p}{h}\mathrm{sgn}(v_0) \tag{3.8}$$

where c $\sim$ 2.07 + 1/(1 + 0.4T) bounded to the interval [2.07, 3.07] [30].

The controllable force in Eqn. (3.7) can also be rewritten as [37]:

$$F_\tau = \left(2.07 + \frac{12Q\eta}{12Q\eta + 0.4wh^2\tau_0}\right)\frac{\tau_0 LA_p}{h}\mathrm{sgn}(v_0) \tag{3.9}$$

which indicates that the controllable force is inversely related to the gap size h. Therefore, a small gap size can achieve a large controllable force, which can increase the effectiveness of the MR damper.

However, a small gap size will greatly reduce the dynamic range, which is indicated in Eqn. (3.7) and Eqn. (3.8). We can see that the viscous force increases

two orders of magnitude faster than the controllable force with a small gap size if one assumes that the magnetic field is saturated; the dynamic range will decrease dramatically or even tends to zero if too small gap size is used. On the other hand, a large gap size will decrease both the controllable force and the viscous force. Since the friction force is a constant, the dynamics range tends to zero when the gap size is too large. It is obvious that there exists an optimal dynamic range [37]. Spencer and his associates [30] have suggested that h/R = 0.02 would be the most effective ratio for their design.

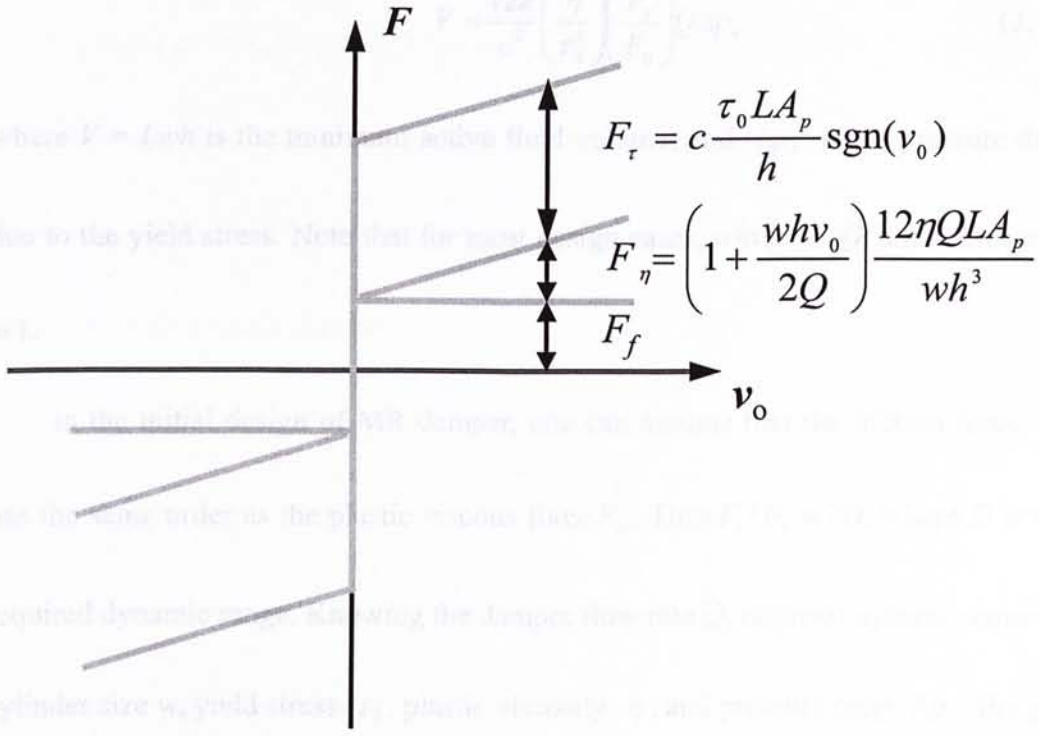

Figure 3.16: Illustration of force decomposition of MR dampers.

3.3.2 Geometry constraints

There are many other parameters to be considered in the design of MR damper.

One of them is the minimum active fluid volume V, which is the volume of MR fluids exposed to the magnetic field and thus responsible for providing the desired MR effect. By using Eqn. (3.7) and Eqn. (3.8), one can obtain

$$wh^2 = \frac{12k}{c}\left(\frac{\eta}{\tau_0}\right)\left(\frac{F_\tau}{F_\eta}\right)Q \tag{3.10}$$

where $k = 1 + (whv_0)/(2Q)$. Because Eqn. (3.8) can also be written as

$$\Delta p_\tau = \frac{F_\tau}{A_p} = \frac{c\tau_0 L}{h} \tag{3.11}$$

Eqn. (3.9) can be further manipulated to give:

$$V = \frac{12k}{c^2}\left(\frac{\eta}{\tau_0^2}\right)\left(\frac{F_\tau}{F_\eta}\right)Q\Delta p_\tau \tag{3.12}$$

where $V = Lwh$ is the minimum active fluid volume; and Δp_τ is the pressure drop due to the yield stress. Note that for most design cases, $whv_0 \ll Q$, and therefore $k \approx 1$.

In the initial design of MR damper, one can assume that the friction force F_τ has the same order as the plastic viscous force F_η. Thus $F_\tau / F_\eta \approx 2\mathrm{D}$, where D is the required dynamic range. Knowing the damper flow rate Q, required dynamic range D, cylinder size w, yield stress τ_0, plastic viscosity η, and pressure drop Δp_τ, the gap size h and active pole length L can be obtained from Eqns. (3.10) and (3.12) [19].

The above expression can be condensed into a pair of simple expressions that can be applied to all MR devices [T18] as shown in Fig. 3.17. Therefore, it is very

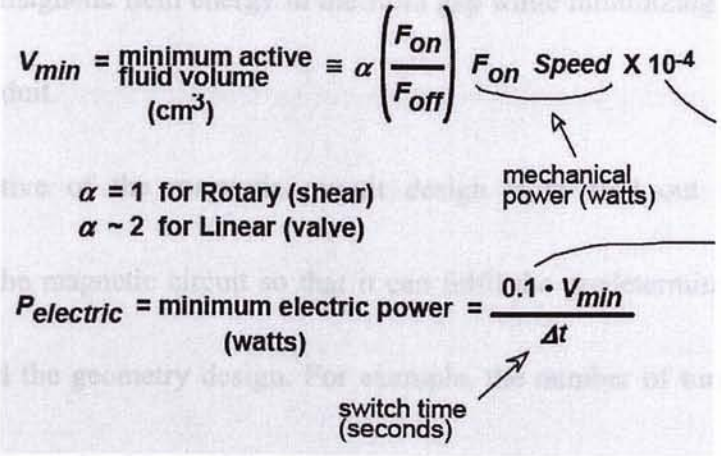

Figure 3.17: Expressions used to evaluate application feasibility for a typical MR fluid [T18].

useful for making a quick evaluation for the fesaibility of a given application.

F_{on} stands for minimum "on-state" force for torque needed (N or N-m), F_{off} stands for maximum "off-state" force or torque that may be tolerated (N or N-m), *Speed* stands for maximum speed or angular velocity for F_{off} (m/s or rad/s) and Δt stands for desired switching time.

3.3.3 Magnetic circuit design

Aftering considering the dynamic range and active fluid volume, it comes to the magnetic circuit design. The guidline of the magnetic circuit design has been described by Lord Corporation [41] and Yang [19]. Those steps are summarized here.

The MR damper magnetic circuit typically uses low carbon steel material to act as the core, which has high magnetic permeablility and saturation. So, it can

maximize the magnetic field energy in the fluid gap while minimizing the enrgy loss in the flux conduit.

The objective of the magnetic circuit design is to find out the necessary amp-turns of the magnetic circuit so that it can fulfil the predetermined application requirment and the geometry design. For example, the number of turns of coil and the required current for the application can be estimated. Typical design process is as follows:

(1) Determine the operating point in MR fluid: it is the magnetic induction B_f value

(2) Determine the magnetic field intensity H_f in the MR fluid such that it can fulfil the application yield stress. Determine H_f from Fig. 3.18 (a), then determine B_f from Fig. 3.18 (b).

(3) Determine the continuity of magnetic flux as follows:

$$B_s = \frac{\phi}{A_s} = \frac{B_f A_f}{A_s} \tag{3.13}$$

where $\phi = B_f A_f$ is the total magnetic induction flux, As is the steel core and A_f is the effective pole area including the fringe of magnetic flux. Fig. 3.19 shows the diagram of the basic magnetic circuit.

(3) Determine the magnetic field intensity H_s of the low carbon steel from Fig. 3.20.

(4) Using the Kirchoff's Law for Magnetic Circuits to determine the necessary number of amp-turns (NI):

$$NI = gH_f + LH_s \tag{3.14}$$

where g is the total length of fluid gaps and L is the length of steel path that is equal to $L_s + L_c$. In the megnetic circuit design as shown in Fig. 3.20, the fluid total length of gap g should be $2h$.

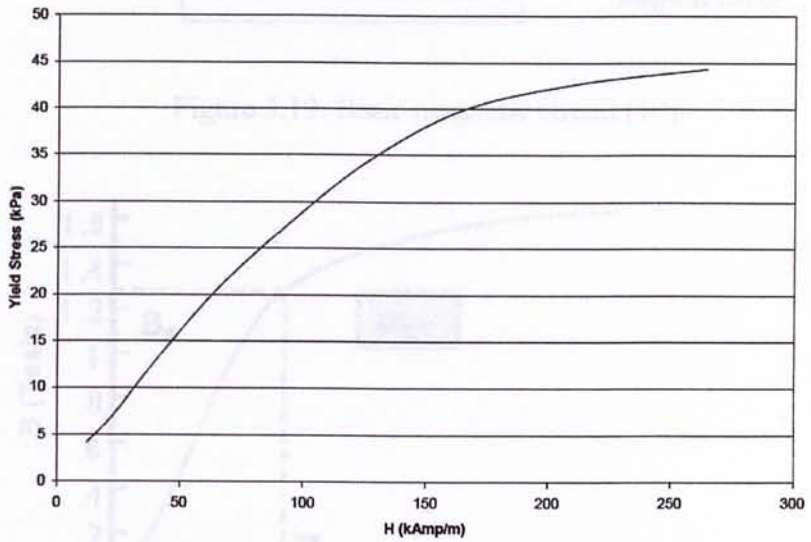

(a)

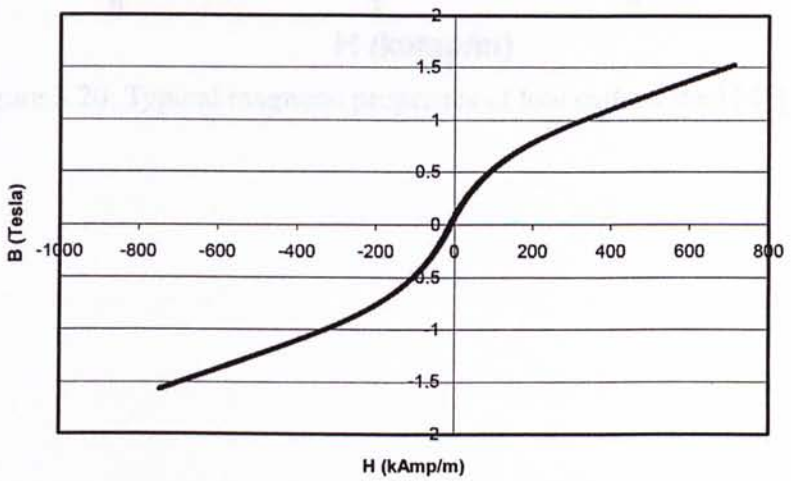

(b)

Figure 3.18: (a) Yield stress versus magnetic induction (b) Typical magnetic properties MRF-132AD [T42].

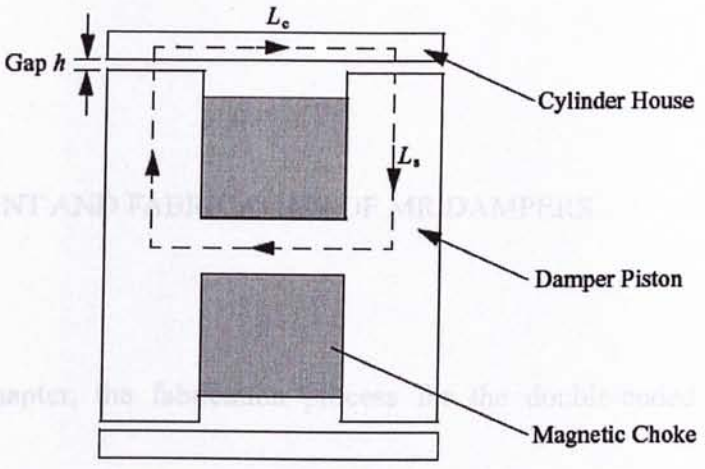

Figure 3.19: Basic magnetic circuit [19].

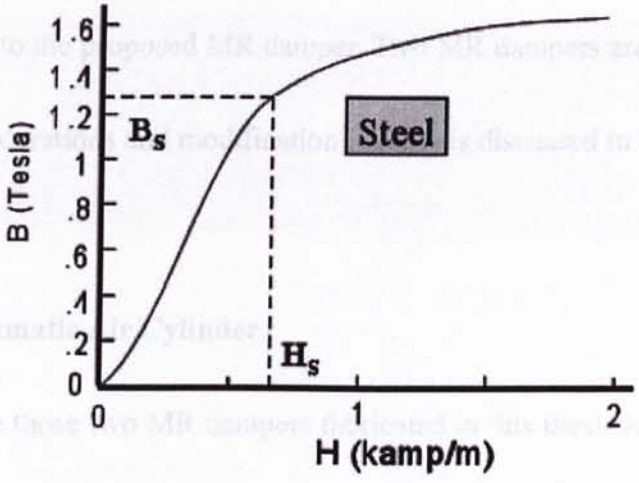

Figure 3.20: Typical magnetic properties of low carbon steel [41].

CHAPTER 4

DEVELOPMENT AND FABRICATION OF MR DAMPERS

In this chapter, the fabrication process for the double-ended MR dampers developed in this thesis is described. A commercially available pneumatic air cylinder that has similar structure to the double-ended MR damper design is modified to the proposed MR damper. Two MR dampers are fabricated in this thesis. The considerations and modification process is discussed in this chapter.

4.1 Pneumatic Air Cylinder

Since those two MR dampers fabricated in this thesis have similar structure and fabrication process, so the discussion will be focused on the second MR damper. The basic components of the air cylinder are discussed as follows:

- *The pneumatic air cylinder*

Fig. 4.1 shows a typical pneumatic air cylinder with similar structure of the proposed double-ended MR damper considered in this thesis. It will be used to be modified to the proposed MR damper. The AirTac© SCD 100×200 will be used for MR damper I and SMC© CA1WBF80-200 will be used for MR damper II.

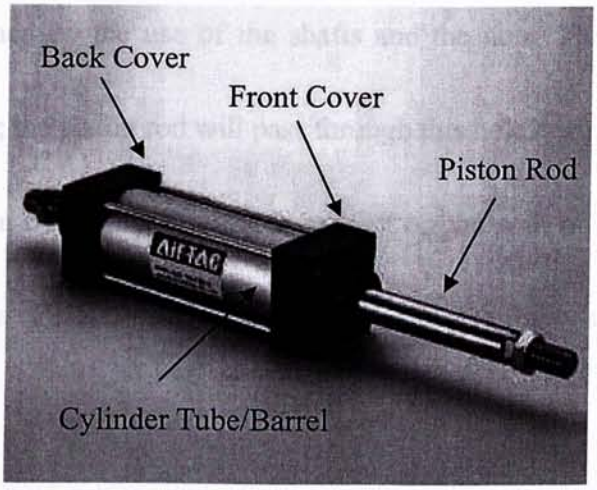

Figure 4.1: AirTac double rod type standard cylinder pneumatic air cylinder (SCD 100×200).

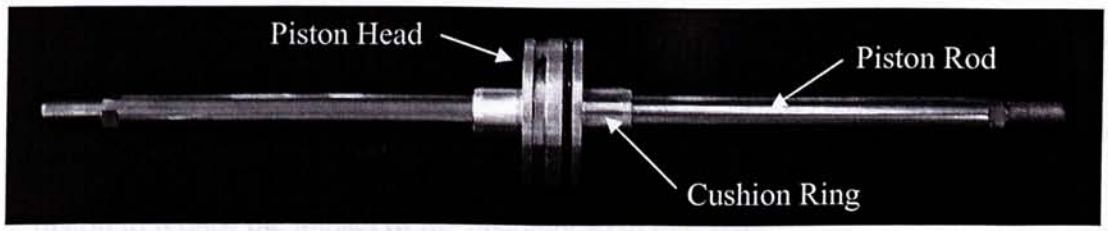

Figure 4.2: The piston.

➢ *Piston*

The piston head and the cushion rings are made of aluminum alloy and the piston rod is made of hi-carbon steel with chrome plated. The piston diameter is 100 mm and 80 mm for damper I and damper II respectively. Since the rod is chrome plated so it can reduce the friction with the internal part and allow a smooth contact with the sealing to improve sealing performance as shown in Fig. 4.2.

➢ *Front and back cover*

Front cover (shown in Fig. 4.3) is used with the back cover to clamp the tube

body that is fastened by the use of the shafts and the nuts. There is a hole at the center of the cover; the piston rod will pass through this hole during the linear motion of the piston driven by the air. Sealing is present on the wall of the internal tunnel. The sealing is made of NBR (Nitrile) that has good compatibility with all kind of MR fluids [40].

There is an air-valve at the top; a nut can be screwed at the air valve, so that MR fluid can be filled at this valve. The function of the cushion needle is to adjust the area of the tunnel that is used to provide the exit for the fluid to flow back to the tube body when the piston is approaching the end cap; this provides a cushion to the piston to reduce the impact of the piston head to the cover.

- *The cylinder body*

The cylinder-body/barrel as shown in Fig. 4.4 is made of aluminum. The stroke length for both prototype dampers is 200 mm, and the inner diameter is 100 mm and the outer diameter is 80 mm for damper I and damper II respectively.

- *The shaft and the tap*

The shaft and the nuts (shown in Fig. 4.5) are used to joint and fasten the whole cylinder by screwing at the front and rear clevis and then the tube body is clamped

between those two cover.

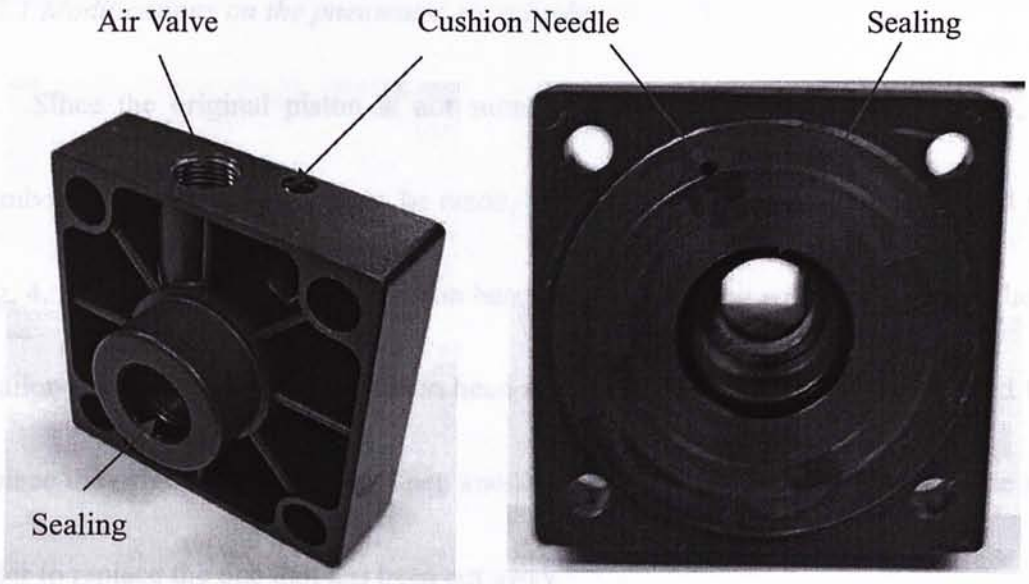

Figure 4.3: The front/back cover.

Figure 4.4: The cylinder-body/barrel.

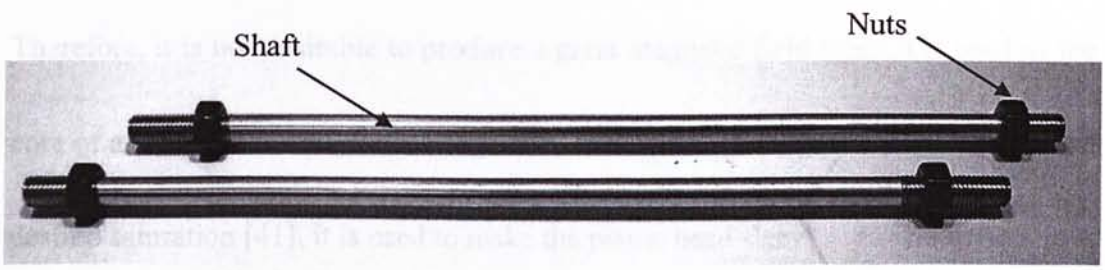

Figure 4.5: The shafts and the nuts.

4.2 Fabrication Process of Double-Ended MR Dampers

4.2.1 Modifications on the pneumatic air cylinder

Since the original piston is not suitable for the MR fluid damper design, a number of modifications have to be made. The modification process is illustrated in Fig. 4.6. First of all, the original piston head and cushion ring will be cut away. Then a tailor-made low-carbon steel piston head sleeve with three slots will be inserted to replace the original piston head. Then another new cushion rings have to be made in order to replace the one that has been cut away.

Since the magnetic coil wrapped on the piston head is the same case as the solenoid with a metal core, the magnetic field produced is governed by the equation:

$$B = k\mu_0 nI \quad \text{where} \quad \mu = k\mu_0 \tag{4.1}$$

where μ_0 is the permeability of the free space, and k is the relative permeability of the core material, n is the number of turns of coil per unit length and I is the applied current.

Because aluminum is not ferromagnetic, it has a relative low permeability. Therefore, it is not desirable to produce a great magnetic field when it is used as the core of a solenoid coil. As low carbon steel having a high magnetic permeability and desired saturation [41], it is used to make the piston head sleeve.

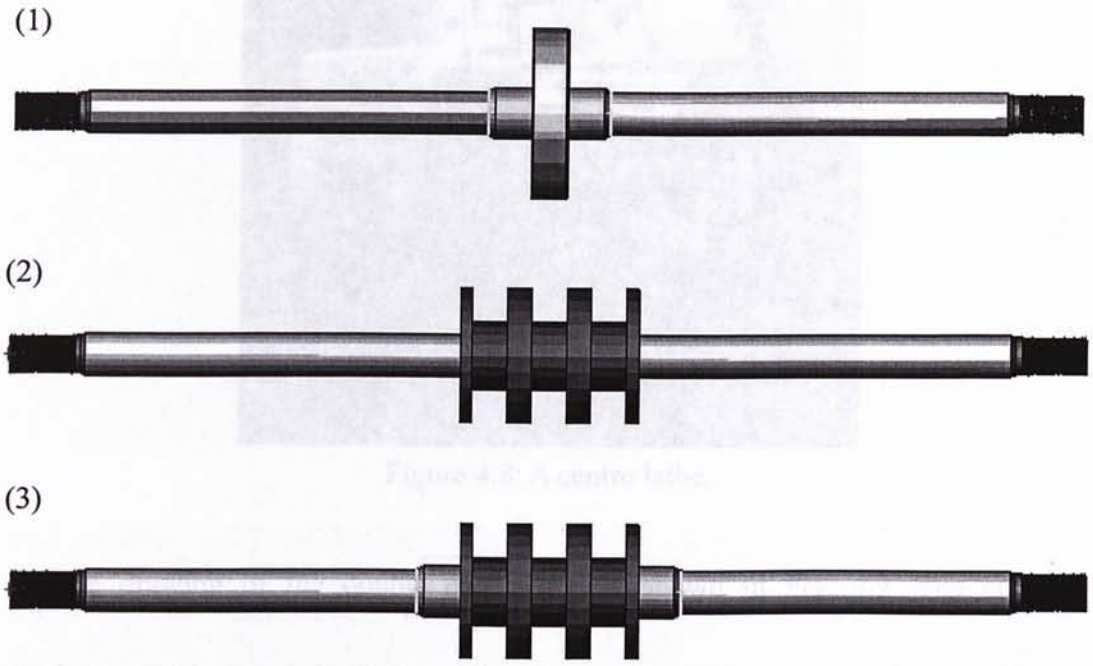

Figure 4.6: (1) The modified piston rod (2) The low-carbon steel piston head sleeve is assembled (3) The new cushion rings is assembled.

4.2.2 Manufacturing processes of the piston sleeve

The manufacturing processes are done in the Industrial Training Center (Machining & Metrology Unit) in the Hong Kong Polytechnic University. The original low carbon steel rod is shown in Fig. 4.7 and its diameter is about 105 mm. All the cutting process of the piston head is done on a center lathe, which is shown in Fig. 4.8.

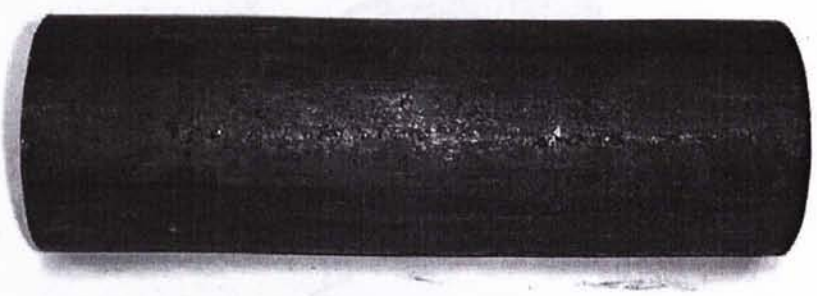

Figure 4.7: Low carbon steel rod.

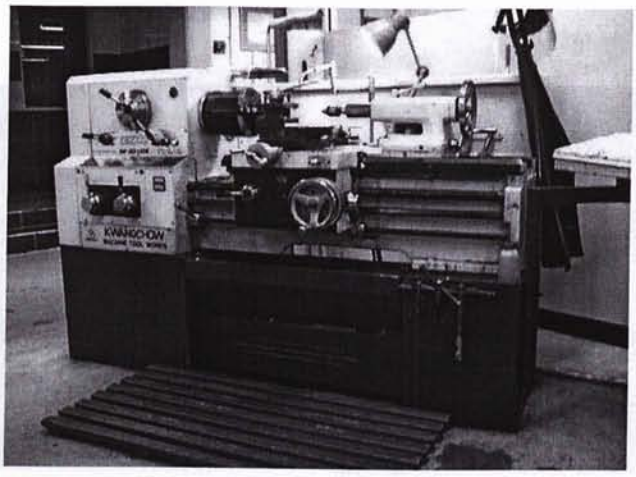

Figure 4.8: A centre lathe.

The drawing of the double end piston is shown in Fig. 4.9. The cutting technique used is set up for facing and under-cutting. The process is shown in Figs. 4.10 (a), 4.10 (b) and 4.10 (c). Fig. 4.10 (a) shows the setup of the low-carbon steel rod being clamped in the centre lathe. Fig. 4.10 (b) shows the piston sleeve finished undercut and three slots that are being cut. Fig. 4.10 (c) shows the drilling process of the center hole and Fig. 4.10 (d) shows the fine boring process of the center hole using boring cutting tool.

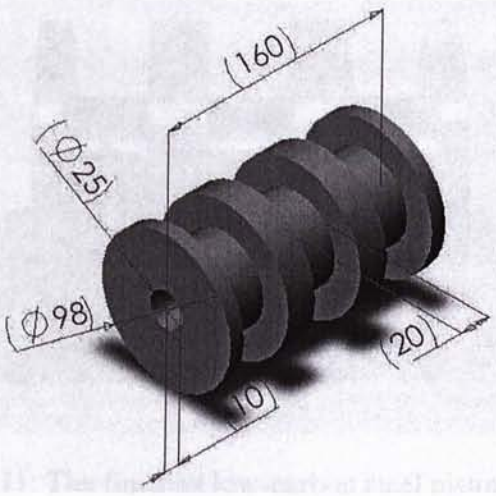

Figure 4.9: Drawing of the double-ended piston head sleeve.

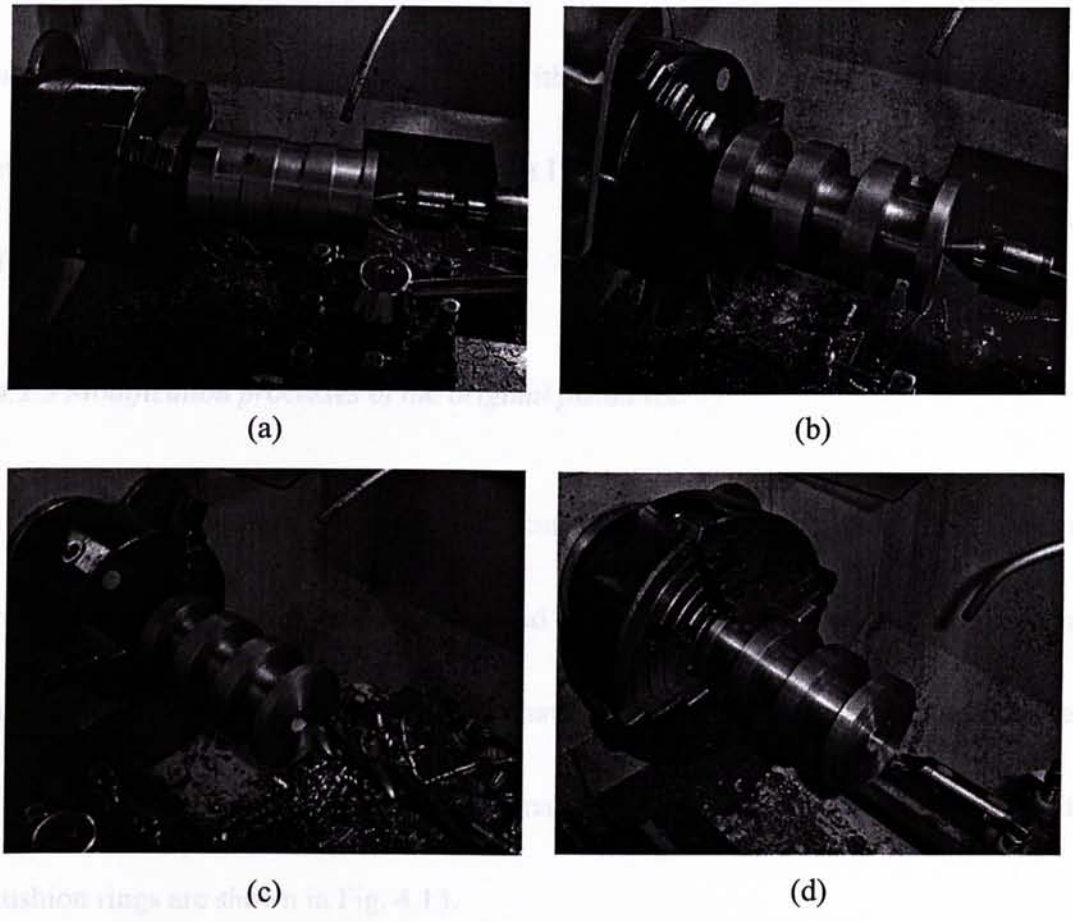

Figure 4.10: (a) The piston sleeve is about to cut (b) The three slots have been cut (c) The hole at the center is being drilled (d) Another boring tool is used to bore the hole with precise dimension.

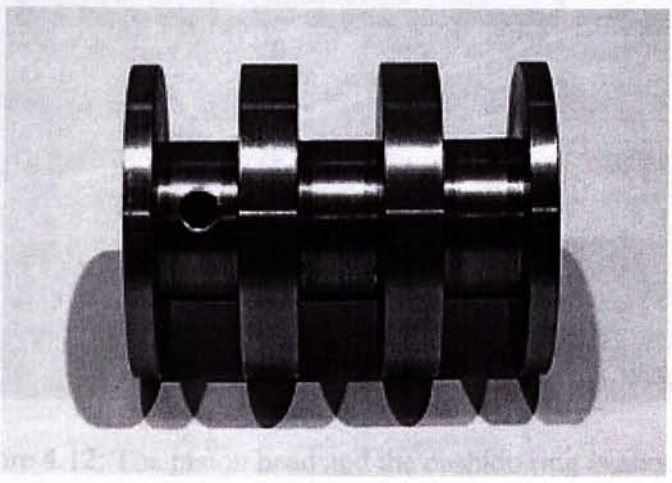

Figure 4.11: The finished low-carbon steel piston sleeve.

The center part of the piston sleeve is undercut to three slots in order to provide space for wrapping wires. Copper wire with AWG 19 gage will be used to wrap the magnetic coil later on. The finished piston I having copper wire wrapped is shown in Fig. 4.11.

4.2.3 Modification processes of the original piston rod

After the piston head sleeve is fabricated, the original piston head and cushion ring have to be cut away as aforementioned . Fig. 4.12 shows the whole piston that is about to cut. Besides, new cushion rings have to be made in order to replace the one cut away. The new cushion rings are made of aluminum and the manufactured cushion rings are shown in Fig. 4.13.

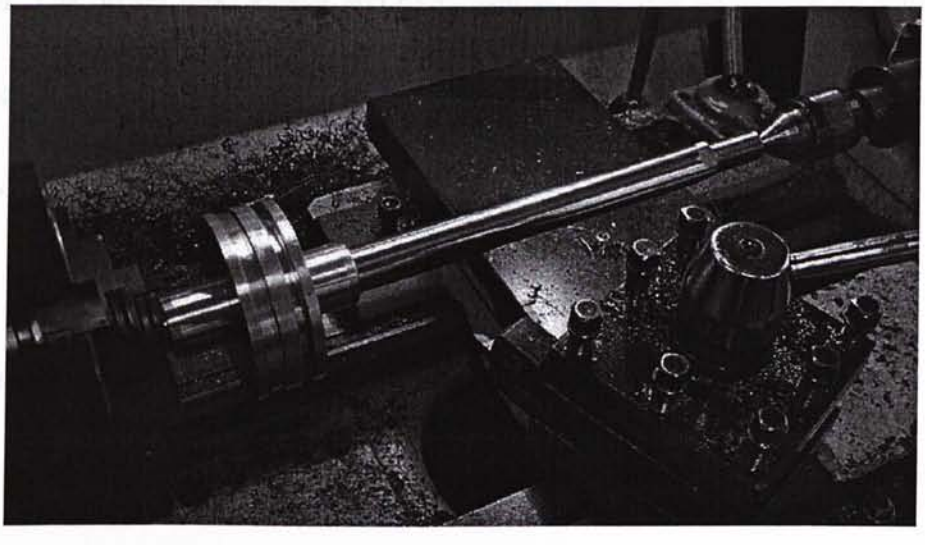

Figure 4.12: The piston head and the cushion ring is about to cut.

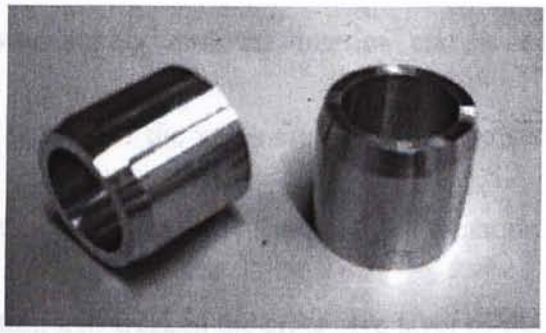

Figure 4.13: The new cushion rings.

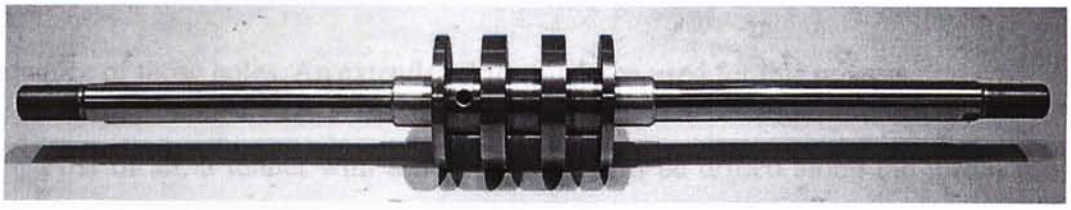

Figure 4.14: The assembled piston rod.

The whole double-ended damper can now be assembled since all parts are obtained. The piston head sleeve and two cushion rings can be assembled with the modified piston rod as mentioned in Fig. 4.6. The assembled piston rod is shown in Fig. 4.14.

4.2.4 Modification of the piston staging area

In order to form the magnetic circuit as required for MR damper, electromagnetic coils are wound around the staging area of of the piston. The electrical wires will be inserted along the hole of the piston rod, the exterior ends are

connected to the power supply and the interior end is connected with the electromagnet that has wound. If the wires are led along the surfaces of the piston rod, the wires will be exposed to the MR fluid and the dynamic motion of the MR fluid and the piston motion will weaken the protective layer of the copper wire which causes short circuited. Therefore, a number of tunnels are drilled along the piston and the piston head in order to insert electrical wires. Fig. 4.15 illustrates the drilling sequence of those holes. An extended drill should be used for this process.

First of all, a tunnel with 8 mm diameter will be drilled along the piston rod until it meets the piston stage area. Since the length of the hole to be drilled is so long and have to align the center, it cannot be done by a normal drilling machine, so it is done at the center lathe again. A shorter length of hole should be drilled first before the extended drill is applied. After this, the extended length drill can be applied and drill the hole up to 250 mm deep. Then, a pilot hole at the end of the center tunnel will be drilled for inserting electrical wires to form the magnetic circuit.

The pilot hole will be sealed by a custom made seal plug to prevent the leakage of the MR fluid during the operation of the MR damper. This seal plug is made by Douglas Engineering, Roskaway, New Jersey, and it can withstand pressure at 200 psi and it has two hermetic sealed #18AWG wires for electrical connection. Fig. 4.16 shows the close up of the modified staging area of the MR damper piston for

inserting the seal plug, and Fig 4.17 shows the dimension of the pilot hole and schematic of the seal plug.

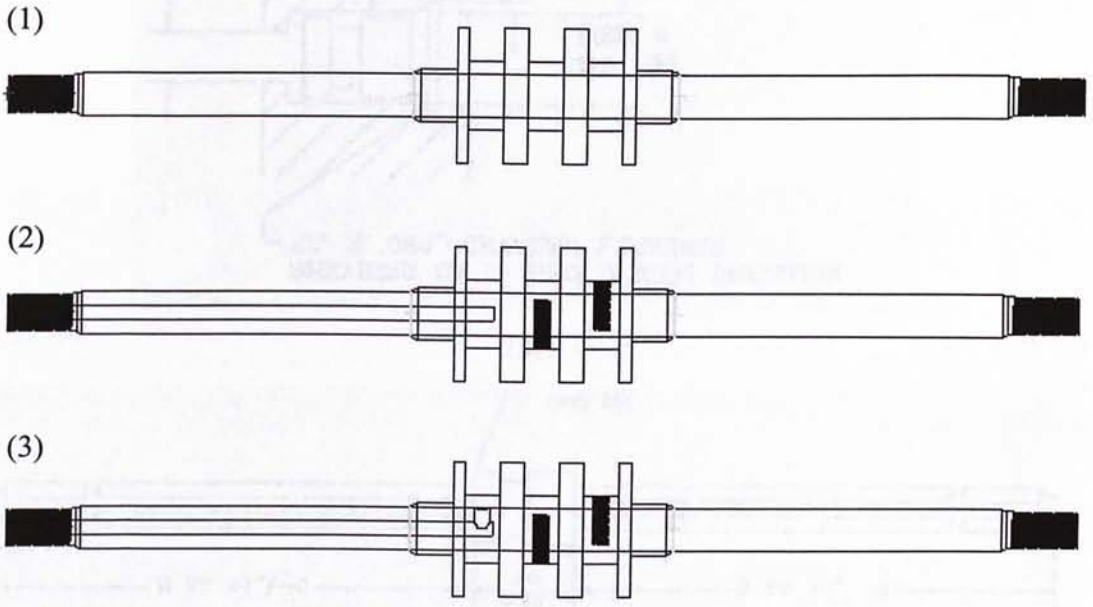

Figure 4.15: (1) No drilling is made (2) Drill a deep hole at the center of the piston (3) Drill a hole at the end of the center deep hole.

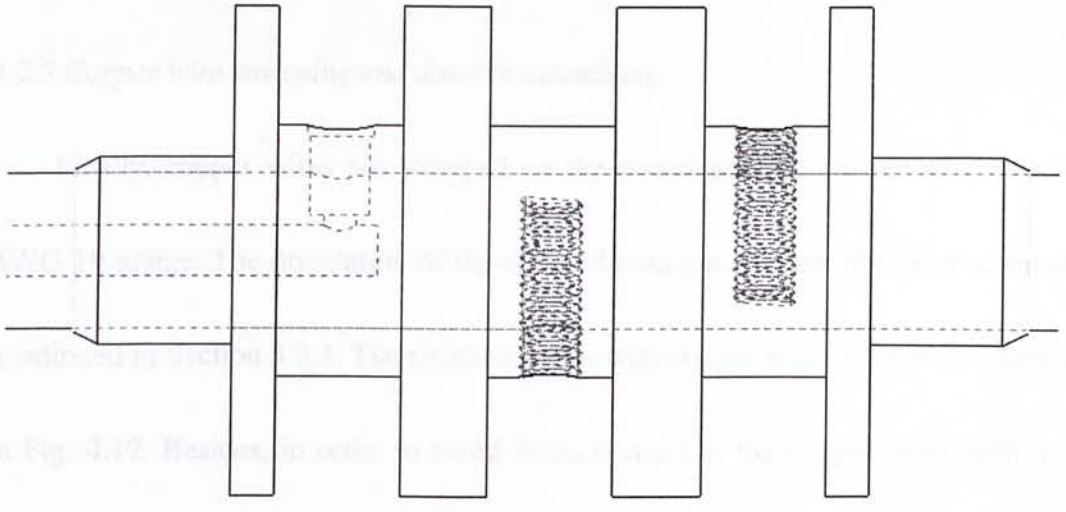

Figure 4.16: Staging area of the modified MR damper piston.

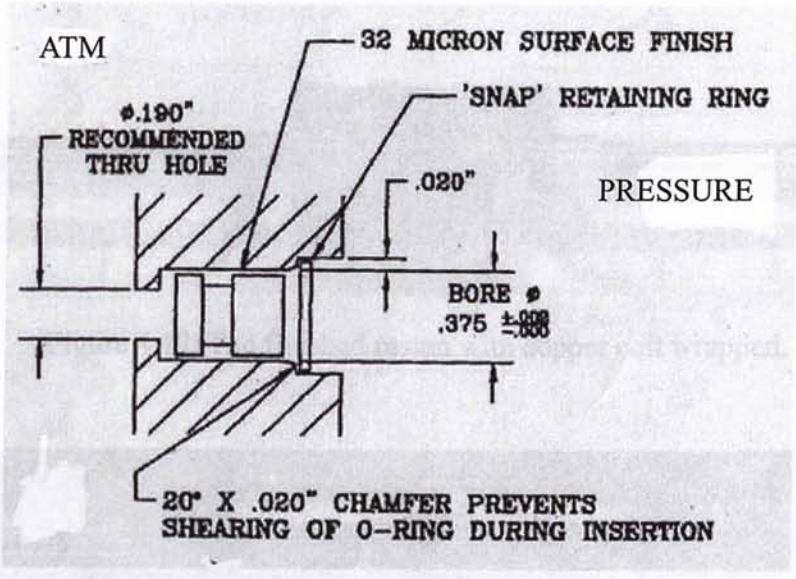

(a)

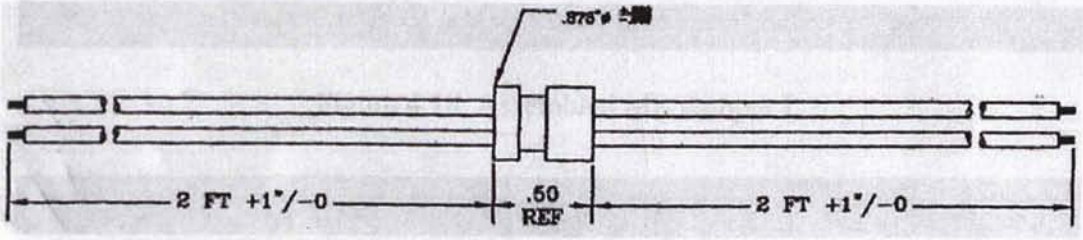

(b)

Figure 4.17: (a) Schematic of the dimenions required for the pilot hole
(b) Schematic of the seal plug [Courtesy of Douglas Engineering].

4.2.5 Copper wire wrapping and damper assembling

Finally, copper wires are wrapped on the piston and the copper wire size is AWG 19 gauge. The orientation of the coil and configuration are the same as those mentioned in Section 3.3.3. The finished piston with copper wires wrapped is shown in Fig. 4.17. Besides, in order to avoid direct contact of the copper wires with the MR fluid, those copper wires in the staging are coated by mutiple layers of epoxy-resin paste.

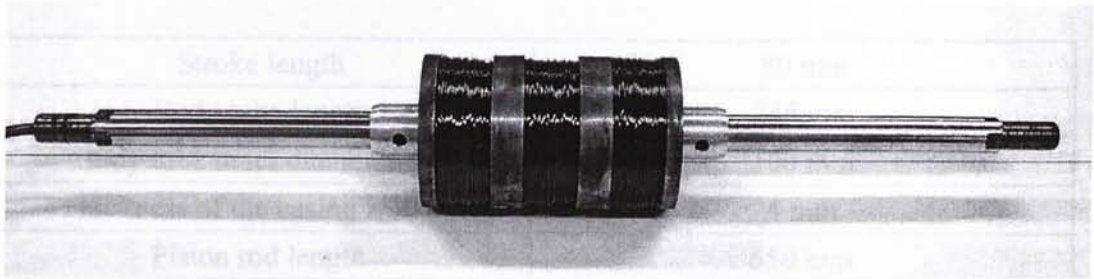

Figure 4.17: The finished piston with copper coil wrapped.

Figure 4.18: Assembled MR damper I.

Figure 4.19: Assembled MR damper II.

Then the whole MR damper can be assembled and MR fluids can be poured from one of the valve openings. MR fluid model MRF-132 AD [42] is used for this damper because it is suitable for damper applications. The dimensions of MR damper I and II are listed in Table 2 and Table 3 respectively. The physical definitions of dimensions can be referred to Fig. 3.12.

TABLE 2: PHYSICAL DIMENSION OF MR DAMPER I.

Stroke length	80 mm
Body tube length	246 mm
Body tube inner diameter, D_b	100 mm
Thickness of the casing wall, t_w	4 mm
Piston rod length	650 mm
Piston rod diameter, D_r	25 mm
Piston diameter (core diameter), D_c	60 mm
Piston pole length, Lp	60 mm
Thickness of gap, t_g	1 mm

TABLE 3: PHYSICAL DIMENSION OF MR DAMPER II.

Stroke length	100 mm
Body tube length	218 mm
Body tube inner diameter, D_b	80 mm
Thickness of the casing wall, t_w	4 mm
Piston rod length	616 mm
Piston rod diameter, D_r	25 mm
Piston diameter (core diameter), D_c	40 mm
Piston pole length, Lp	42 mm
Thickness of gap, t_g	0.8 mm

CHAPTER 5

EXPERIMENTAL SETUP AND RESULTS

The double-ended MR damper is tested under various conditions in order to find out its behaviors. The force-displacement and force-velocity results are investigated. The MR damper I has encountered the force-lag problem that deteriorate the damper performance. After gaining the experience and analyzing experimental data from the testing results for the MR damper I; a special MR fluid filling setup is used to increase the internal pressure for the MR damper II to solve the force-lag problem. Therefore, the force-lag phenomenon, the MR fluid filling setup and the effect of the internal pressure on the MR damper is discussed in this chapter. At last, the experimental results of the MR damper are presented.

5.1 Experimental Setup for the Double-Ended MR Damper

5.1.1 Instron 8801 loading machine

The double-ended MR damper will be tested on the Instron's FastTrack™ 8801 servohydraulic testing system, which is used for higher capacity fatigue and static testing of biomedical, advanced materials and manufactured components. The

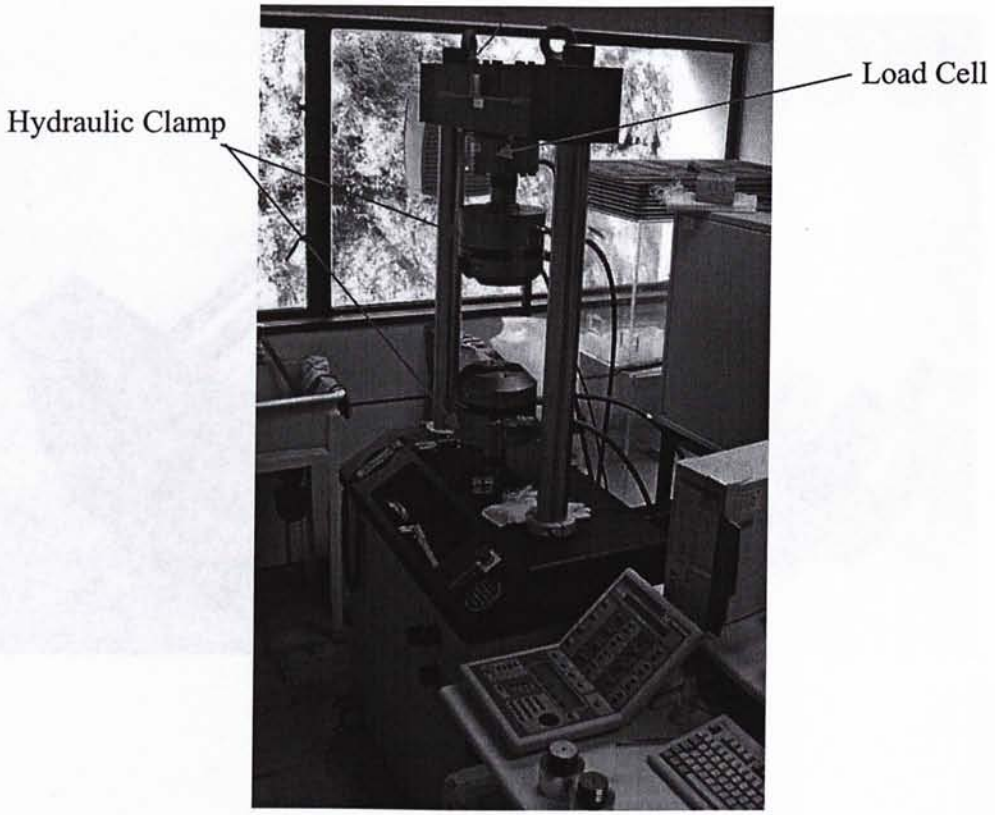

Figure 5.1: Instron 8801 loading machine.

Instron 8801 loading machine is combined with the FastTrack™ 8800 digital controller and Instron's patented Dynacell™. Figure 5.1 shows the Instron 8801 loading machine, which is located in the Physics Department of the Chinese University of Hong Kong.

5.1.2 Experimental setup for testing the MR damper

As shown in figure 5.1, there are two hydraulic clamps, which are provided to hold the test sample. Therefore, a special mount is needed in order to mount the MR damper on the loading machine. The mountings are shown in Fig. 5.2.

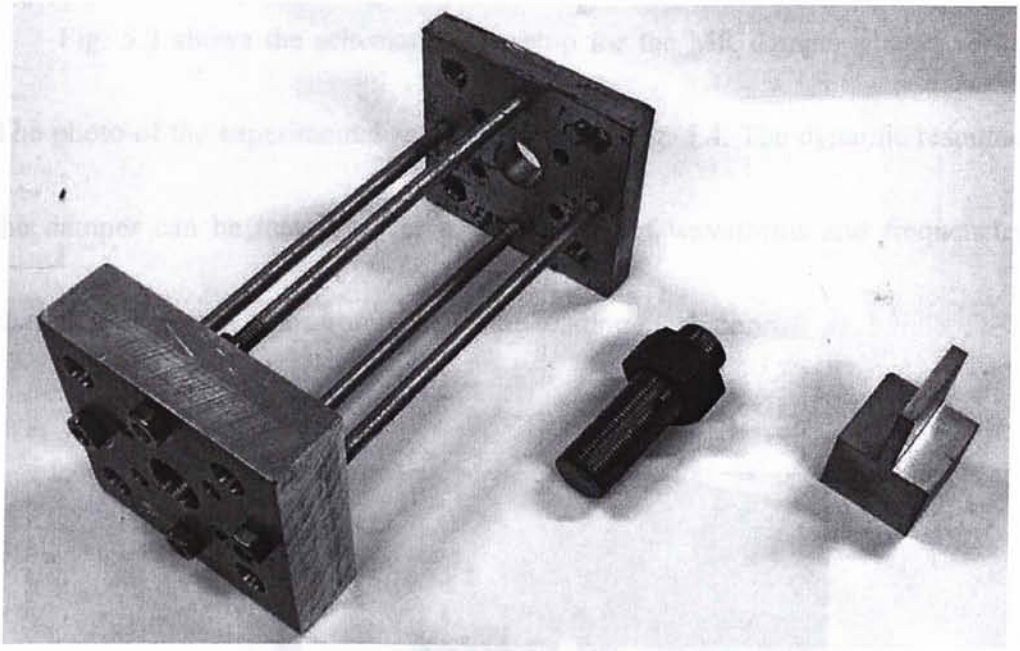

Figure 5.2: The mountings.

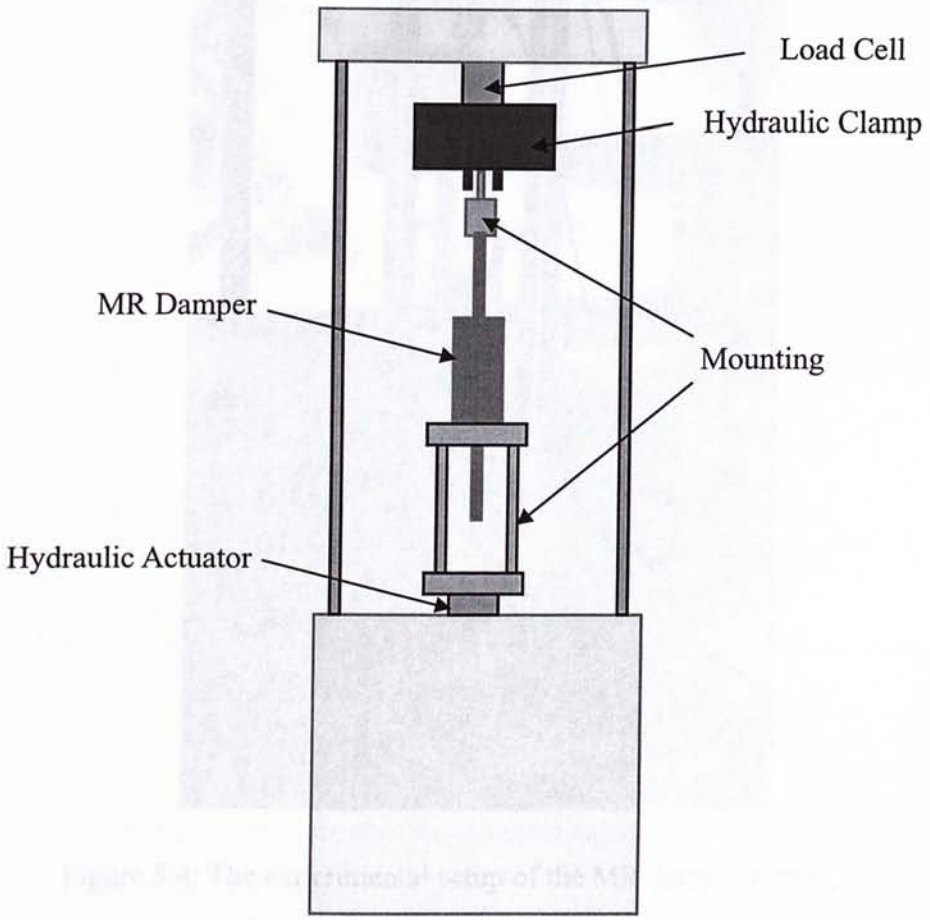

Figure 5.3: Schematic diagram of the MR damper experimental setup.

Fig. 5.3 shows the schematic test setup for the MR damper placed vertically. The photo of the experimental setup is shown in Fig. 5.4. The dynamic responses of the damper can be measured for a wide range of waveforms and frequencies by changing the signal to the controller of the loading machine.

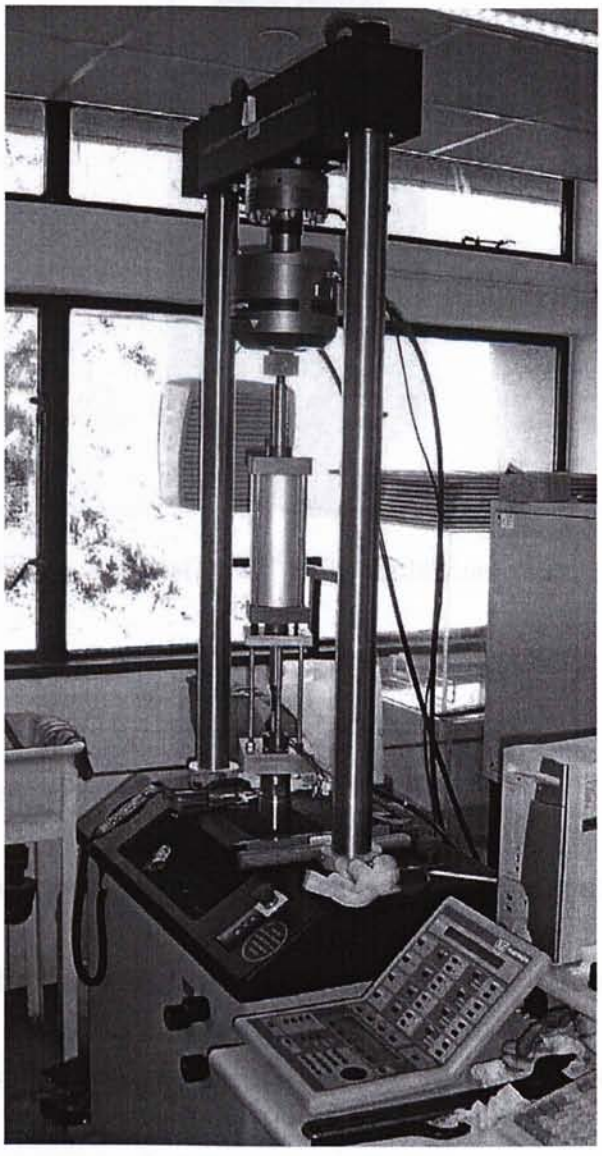

Figure 5.4: The experimental setup of the MR damper testing.

The output signals from the load cell (force) and the displacement will be sent to the FastTrack™ 8800 digital controller, which is shown in Fig. 5.5 to record the data. The time domain data are obtained and the results can be plotted in the PC.

Figure 5.5: FastTack™ 8800 digital controller.

5.2 Force-Lag Phenomenon of MR Damper

5.2.1 Force-lag phenomenon

The MR damper will be tested by applying fixed magnitude of sinusoidal excitations with different input currents applied. The testing results will be analyzed and will be used as the parameter identification for the mathematical model later on. The variable input current method will be used to test the MR damper. Four different constant currents, 0 A, 0.5 A, 1 A, 1.5 A, are applied to test the MR damper I.

The MR damper force-time and force-displacement behaviors under a 20 mm, 0.5 Hz triangular displacement excitation at various input current levels are shown in Figs. 5.6 and 5.7 respectively. It can be observed from Figs 5.6 and 5.7 that the effects of changing the applied current on the damping force are obvious. When no current is applied, the MR damper acts as a viscous damper and the damping force of the MR damper is about 3 KN. When 1.5 A current is applied, the force required to yield the MR fluid increases and the damping force of the MR damper is about 22 KN. When input current is applied to the MR damper, the MR fluids are magnetized to cause the yield force of the MR fluids increase. Thus, the magnitude of the plastic-viscosity region increases, which can be observed from Fig. 5.6. The dynamic range for this MR damper is about 7 and the damping force range is between 3 KN to 22 KN.

However, as shown in Figs. 5.6 and 5.7, there exists force lag (compliance) in the MR damper response, which is caused by the trapped air in the MR damper and the vacuum/cavitations due to the high viscosity of the MR fluid. In order to solve the force lag problem, a special MR fluid filling setup will be used and the MR damper will be pressurized as well. Besides, after gaining the experimental data for MR damper I, MR damper II with more concise dimension that is suitable for railway application is fabricated.

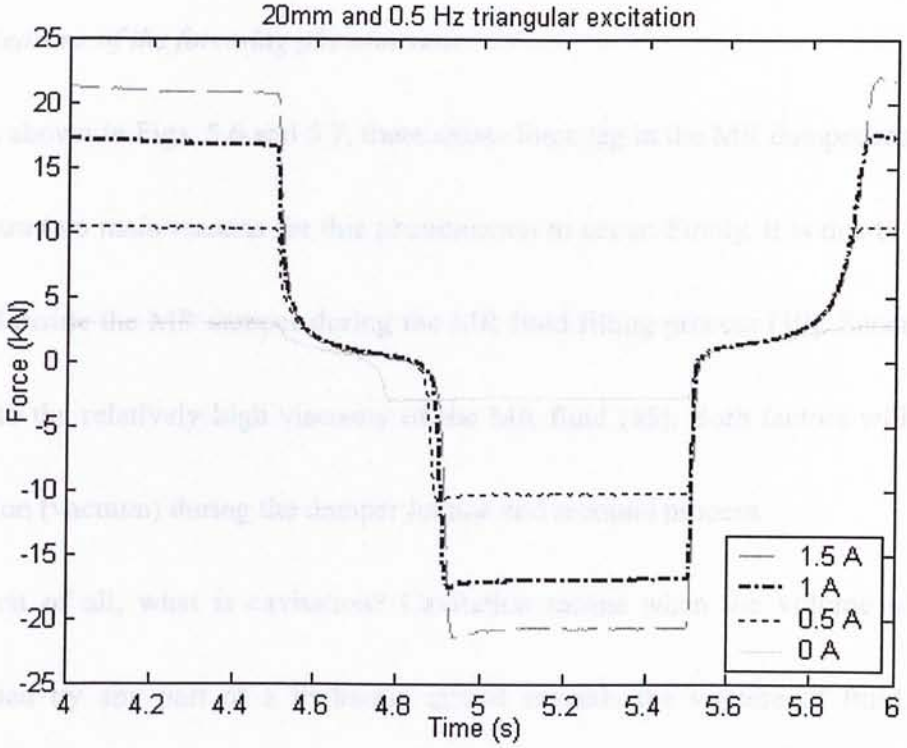

Figure 5.6: Force versus time graph under 0.5 Hz and 20 mm amplitude excitation.

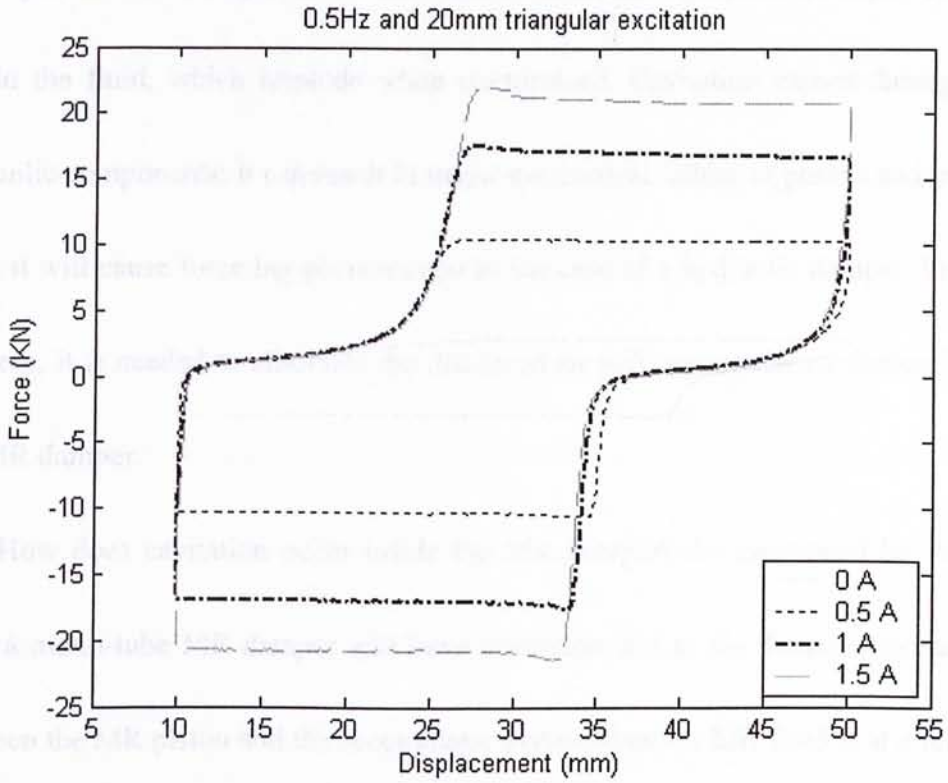

Figure 5.7: Force versus displacement diagram under 0.5 Hz and 20 mm amplitude excitation.

5.2.2 Reasons of the force-lag phenomenon

As shown in Figs. 5.6 and 5.7, there exists force lag in the MR damper response. There are two main reasons for this phenomenon to occur. Firstly, it is due to the air trapped inside the MR damper during the MR fluid filling process [19]. Secondly, it is due to the relatively high viscosity of the MR fluid [35]. Both factors will cause cavitation (vacuum) during the damper jounce and rebound process.

First of all, what is cavitation? Cavitation means when the volume of fluid demanded by any part of a hydraulic circuit exceeds the volume of fluid being supplied. This causes the absolute pressure in that part of the circuit to fall below the vapor pressure of the hydraulic fluid. This result in the formation of vapor bubbles within the fluid, which implode when compressed. Cavitation causes damages to hydraulic components; it can result in major mechanical failure of pumps and motors. Then it will cause force lag phenomenon in the case of a hydraulic damper. In view of these, it is needed to eliminate the dissolved air and prevent the cavitation inside the MR damper.

How does cavitation occur inside the MR damper? As mentioned by Poynor [35], a mono-tube MR damper will have cavitation due to the dynamic interaction between the MR piston and the accumulator piston when the MR fluid is at a relative high viscosity. They can be explained by Figs. 5.8 and 5.9.

In Fig. 5.8, it shows a mono tube MR damper functioning properly. During the jounce and rebound cycle, the piston moves up and down and then the MR fluid flows through the MR valve smoothly. At the same time, the accumulator piston will move accordingly to compensate the volume change of the damper rod volume as it moves in and out in the fluid chamber. In this case, during both the compression and expansion, fluid chamber is filled with MR fluid and no cavitation occurs.

In Fig. 5.9, it shows a mono tube MR damper that functions improperly when cavitation occurs. During the on-state of MR fluid damper, the high current supplied to the electromagnetic circuit will magnetize the MR fluid to high viscosity to the point that it acts like a seal between two fluid chambers that are divided by the MR piston. Thus, the MR fluid cannot pass from the compression chamber to the expansion chamber during the jounce and rebound cycle. In the jounce case, the fluid in the lower chamber (compression chamber) pushes against the accumulator piston and moves it down by the same volume as the piston rod displaced. However, the increased pressure of the compressed accumulator is not sufficient enough to yield the fluid plug created at the MR valve. Therefore, MR fluid plug acts like an O-ring seal and slides down with the piston along the tube body, not allowing any fluid to pass through the MR valve. This situation causes cavitation to occur in the upper fluid chamber (expansion chamber) and significantly reduces the damping force with

force lag. In the rebound case, the situation is vice versa.

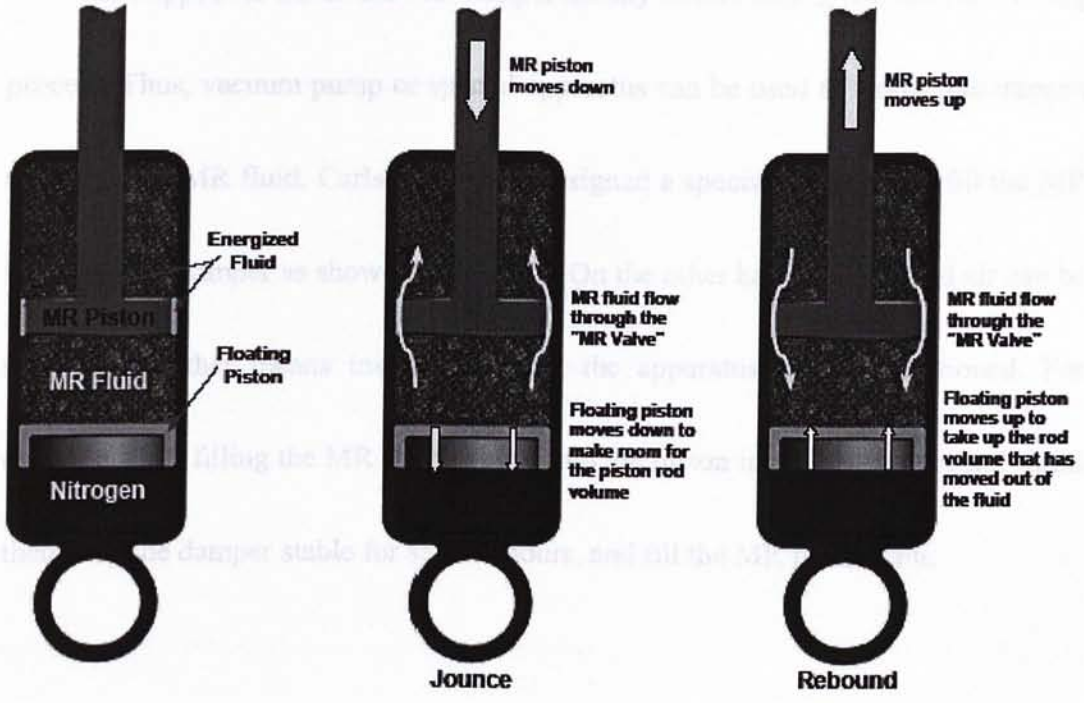

Figure 5.8: Mono-tube MR damper functioning properly [35].

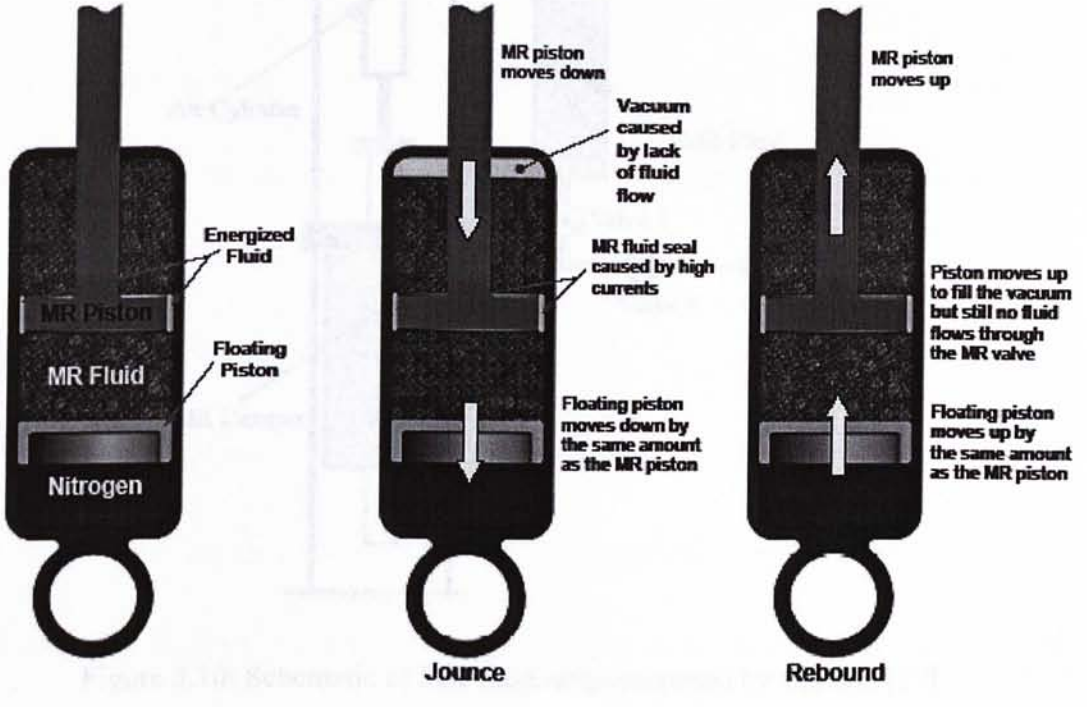

Figure 5.9: Mono-tube MR damper cavitation due to lack of fluid transfer [35].

5.2.3 Methods to eliminate the force-lag phenomenon

The trapped air inside the MR damper mainly occurs during the MR fluid filling process. Thus, vacuum pump or special apparatus can be used to reduce the trapped air inside the MR fluid. Carlson [19] has designed a special apparatus to fill the MR fluid into the damper as shown in Fig. 5.10. On the other hand, the trapped air can be reduced by other means instead of using the apparatus as aforementioned. For example, after filling the MR fluid, we can run the piston in and out for several times, then keep the damper stable for several hours, and fill the MR fluid again.

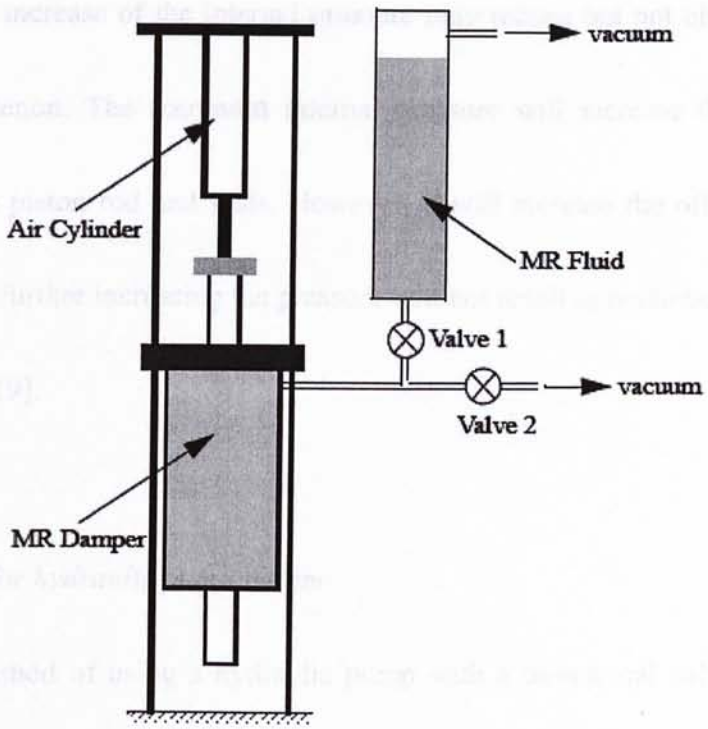

Figure 5.10: Schematic of MR fluid setup proposed by Carlson [19].

Due to the relatively high viscosity of the MR fluid, eliminating air pockets in the damper and air dissolved in the fluid is very difficult, even though special care is taken to do so. Therefore, the ultimate solution is to increase the internal pressure of the fluid chamber so that it can reduce the effect of the trapped air and to overcome the seal plug problem due to high fluid viscosity.

For the double-ended MR damper in this thesis, the internal pressure of the fluid chamber can be increased by using external accumulator or using hydraulic pump with hydraulic valve. It should be noted that increasing the internal pressure can only compensate for a limited volume of air trapped in the damper. If there is too much air present, the increase of the internal pressure may reduce but not eliminate the force lag phenomenon. The increased internal pressure will increase the friction force between the piston rod and seals. However, it will increase the off-state force very slightly and further increasing the pressure will not result in continued increase of off state force [19].

5.2.4 Setup for hydraulic pump system

The method of using a hydraulic pump with a directional valve is adopted to increase the internal pressure of the MR damper. The setup is shown in Fig. 5.11. This setup includes the ENERPAC® P-142 hand pump, two pressure gauges,

FASTER® ANV 14 GAS quick-release coupler (as shown in Fig. 5.12), etc.

The MR fluid will be pumped to the MR damper by using the ENERPAC® hand pump. Pressure gauge 1 is used to monitor the outlet pressure of the hand pump and the pressure gauge 2 is used to monitor the internal pressure of the MR damper. The quick couplers are used in a hydraulic system to quickly connect lines without losing fluid or fluid pressure. All couplings consist of two mating halves: the plug (male) half and the coupler (female) half. The female coupler itself acts as a directional valve, which can withstand working pressure as high as 5000 psi. The quick coupler at fluid port one is used to connect the hand pump and then the quick coupler at fluid port two is used connect the pressure gauge 2. Both connections can be unplugged during the experiment.

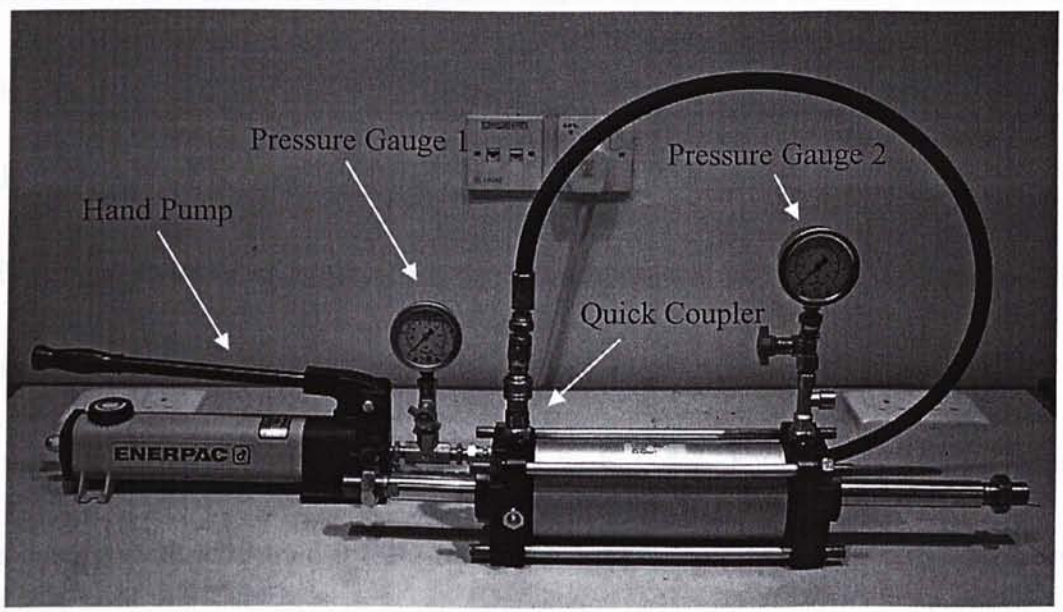

Fig. 5.11: The hydraulic pump set up.

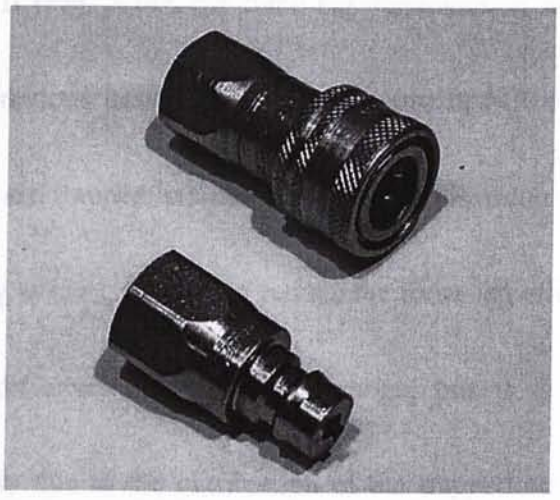

Fig 5.12: Faster® ANV 14 GAS quick-release coupler.

5.2.5 Results and effects of the pressurized MR damper

Figs. 5.13 - 5.16 show the testing results of the MR damper with different internal pressures. Fig. 5.13 shows the results of the test under a 20 mm, 0.1 Hz triangular displacement excitation, operation current at 1.5 A with different internal pressures (0, 25, 50, 75 and 100 psi). It can be seen that the force-lag phenomenon can be reduced when the internal pressure is increased. When the internal pressure of the MR damper is raised to 100 psi, the force-lag phenomenon is nearly eliminated. Therefore, the internal pressure for the MR damper will be raised to 100 psi for the remaining tests in this thesis.

Comparing the results in Fig. 5.14 to Fig. 5.7, both are under the same excitation with a 20 mm, 0.1 Hz triangular displacement with no internal pressure added. It is worth noting that after using the hydraulic pump system to fill in the MR

fluid in MR damper II (Fig. 5.14), the force-lag phenomenon is reduced obviously compared with the previous case without special care in MR damper I (Fig. 5.7). This is because the air trapped inside the MR fluid is minimized by using the hydraulic pump filling system, which can reduce the force-lag effect. Although those two dampers have different size and force range, but it is believed that the improvement is mainly due to the elimination of the trapped air. As shown in Fig. 5.14, even the trapped air is minimized; the force-lag phenomenon cannot be avoided due to seal plug effect when the input current is increased.

Thus, the internal pressure of the MR damper is increased accordingly until the force-lag phenomenon is minimized. As shown in Figs. 5.15 – 5.16, the force-lag phenomenon has been reduced gradually when the internal pressure is increased. It is worth noting that in Fig. 5.15, even the internal pressure is increased; the force-lag phenomenon can be eliminated in the lower input current case ($\leq$ 1A) but not for the higher input current case (2A). It proves the existence of seal plug phenomenon that when the input current increases, the viscosity of the MR fluid increases, then a higher internal pressure is needed to overcome the seal plug effect. At last, it is shown in Fig. 5.16 that the force-lag phenomenon is almost eliminated when the MR damper is operated with internal pressure of 100 psi.

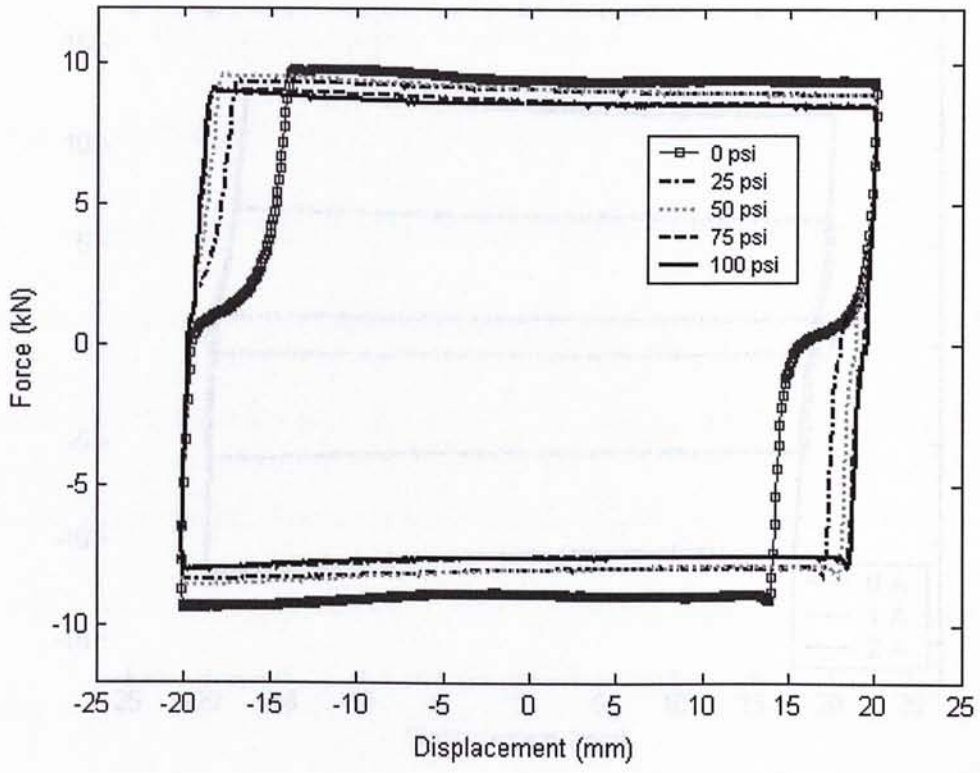

Figure 5.13: Internal pressure effects test under a 20 mm, 0.1 Hz triangular displacement excitation with operation current at 1.5 A.

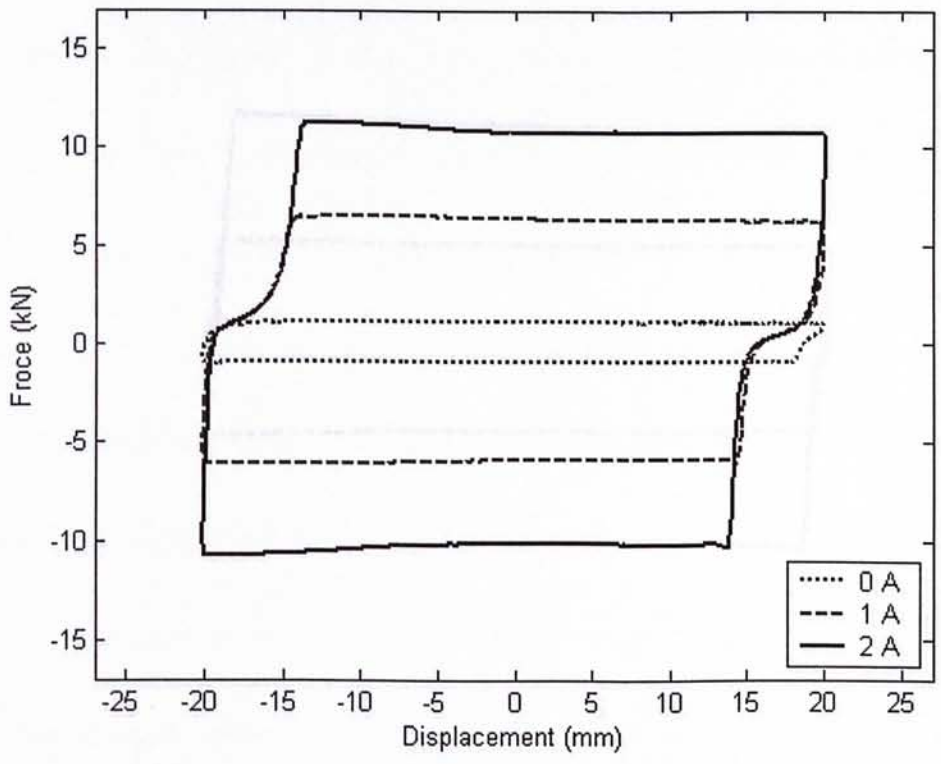

Figure 5.14: Operation current effects test under a 20 mm, 0.1 Hz triangular displacement excitation with operation pressure at 0 psi.

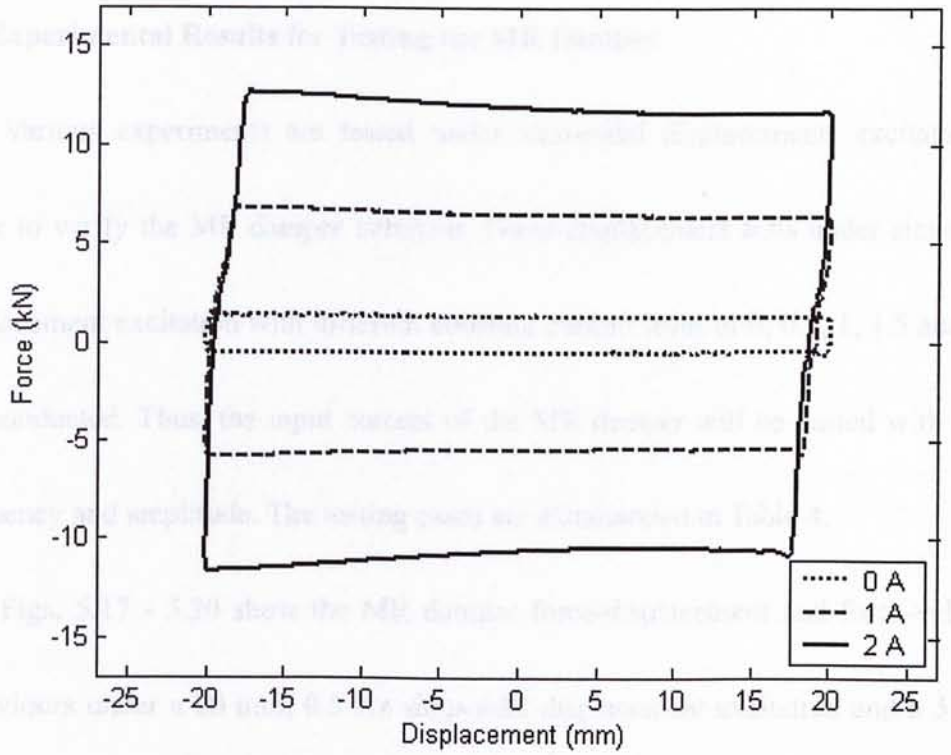

Figure 5.15: Operation current effects test under a 20 mm, 0.1 Hz triangular displacement excitation with operation pressure at 50 psi.

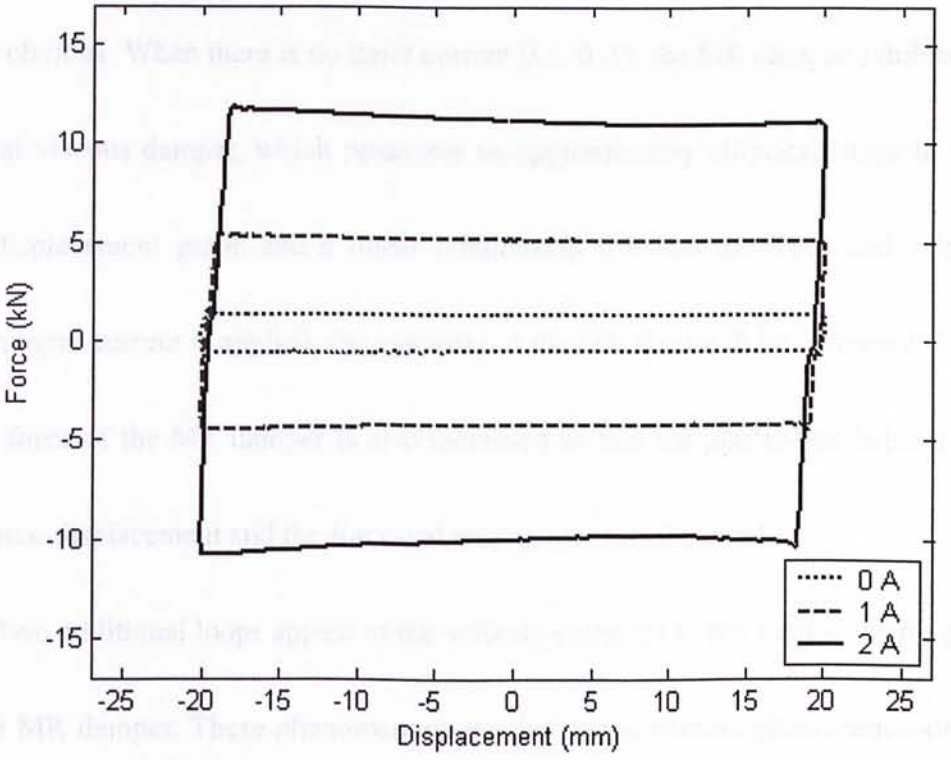

Figure 5.16: Operation current effects test under a 20 mm, 0.1 Hz triangular displacement excitation with operation pressure at 100 psi.

5.3 Experimental Results for Testing the MR Damper

Various experiments are tested under sinusoidal displacements excitation in order to verify the MR damper behavior. Force-displacement tests under sinusoidal displacement excitation with different constant current level of 0, 0.5, 1, 1.5 and 2 A are conducted. Thus, the input current of the MR damper will be varied with fixed frequency and amplitude. The testing cases are summarized in Table 4.

Figs. 5.17 - 5.20 show the MR damper force-displacement and force-velocity behaviours under a 20 mm, 0.5 Hz sinusoidal displacement excitation and a 5 mm, 3.5 Hz sinusoidal displacement excitation respectively at various input current levels. It can be seen that the effects of changing input current on the damping force are quite obvious. When there is no input current (i.e. 0 A), the MR damper exhibits as a normal viscous damper, which possesses an approximately elliptical shape in force and displacement graph and a linear relationship between the force and velocity. When input current is applied, the viscosity of the MR fluid will be increased. So the yield force of the MR damper is also increased so that the plastic-like behaviors in the force-displacement and the force-velocity graphs are observed.

Two additional loops appear at the velocity extremes in the force-velocity graph of the MR damper. These phenomenons are due to the stiction phenomenon of MR fluids, fluid inertial force and the force overshoots at displacement maximums [19].

More experimental results are shown in Appendix.

TABLE 4: FORCE-DISPLACEMENT TESTS UNDER SINUSOIDAL DISPLACEMENT EXCITATION

Amplitude (mm)	Frequencies (Hz)							
40	0.05	X	X	X	X	X	X	X
30	0.05	0.1	X	X	X	X	X	X
20	0.05	0.1	0.5	X	X	X	X	X
10	0.05	0.1	0.5	1	1.5	X	X	X
5	0.05	0.1	0.5	1	1.5	2	3.5	X
2	0.05	0.1	0.5	1	1.5	2	3.5	5

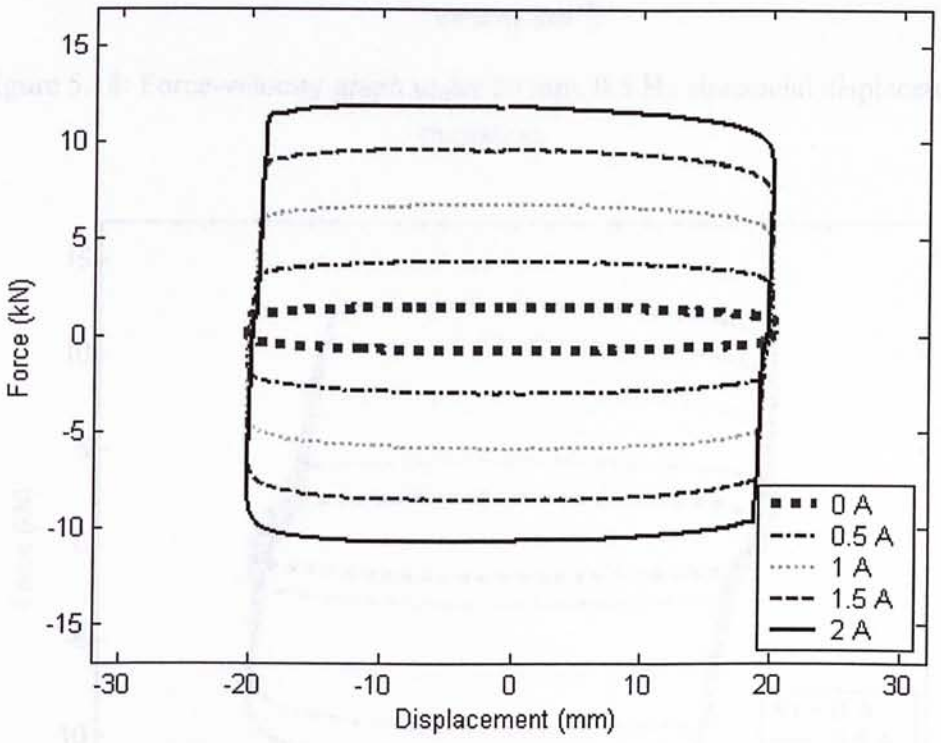

Figure 5.17: Force-displacement graph under 20 mm, 0.5 Hz sinusoidal displacement excitation.

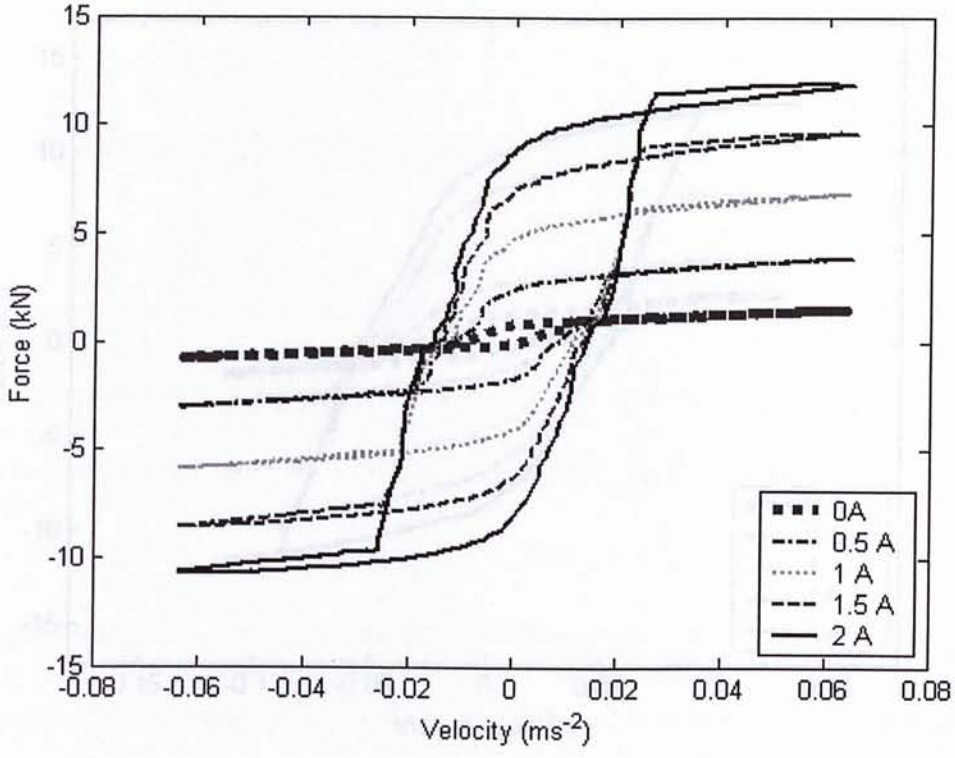

Figure 5.18: Force-velocity graph under 20 mm, 0.5 Hz sinusoidal displacement excitation.

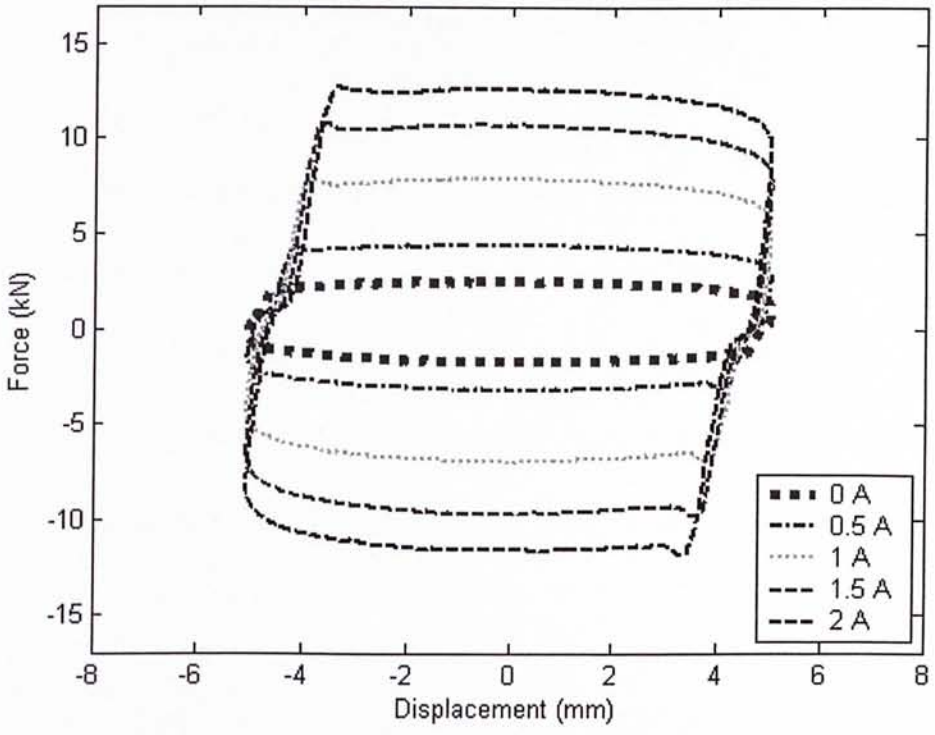

Figure 5.19: Force-displacement graph under 5 mm, 3.5 Hz sinusoidal displacement excitation.

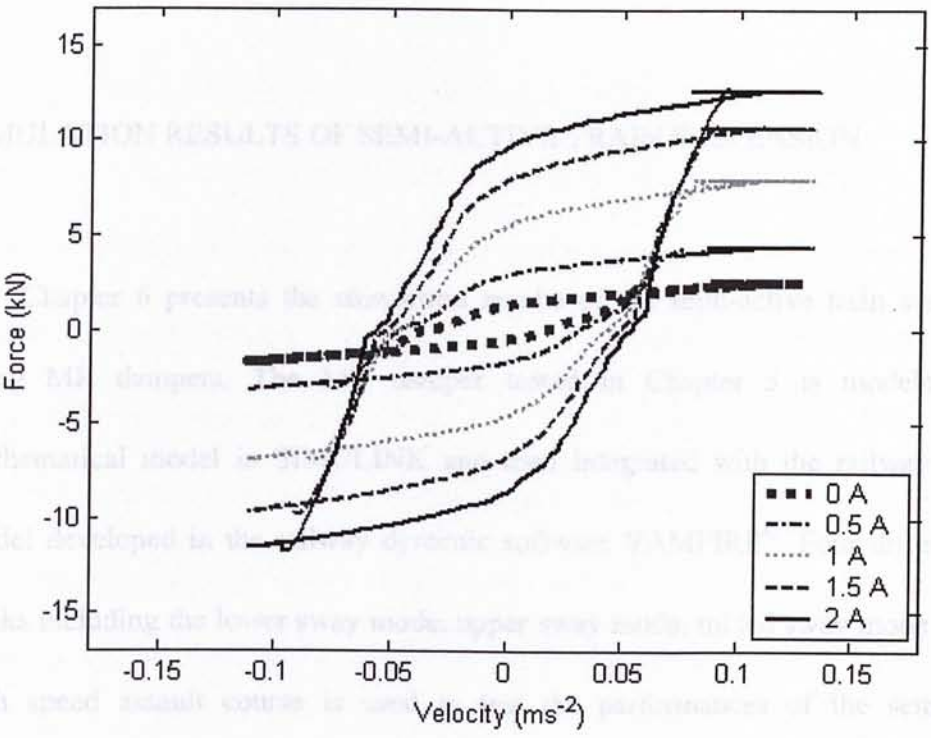

Figure 5.20: Force-displacement graph under 5 mm, 3.5 Hz sinusoidal velocity excitation.

CHAPTER 6

SIMULATION RESULTS OF SEMI-ACTIVE TRAIN SUSPENSION

Chapter 6 presents the simulation results of the semi-active train suspension using MR dampers. The MR damper tested in Chapter 5 is modeled by a mathematical model in SIMULINK and then integrated with the railway vehicle model developed in the railway dynamic software VAMPIRE©. Four different test tracks including the lower sway mode, upper sway mode, mixed sway mode and BR high speed assault course is used to test the performances of the semi-active suspension system. Then different suspension systems as well as human ride comfort are discussed.

6.1 MR Damper Model

The experimental data obtained in Chapter 5 will be used to validate the MR damper model. The dynamic phenomenological model proposed by Yang [19] is adopted here to describe the MR damper behaviors. This model is based on the Bouc-Wen Model, which considers the MR fluid stiction phenomenon, as well as the shear thinning effects. The schematic of the model is illustrated in Fig. 6.1. The damper force is given by:

$$\dot{z} = -\gamma|\dot{x}|z|z|^{n-1} - \beta\dot{x}|z|^{n} + A\dot{x} \tag{6.1}$$

$$f - f_0 = \alpha z + kx + c(\dot{x})\dot{x} + m\ddot{x} \tag{6.2}$$

$$c(\dot{x}) = a_1 e^{-(a_2|\dot{x}|)^p} \tag{6.3}$$

Eqn. (6.1) represents the Bouc-Wen model, which is extremely versatile and can describe a wide variety of hysteretic behaviors. The evolutionary variable z is governed by the parameters γ, β, A and n. By adjusting these parameters, one can control the linearity in the unloading and the smoothness of the transition from the pre-yield to the post-yield region [36].

The total damper resisting force is given by Eqn. (6.2), where α is the functional dependent parameter on the input current; k is the accumulator stiffness; f_0 is the friction force due to the damper seals as well as measurement bias; $c(\dot{x})$ is the post-yield plastic damping coefficient; m is used to emulate the MR fluid stiction phenomenon and fluid inertia effect.

Eqn. (6.3) is the damping coefficient $c(\dot{x})$, which is defined as the mono-decreasing function with respect to the absolute velocity $|\dot{x}|$. It is used to describe the MR fluid shear thinning effect, which results in the force roll-off of the damper resisting force in the low velocity region, where a_1, a_2 and p are positive constants.

The comparison between the experimental data and the mathematical model is shown in Figs. 6.2 – 6.5. From Figs 6.2 - 6.5, the force-displacement and force-velocity graphs under sinusoidal excitation with 0.5 Hz, 20 mm and 3.5 Hz, 5 mm are shown respectively. Input currents 0.5 A, 1 A and 1.5 A are used respectively in each comparison. The resulting values of those parameters of the MR damper model are given in Tables 5 and 6. Table 5 shows the damper parameters that

are not varied with the input current, and Table 6 shows the input current dependent parameters.

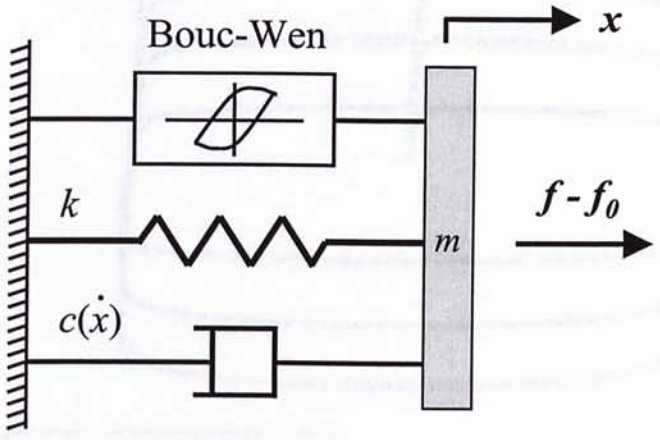

Figure 6.1: Schematic of dynamic phenomenological model for MR damper.

TABLE 5: MR DAMPER PARAMETERS.

Parameter	Value	Parameter	Value
γ	32000 m^{-1}	m	100 kg
β	22 m^{-1}	k	2500 N/m
A	220 m^{-1}	p	0.54

TABLE 6: MR DAMPER PARAMETERS AT VARIOUS INPUTS CURRENT.

Current (A)	α (N)	a_1 (N·sec/m)	a_2 (sec/m)	n	f_0 (N)
0.5 A	15000	32000	6	2.7	400
1 A	27000	65000	8	2.7755	500
1.5 A	40000	85000	8	2.7755	500

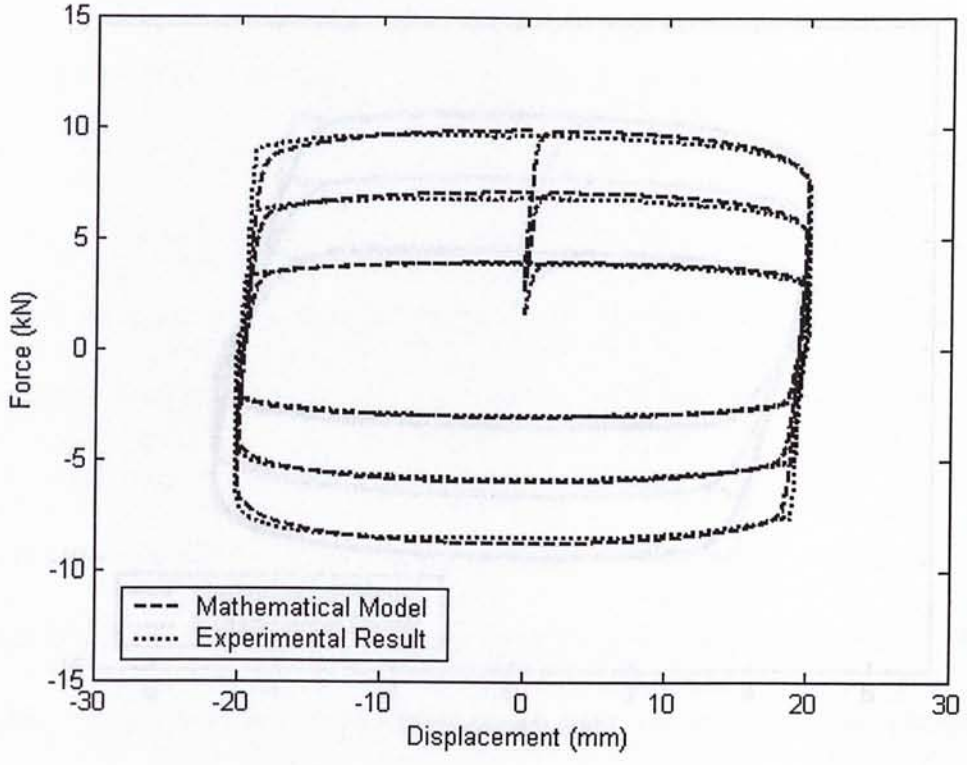

Figure 6.2: Force-displacement graph under 0.5 Hz, 20 mm sinusoidal excitation.

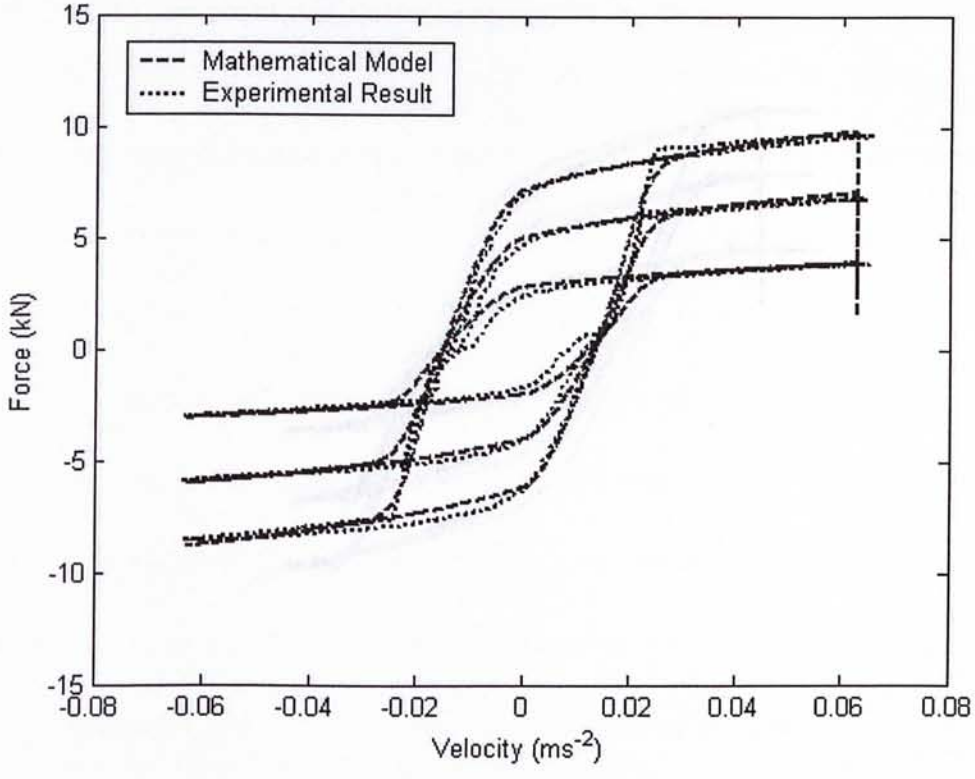

Figure 6.3: Force-velocity graph under 0.5 Hz, 20 mm sinusoidal excitation.

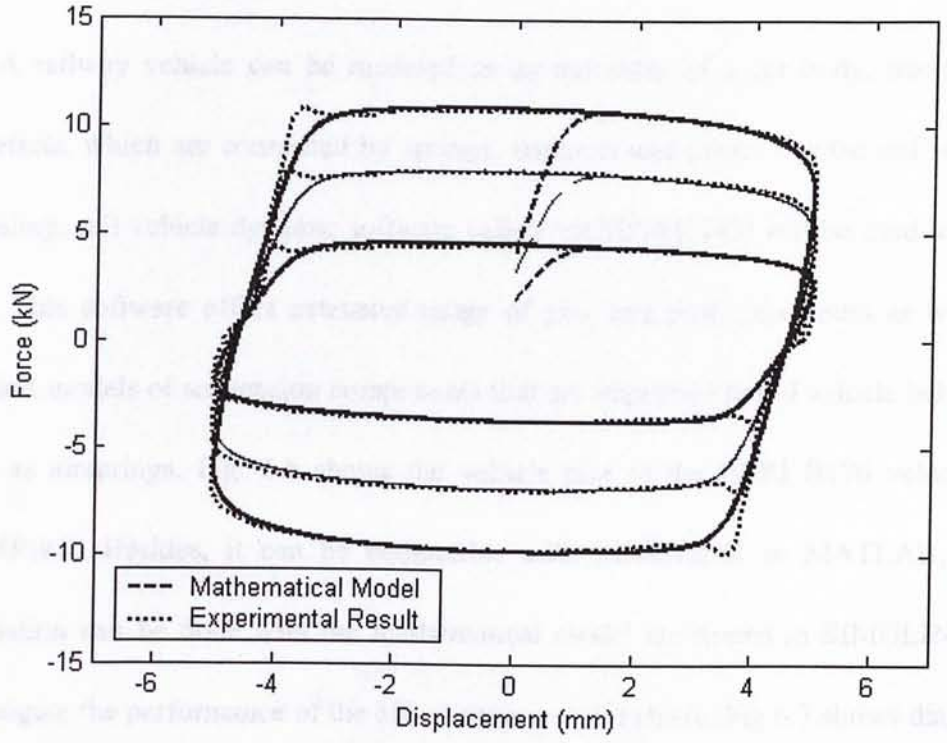

Figure 6.4: Force-displacement graph under 3.5 Hz, 5 mm sinusoidal excitation.

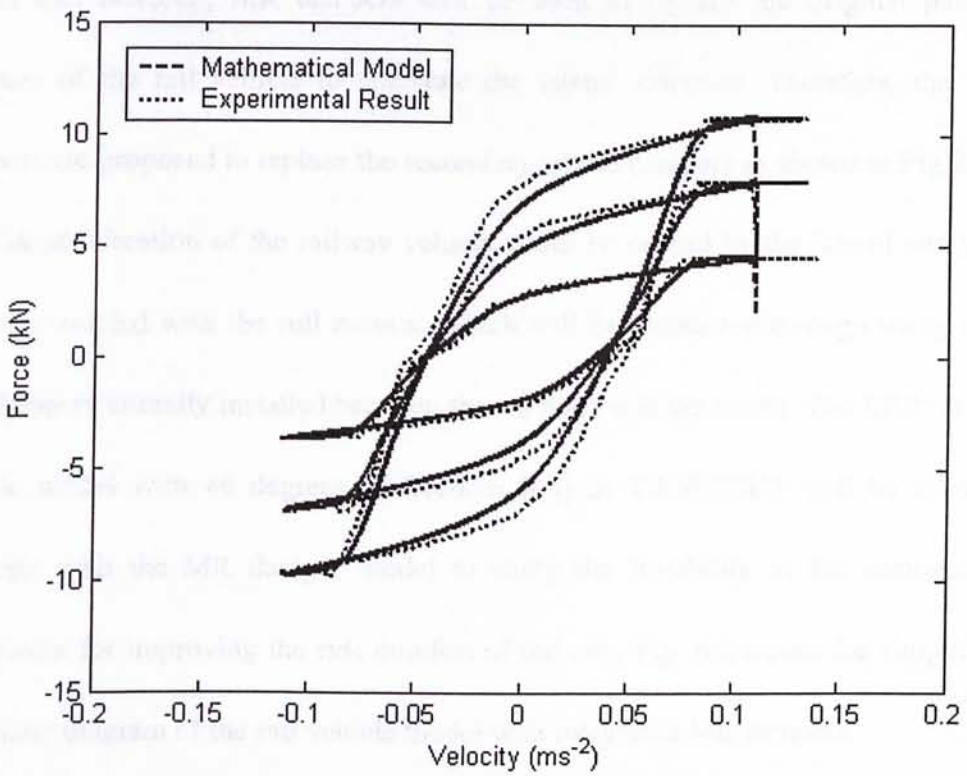

Figure 6.5: Force-velocity graph under 3.5 Hz, 5 mm sinusoidal excitation.

6.2 Rail Vehicle Model

A railway vehicle can be modeled as an assembly of a car body, trucks and wheelsets, which are connected by springs, dampers and joints. For the rail vehicle modeling, rail vehicle dynamic software called VAMPIRE [43] will be used for this task. This software offers extensive range of pre- and post- processors as well as detailed models of suspension components that are important to rail vehicle behavior such as airsprings. Fig. 6.6 shows the vehicle plot of the ERRI B176 vehicle in VAMPIRE. Besides, it can be compatible with SIMULINK in MATLAB, thus simulation can be done with the mathematical model developed in SIMULINK to investigate the performance of the MR damper in rail vehicle. Fig 6.7 shows diagram of the simulation system integration.

In this research, MR dampers will be used to replace the original passive dampers of the rail vehicle to attenuate the lateral vibration. Therefore, the MR dampers are proposed to replace the secondary lateral dampers as shown in Fig 2.15. The lateral vibration of the railway vehicle could be caused by the lateral and yaw motions coupled with the roll motion, which will be attenuated through using four MR dampers laterally installed between the car body and the trucks. The ERRI B176 vehicle model with 46 degrees of freedom [44] in VAMPIRE® will be used to integrate with the MR damper model to study the feasibility of the semi-active suspension for improving the ride comfort of the rain. Fig. 6.8 shows the simplified schematic diagram of the rail vehicle model with integrated MR dampers.

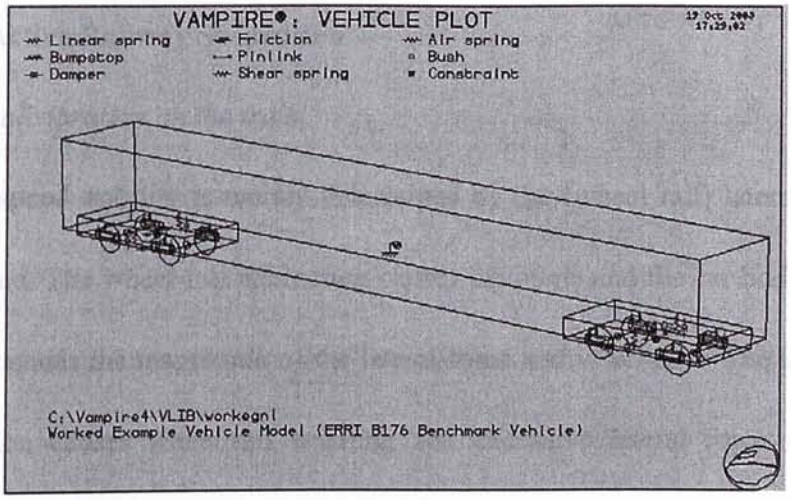

Figure 6.6: ERRI B176 benchmark vehicle.

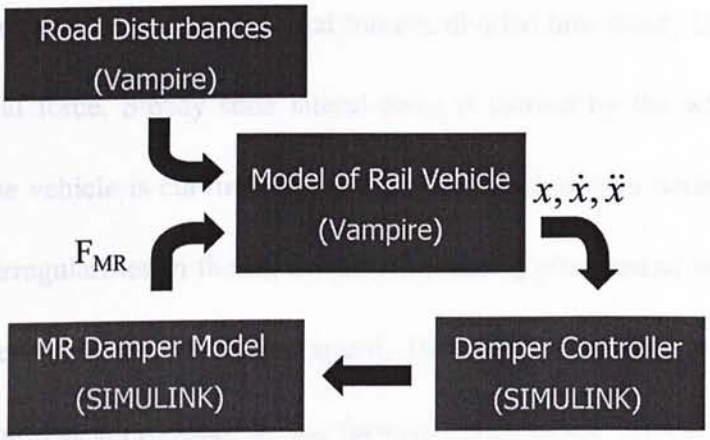

Figure 6.7: Diagram of the simulation system integration.

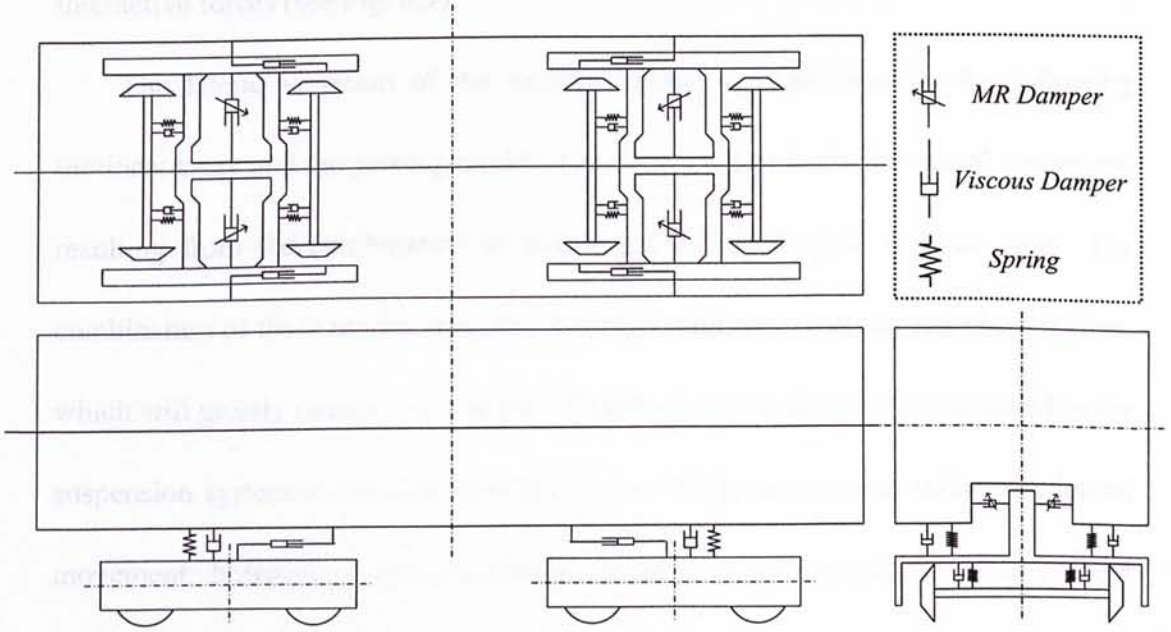

Figure: 6.8: Simplified schematic diagram of the rail vehicle model with MR dampers.

6.3 Semi-Active Railway Suspension

6.3.1 Lateral vibration on the train

High speed stability is mainly determined by the (wheel rail) lateral force and critical speed. The wheel-rail interaction causes the bogie and the car body to vibrate which aggravates the magnitude of the lateral force and vice versa. The lateral force and vibration causes wheel/rail wearing, and excessive lateral force will causes derailment too. Therefore, lateral vibration should be reduced to reduce maintenance cost and improve curving safety. Lateral force is divided into steady lateral force and dynamic lateral force. Steady state lateral force is caused by the wheel-rail attack angle when the vehicle is curving. Dynamic lateral force occurs when the vehicle is passing over irregularities in the rails. Besides, hunting phenomena will occur when the train is reached/over its critical speed. Hunting phenomena is a self-excited lateral vibration that is produced by the forward speed of the vehicle and wheel rail interactive forces (see Fig. 6.9).

The lateral vibration of the railway vehicle is dominated by the following motions: sway and the yawing modes. The sway motion is the horizontal movement resulting from the combination of lateral and roll motions at a given point. The combination of these modes at a critical speed could cause the hunting phenomenon, which will greatly reduce ride comfort. Therefore, lateral dampers are installed in the suspension system to increase the damping for the lower sway to reduce the lateral movement; however, it could sacrifice the stability of the railway vehicle under higher frequency excitation. Hence, the strategy of the semi-active suspension for

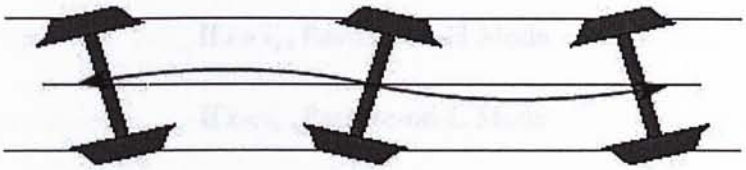

Figure 6.9: Wheelset Hunting [26].

coping with lateral vibration is to increase the damping for the lower sway mode without degrading the performance of the rail vehicle for higher frequency upper sway mode.

6.3.2 Semi-active control strategy

The control strategy adopted here is based on the measurement of the absolute lateral velocity of the car body and compared with predetermined threshold velocity [8], which is chosen to be the one generated by low frequency irregularities (wavelength about 100 m) at the maximum speed of the rail vehicle. This control strategy yields substantial benefits over a pure passive system [8]. The concept is that the MR damper will be set to a relative lower damping rate in passive-on mode with 0.5 A (passive-on-L mode), until a resonance is detected then the MR damper will be set to a relative higher damping rate in passive-on mode with 1 A (passive-on-H mode). The range of the current can be applied to the MR damper is from 0 A to 1.5 A, since the MR damper with too low or too high damping rate is not favorable in the suspension system , so 0.5 A and 1 A is chosen as the applied current in the passive-on-L and passive-on-H mode respectively. The switching speed is chosen as the maximum allowable absolute lateral velocity of the car body, which is caused by the low frequency irregularities. The algorithm is as follows:

$$\begin{aligned} &\text{If } \dot{x} > v_s, \text{ Passive-on-H Mode} \\ &\text{If } \dot{x} < v_s, \text{ Passive-on-L Mode} \end{aligned} \tag{6.4}$$

where v_s is the threshold velocity. The absolute lateral velocity of the car body above the leading and trailing bogies will be measured individually. Then, the change of the damping rate of those two sets of the MR dampers installed in the leading bogie and the trailing bogie will be controlled individually according to the velocity measured.

Four secondary suspensions are considered. They are: (1) semi-active, (2) passive-on-H, (3) passive-on-L, and (4) passive systems. Their definitions are as follows: (1) semi-active: controlled MR dampers are used to replace the traditional passive dampers placed laterally in the secondary suspension system between the trucks and the car body of the rail vehicle; (2) passive-on-H: the uncontrolled MR dampers in passive-on mode (constant applied current 1 A) with relative higher damping rate are used to replace the traditional passive dampers in the secondary suspension system; (3) passive-on-L: uncontrolled MR dampers in passive-on mode (0.5 A) with relative lower damping rate are used to replace the traditional passive dampers in the secondary suspension system; (4) passive system: traditional viscous dampers are used in the secondary suspension system.

The rail vehicle model is simulated to run on different kinds of track irregularities at 90 m/s with four suspension systems as aforementioned. There are four different kinds of track: (I) lower sway mode test track, (II) upper sway mode test track, (III) mixed mode test track and (IV) BR high speed assault course test track. All of the track irregularities have the same length with 1200 m in total.

The lower sway mode test track is the long wavelength track irregularities, which are used to excite the lower sway mode of the rail vehicle at 0.551 Hz. It is a sinusoidal excitation with 40 mm amplitude and 4 cycles as shown in Fig. 6.10. Then, the upper sway mode test track is the short wavelength track irregularities, which are used to excite the upper sway mode at 3.648 Hz of the rail vehicle. It is a sinusoidal excitation with 20 mm amplitude and 5 cycles as shown in Fig. 6.11.

The mixed mode test track is the coupled track irregularities with both long and short wavelength excitations in order to excite both the lower and upper sway modes of the rail vehicle. As shown in Fig. 6.12, the track irregularities consist of the long wavelength excitation with 40 mm amplitude and 2 cycles and then follow by a short wavelength excitation with 20 mm amplitude and 4 cycles.

Finally, the BR high speed assault course is a sinusoidal excitation with increasing frequency and decreasing amplitude. It is conventionally used to seek out the undesirable resonances in the suspension. As shown in Fig. 6.13, it is a swept sine lateral track perturbation with amplitude start from 50 mm with increasing `frequency and decreasing amplitude.

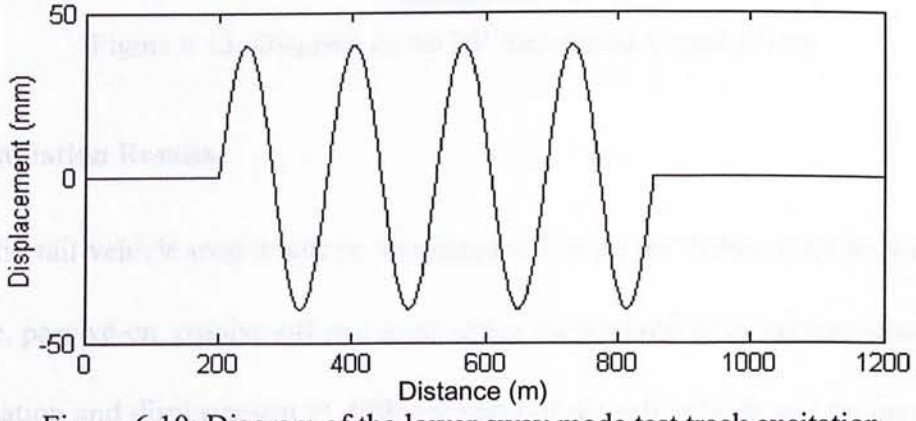

Figure 6.10: Diagram of the lower sway mode test track excitation.

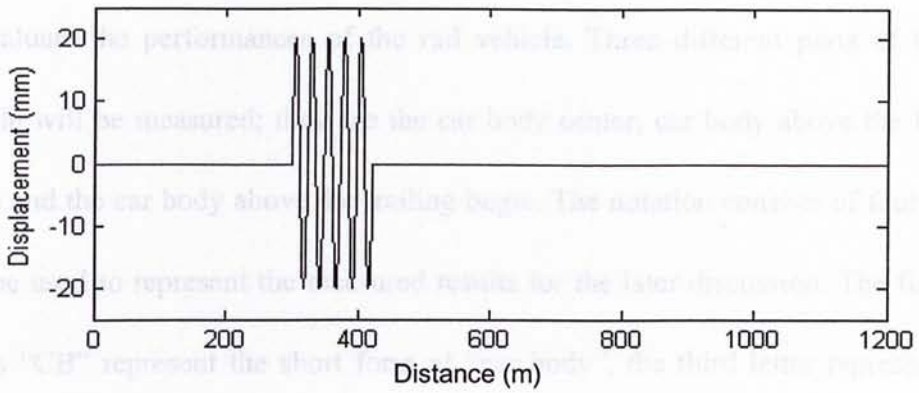

Figure 6.11: Diagram of the upper sway mode test track excitation.

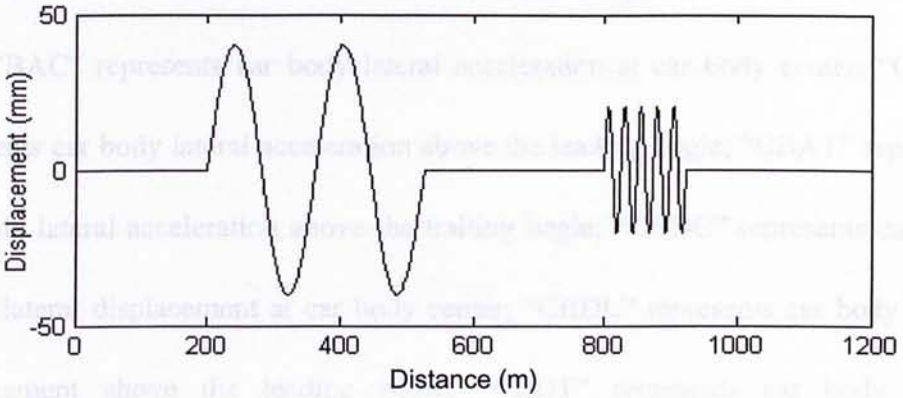

Figure 6.12 Diagram of the mixed mode test track excitation.

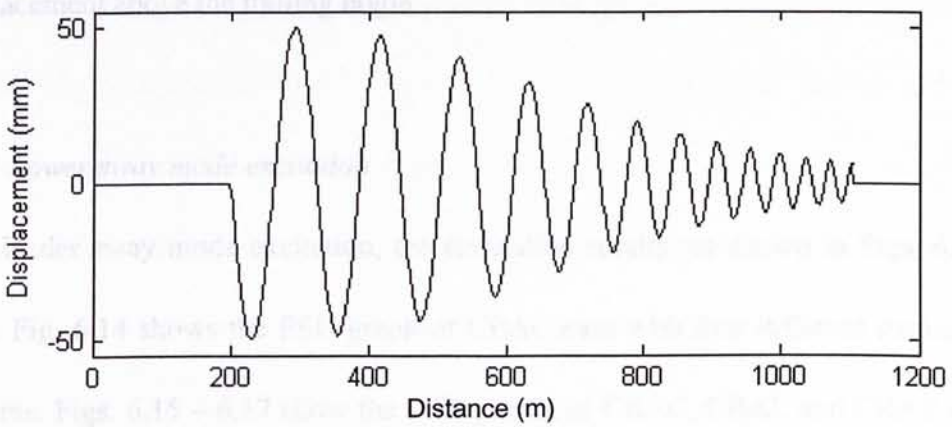

Figure 6.13: Diagram of the BR high speed assault course

6.4 Simulation Results

The rail vehicle model will be simulated to run on the different tracks with the passive, passive-on, passive-off and semi-active suspensions as aforementioned. The acceleration and displacement at different parts of the rail vehicle will be measured

to evaluate the performances of the rail vehicle. Three different parts of the rail vehicle will be measured; they are the car body center, car body above the leading bogie and the car body above the trailing bogie. The notation consists of four letters will be used to represent the measured results for the later discussion. The first two letters "CB" represent the short form of "car body", the third letter represents the type of measurement and the fourth letter represents the position of the measurement. So, "CBAC" represents car body lateral acceleration at car body center; "CBAL" represents car body lateral acceleration above the leading bogie; "CBAT" represents car body lateral acceleration above the trailing bogie; "CBDC" represents car body center lateral displacement at car body center; "CBDL" represents car body lateral displacement above the leading bogie; "CBDT" represents car body lateral displacement above the trailing bogie

6.4.1 Lower sway mode excitation

Under sway mode excitation, the simulation results are shown in Figs. 6.14 – 6.20. Fig. 6.14 shows the PSD graph of CBAC case with four different suspension systems. Figs. 6.15 – 6.17 show the PSD graphs of CBAC, CBAL and CBAT cases respectively for both passive suspension and semi-active suspension. Figs. 6.18 – 6.20 show the displacement time responses of CBDC, CBDL and CBDT cases respectively for both passive suspension and semi-active suspension.

It can be seen from Fig. 6.14 that the passive suspension system can attenuate the higher frequency (> 1 Hz) vibration of the car body quite well under the lower

sway. However, its performance is not favorable in the low frequency region (~ 0.55 Hz), where higher damping force is desired.

On the other hand, the passive-on-H and passive-on-L cases have two extreme attenuation abilities for the low frequency (~ 0.55 Hz) and higher frequency (> 1 Hz) vibrations. The passive-on-H suspension system has the best attenuation ability at the low frequency region under the excitation of the lower sway and the passive-on-L case yields the best performance (attenuation) at the higher frequency region. However, the passive-on-H suspension system fails to attenuate the higher frequency vibration while the passive-on-L suspension system fails to attenuate the low frequency vibration.

On the other hand, the semi-active suspension system possesses the vibration attenuation ability of both the passive-on-H and passive-on-L suspension systems. At the low frequency region (~ 0.55 Hz), the semi-active suspension highly resembles the performance of the passive-on-H suspension system at this lower sway mode excitation. For the higher frequency region (> 1 Hz), the semi-active suspension has better vibration attenuation ability than passive-on-H suspension system.

As shown in Figs. 6.15 – 6.17, semi-active suspension system has better attenuation ability for CBAC, CBAL and CBAT cases than the passive suspension system for frequency region below 2.5 Hz. However, semi-active suspension has bigger amplitude of vibration at around 3.5 Hz than the passive suspension system for CBAC, CBAL and CBAT cases.

Nevertheless, as observed in Figs. 6.18 – 6.20, it can be seen that the

semi-active suspension system yield smaller displacement amplitude than the passive system for those CBDC, CBDL and CBDT cases. That shows the semi-active suspension has better performance for displacement reduction than the passive system with the trade- off that it lead to a higher acceleration rate than the passive system in higher frequency region under this lower sway mode test.

At the same time, as shown in Table 7, semi-active suspension yields smaller lateral RMS. acceleration for all case when compared to the passive system. This means that the semi-active suspension system has better overall performance than the passive suspension system. It is worth noting that the passive-on-H and passive-on-L cases have the worst RMS. values as compared to the passive and semi-active systems for all cases except that the passive-on-H system has better performance than the passive system for CBAC case.

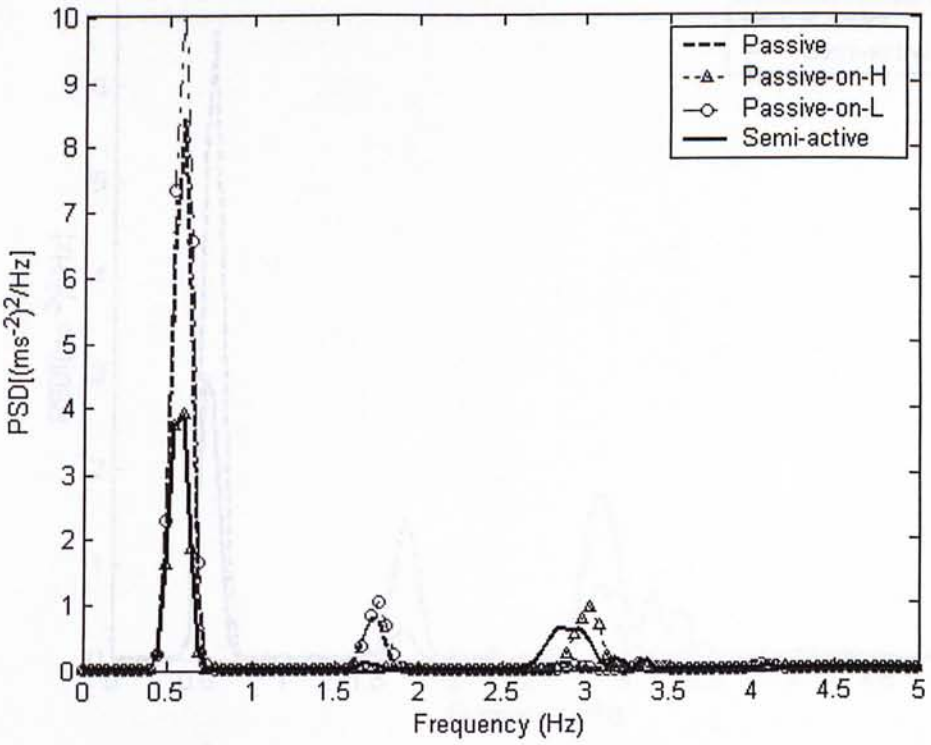

Figure 6.14: PSD graph of CBAC under lower sway mode excitation.

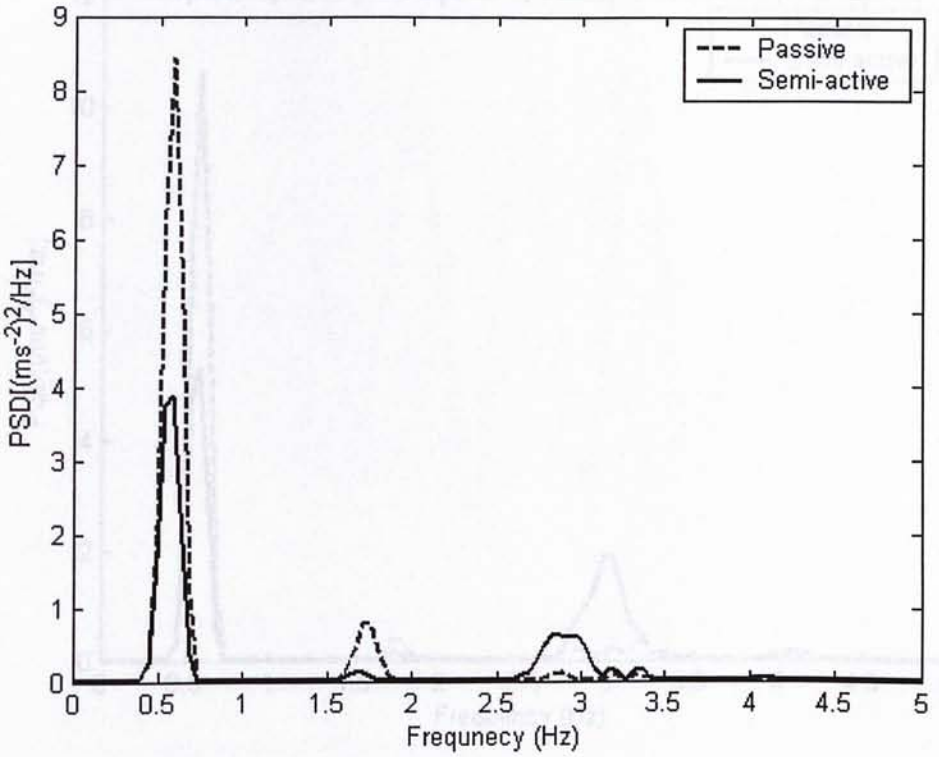

Figure 6.15: PSD graph of CBAC under lower sway mode excitation.

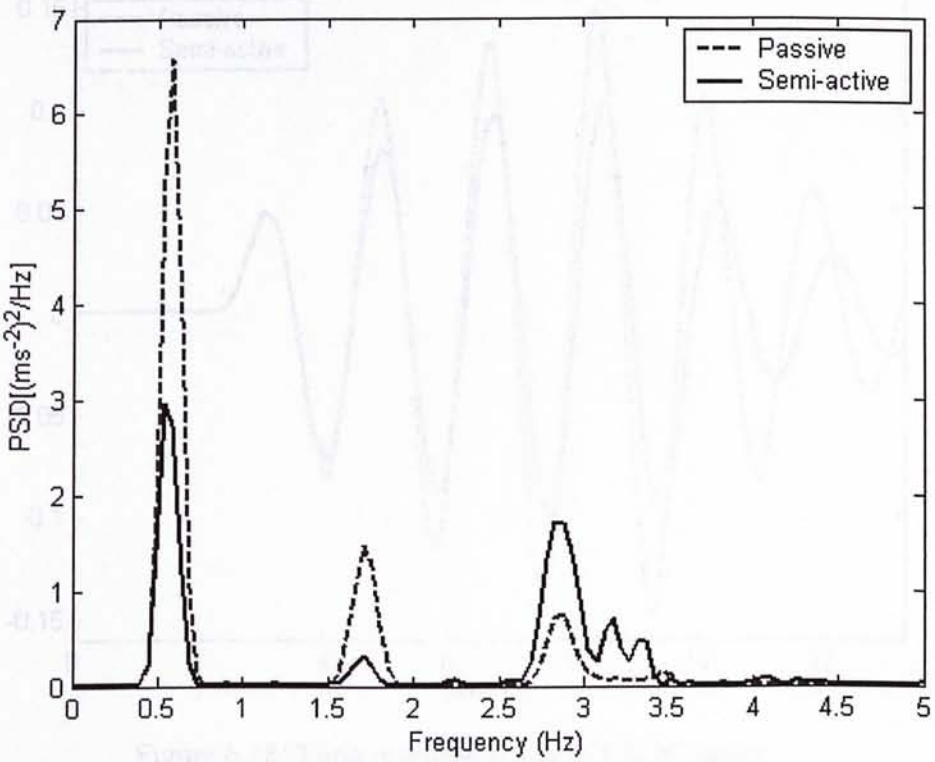

Figure 6.16: PSD graph of CBAL under lower sway mode excitation.

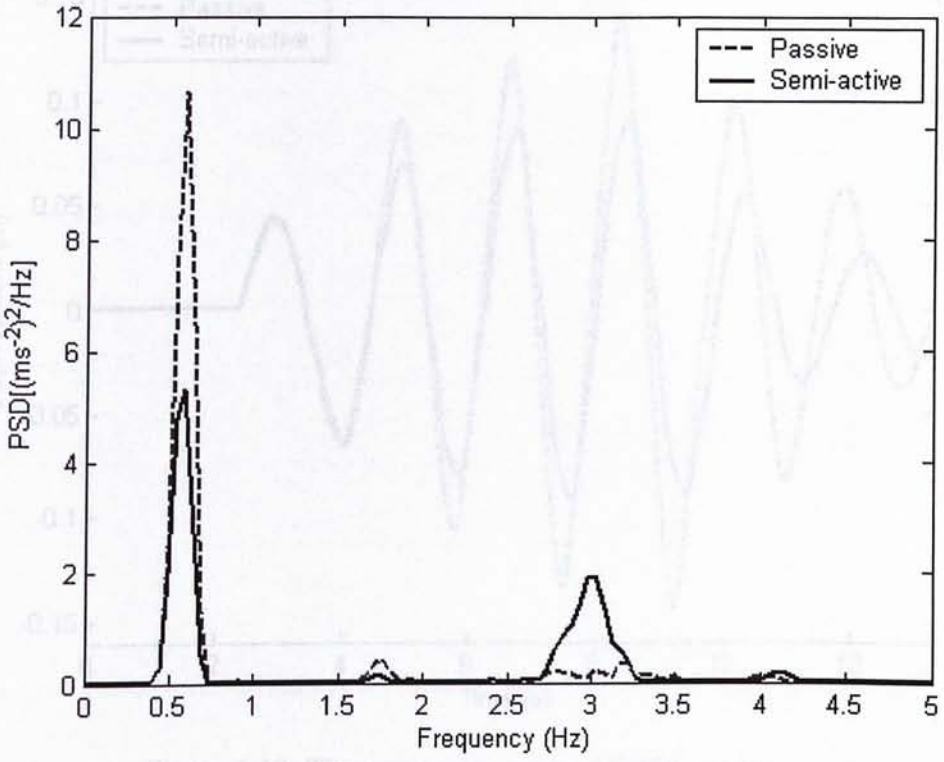

Figure 6.17: PSD graph of CBAT under lower sway mode excitation.

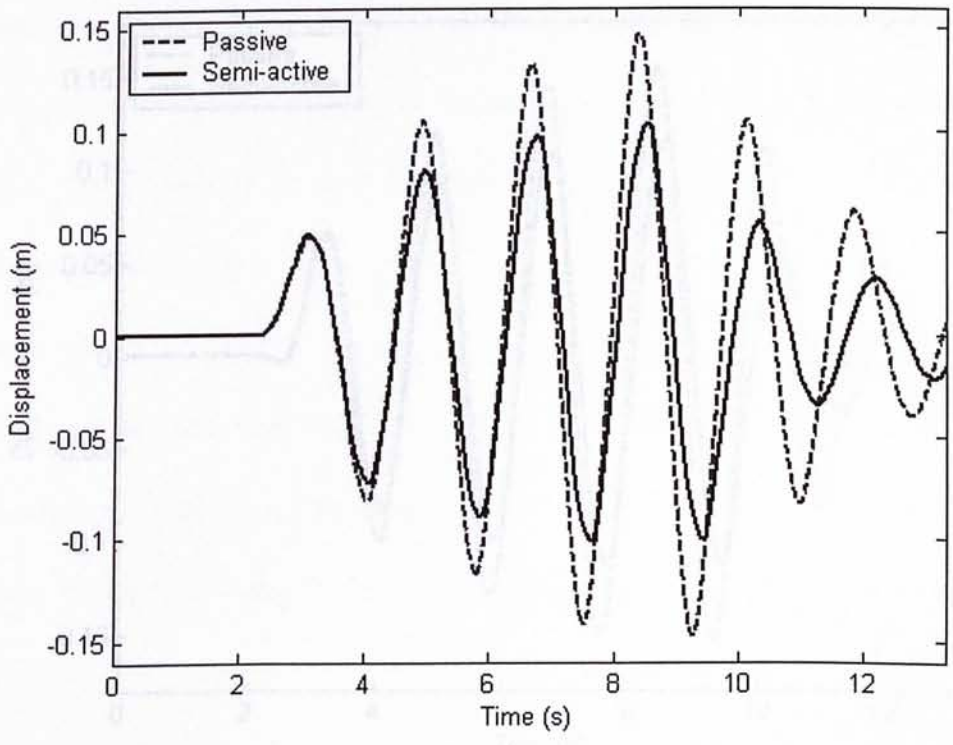

Figure 6.18: Time response graph of CBDC under lower sway mode excitation.

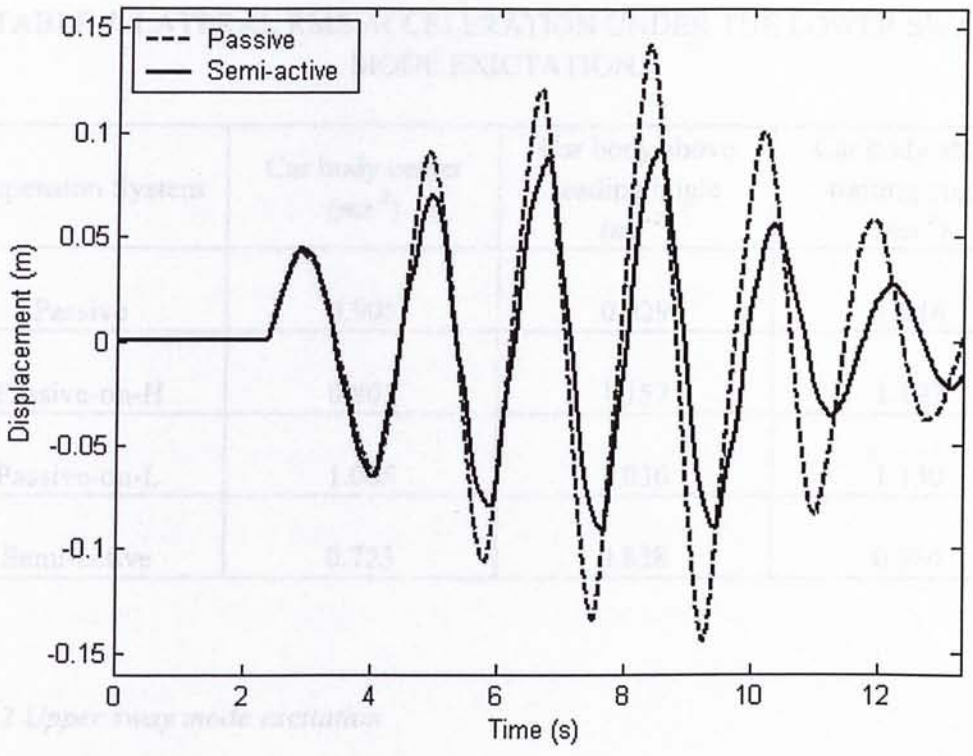

Figure 6.19: Time response graph of CBDL under lower sway mode excitation.

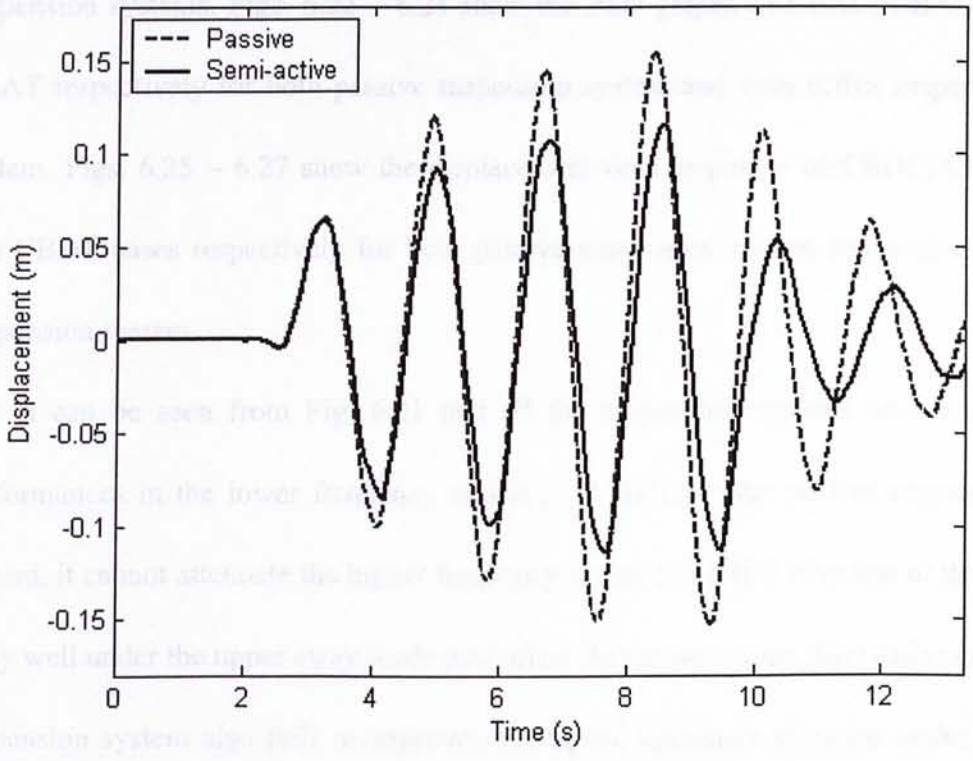

Figure 6.20: Time response of CBDT under lower sway mode excitation.

TABLE 7: LATERAL RMS ACCELERATION UNDER THE LOWER SWAY MODE EXICTATION.

Suspension System	Car body center (ms^{-2})	Car body above leading bogie (ms^{-2})	Car body above trailing bogie (ms^{-2})
Passive	0.905	0.929	1.048
Passive-on-H	0.803	1.157	1.197
Passive-on-L	1.005	1.036	1.130
Semi-active	0.723	0.828	0.934

6.4.2 Upper sway mode excitation

Under upper sway mode excitation, the simulation results are shown in Figs. 6.21 – 6.27. Fig 6.21 shows the PSD graph of CBAC case with four different suspension systems. Figs. 6.22 – 6.24 show the PSD graphs of CBAC, CBAL and CBAT respectively for both passive suspension system and semi-active suspension system. Figs. 6.25 – 6.27 show the displacement time responses of CBDC, CBDL and CBDT cases respectively for both passive suspension system and semi-active suspension system.

It can be seen from Fig. 6.21 that all the suspension systems have similar performances in the lower frequency region (< 2 Hz). For the passive suspension system, it cannot attenuate the higher frequency region (~3.6 Hz) vibration of the car body well under the upper sway mode excitation. At the same time, the passive-on-H suspension system also fails to attenuate the higher frequency vibration under this upper sway mode excitation, which requires a relative soft damping force. On the

other hand, the passive-on-L case yields the best performance (attenuation) in the higher frequency region (~3.6 Hz) as expected under the upper sway mode excitation. For the semi-active suspension system, it resembles the vibration attenuation ability of the passive-on-L suspension system under this upper sway mode excitation. As shown in Fig. 6.21, the semi-active suspension system yields the same performance as the passive-on-L case, which has better performance than the passive and passive-on-H suspension systems for the CBAC case.

As shown in Figs. 6.22 – 6.24, semi-active suspension system has better attenuation ability for CBAC, CBAL and CBAT cases compared to the passive system for the whole frequency range shown. As aforementioned, since the semi-active suspension resembles the passive-on-L case under this upper sway mode excitation, it possesses better attenuation ability for CBAC, CBAL and CBAT cases.

Besides, it can be seen from Figs. 6.25 – 6.27 that the semi-active suspension system has similar displacement amplitude compared to the passive system for those CBDC, CBDL and CBDT cases. However, it is worth noting that the semi-active suspension system has smaller amplitudes in the ripples of each displacement time response compared to the passive system for all cases.

Furthermore, as shown in Table 8, the semi-active suspension system yields smaller lateral R.M.S. acceleration for all case compared to the passive system. It should be noted that the semi-active system has the same performance as the passive-on-L case and the passive-on-H case does not perform well under the upper sway mode excitation.

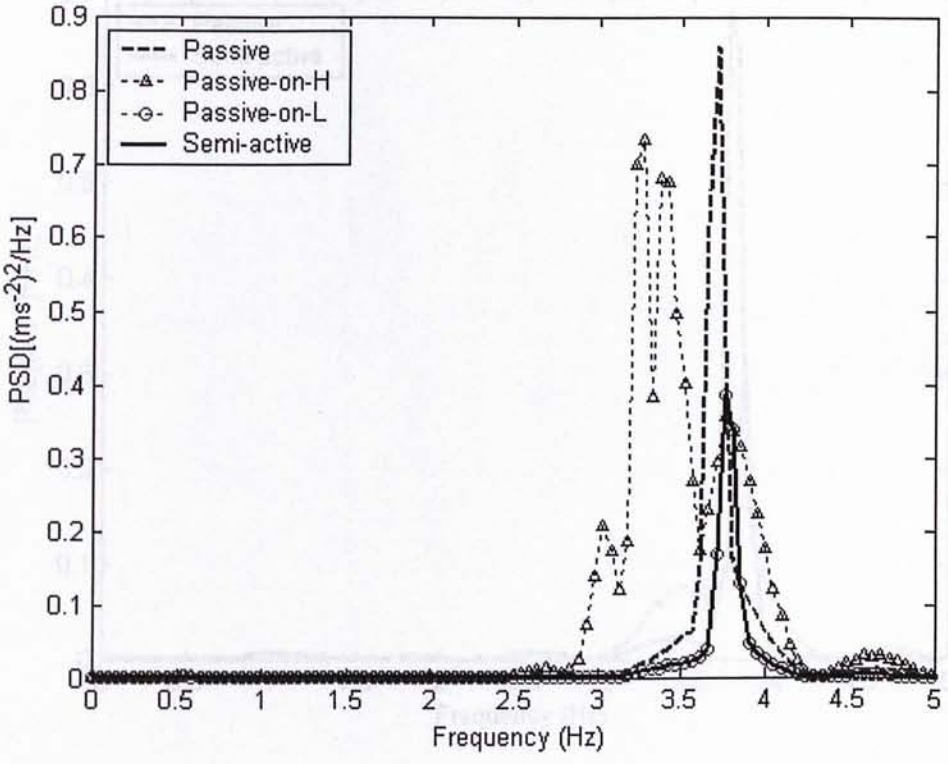

Figure 6.21: PSD graph of CBAC under upper sway mode excitation.

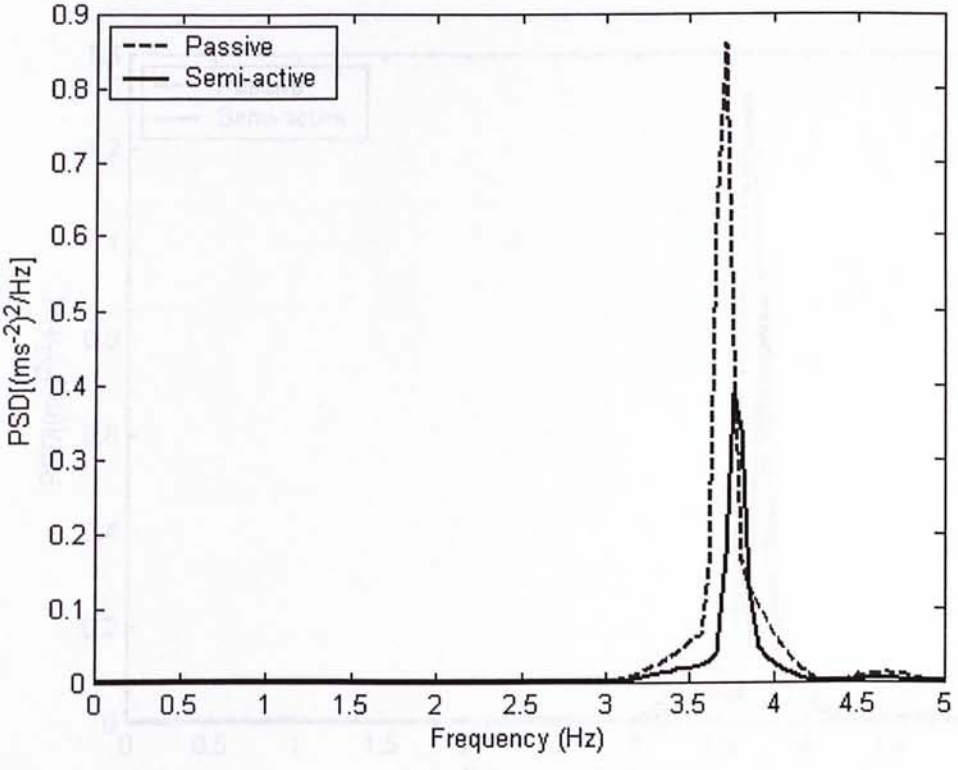

Figure: 6.22: PSD graph of CBAC under upper sway mode excitation.

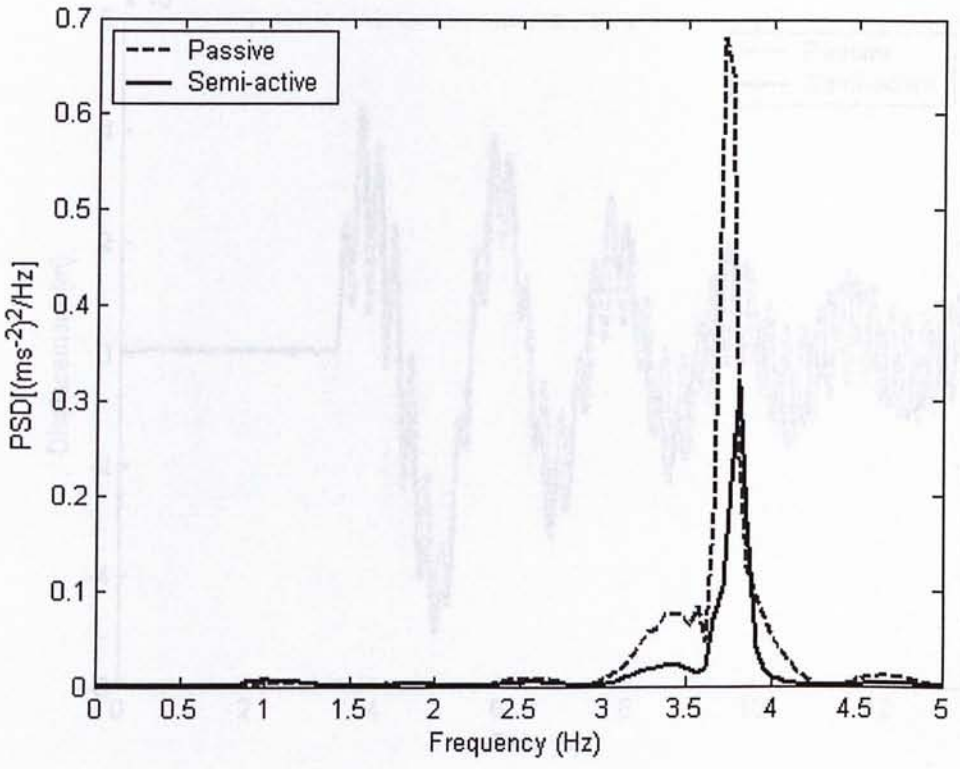

Figure: 6.23: PSD graph of CBAL under upper sway mode excitation.

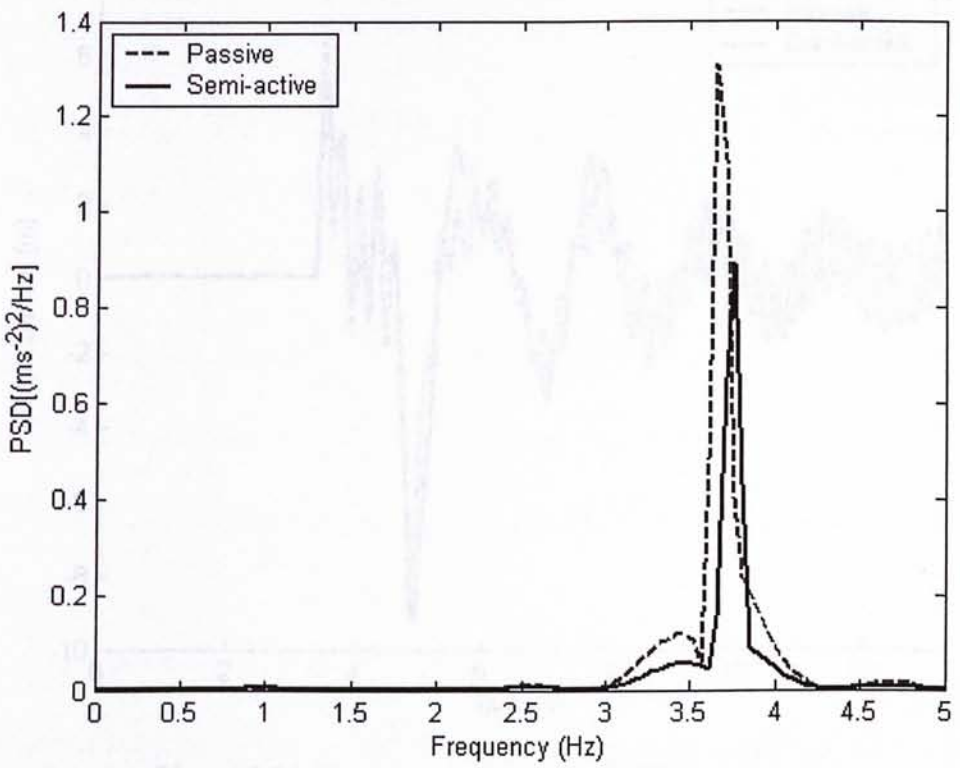

Figure 6.24: PSD graph of CBAT under upper sway mode excitation.

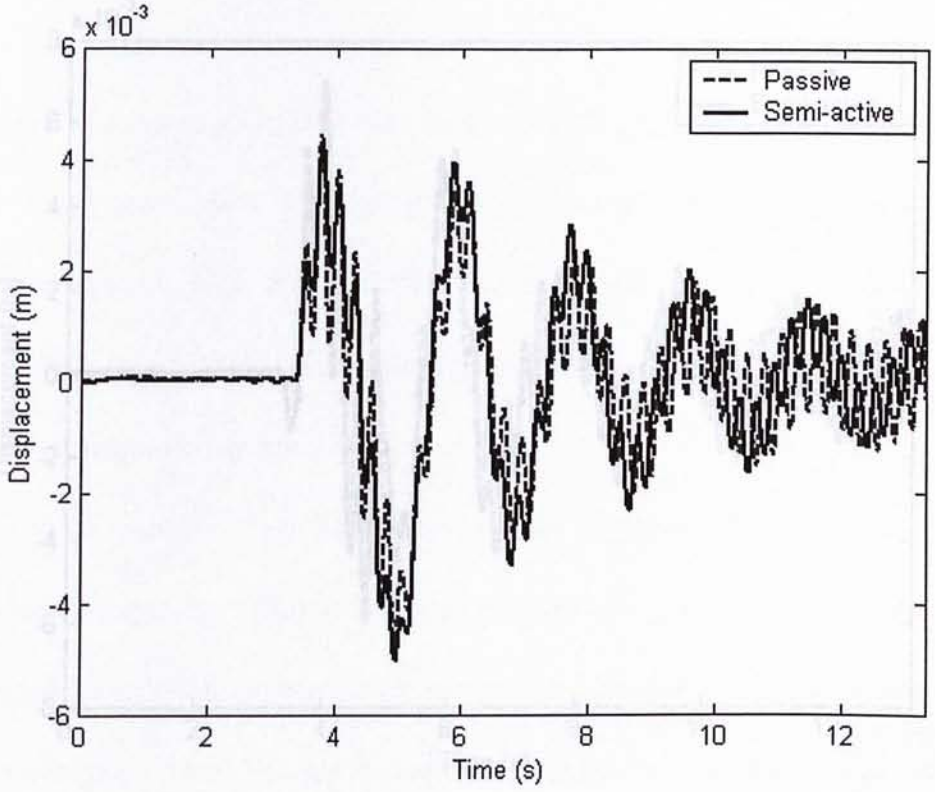

Figure 6.25: Time response graph of CBDC under upper sway mode excitation.

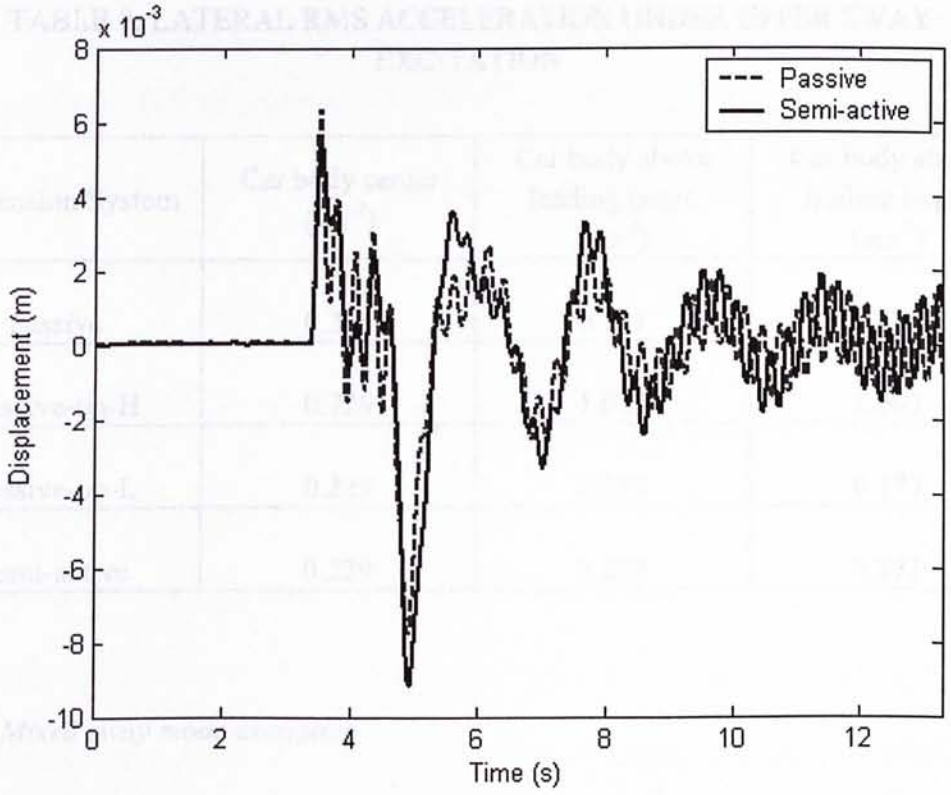

Figure 6.26: Time response graph of CBDL under upper sway mode excitation.

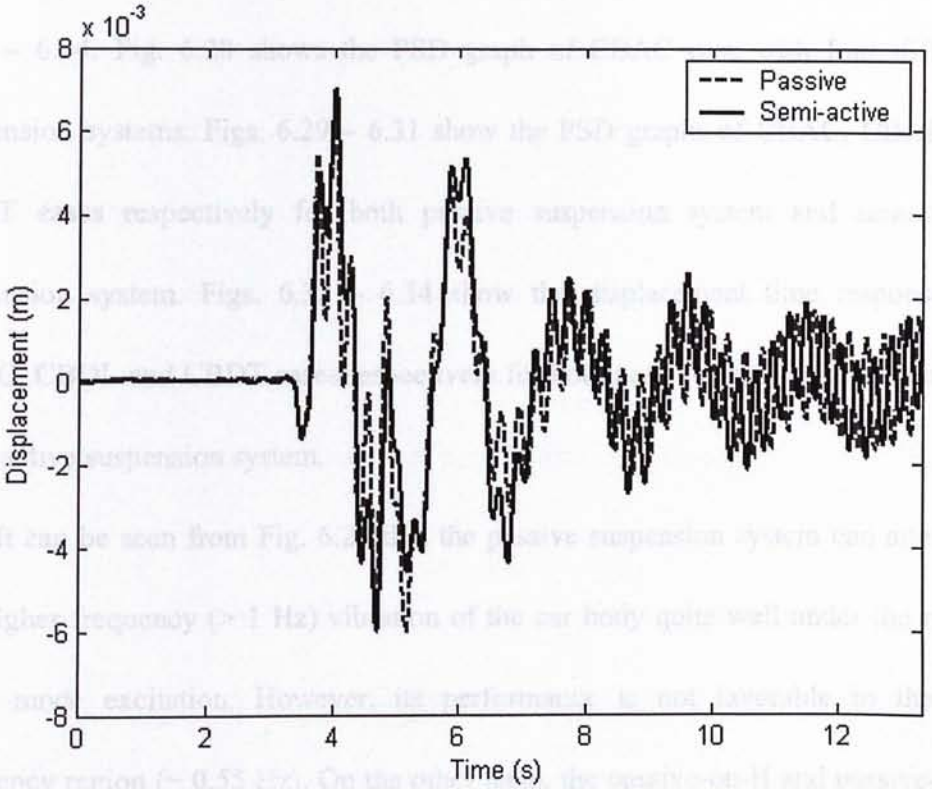

Figure 6.27: Time response graph of CBDT under upper sway mode excitation.

TABLE 8: LATERAL RMS ACCELERATION UNDER UPPER SWAY EXCITATION.

Suspension System	Car body center (ms^{-2})	Car body above leading bogie (ms^{-2})	Car body above trailing bogie (ms^{-2})
Passive	0.358	0.391	0.481
Passive-on-H	0.729	1.078	1.063
Passive-on-L	0.229	0.279	0.373
Semi-active	0.229	0.279	0.373

6.4.3 Mixed sway mode excitation

Under mixed sway mode excitation, the simulation results are shown in Figs.

6.28 – 6.34. Fig. 6.28 shows the PSD graph of CBAC case with four different suspension systems. Figs. 6.29 – 6.31 show the PSD graphs of CBAC, CBAL and CBAT cases respectively for both passive suspension system and semi-active suspension system. Figs. 6.32 – 6.34 show the displacement time responses of CBDC, CBDL and CBDT cases respectively for both passive suspension system and semi-active suspension system.

It can be seen from Fig. 6.28 that the passive suspension system can attenuate the higher frequency (> 1 Hz) vibration of the car body quite well under the mixed sway mode excitation. However, its performance is not favorable in the low frequency region (~ 0.55 Hz). On the other hand, the passive-on-H and passive-on-L suspension systems have two extreme attenuation abilities for the low frequency (~ 0.55 Hz) and higher frequency (> 1 Hz) vibrations. The passive-on-H suspension system has the best attenuation ability in the low frequency region (~ 0.55 Hz) and the passive-on-L case yields the best performance in the higher frequency region. However, the passive-on-H suspension system fails to attenuate the higher frequency (> 2 Hz) vibration and the passive-on-L suspension system fails to attenuate the low frequency vibration (~ 0.55 Hz). For the semi-active suspension, it possesses the vibration attenuation ability of both the passive-on-H and passive-on-L suspension systems. In the low frequency region (~ 0.55 Hz), the semi-active suspension highly resembles the performance of the passive-on-H case. For the higher frequency region (> 1 Hz), the semi-active suspension has better vibration attenuation ability than the passive-on-H suspension system.

As shown in Fig. 6.29, semi-active suspension system has better attenuation ability for CBAC case than the passive system for almost whole frequency range shown. For the CBAL and CBAT cases as shown in Figs. 6.30 and 6.31, the semi-active suspension system has better attenuation ability than the passive system in frequency region below 2 Hz. However, the semi-active suspension has bigger vibration amplitude at around 3.5 Hz than the passive system for the CBAL and CBAT cases.

On the contrary, it can be seen from Figs. 6.32 – 6.34 that the semi-active suspension system yields smaller displacement amplitude than the passive system for those CBDC, CBDL and CBDT cases. As mentioned in Section 6.4.1, the semi-active suspension has better performance for displacement reduction than the passive system with the trade-off that it leads to a higher acceleration rate than the passive system in higher frequency region under this mixed sway mode test.

When R.M.S values as shown in Table 9 are considered, it should be noted that the semi-active suspension system has better performance for the CBAC and CBAT cases and similar performance for CBAL case. The key is that the semi-active suspension can have better or similar acceleration attenuation ability while it possesses smaller displacement amplitude compared to the passive suspension system. That means the semi-active suspension system has better overall performance than the passive suspension system. For the passive-on-H and passive-on-L cases, they posses worse R.M.S. values than the passive and semi-active systems for all cases; that means they cannot adapt to the changing needs

of the vibration attenuation in general.

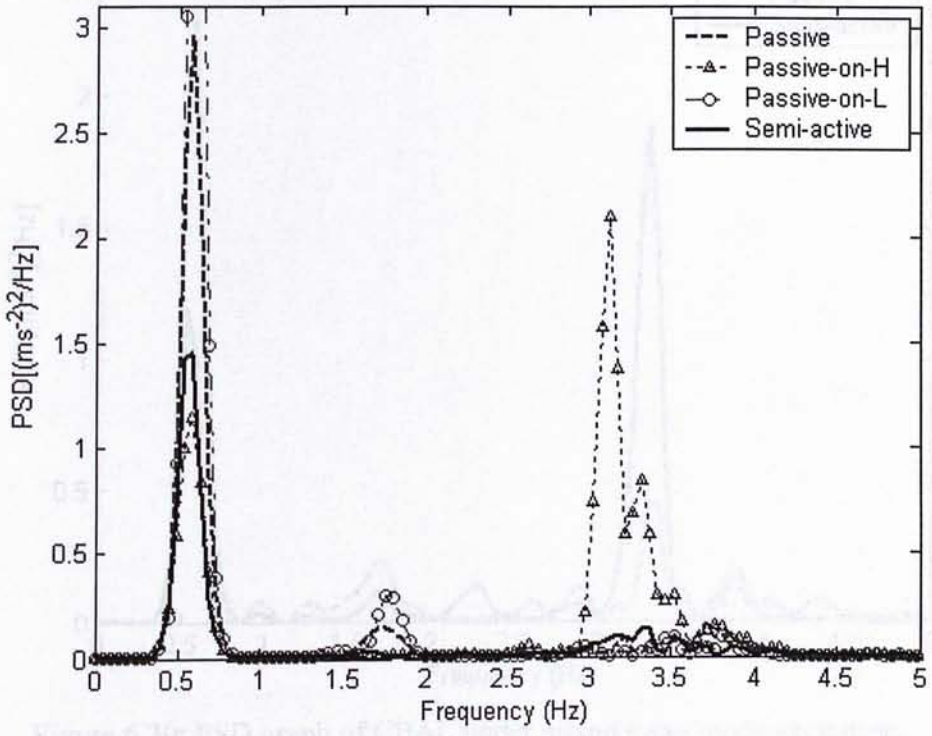

Figure 6.28: PSD graph of CBAC under mixed sway mode excitation.

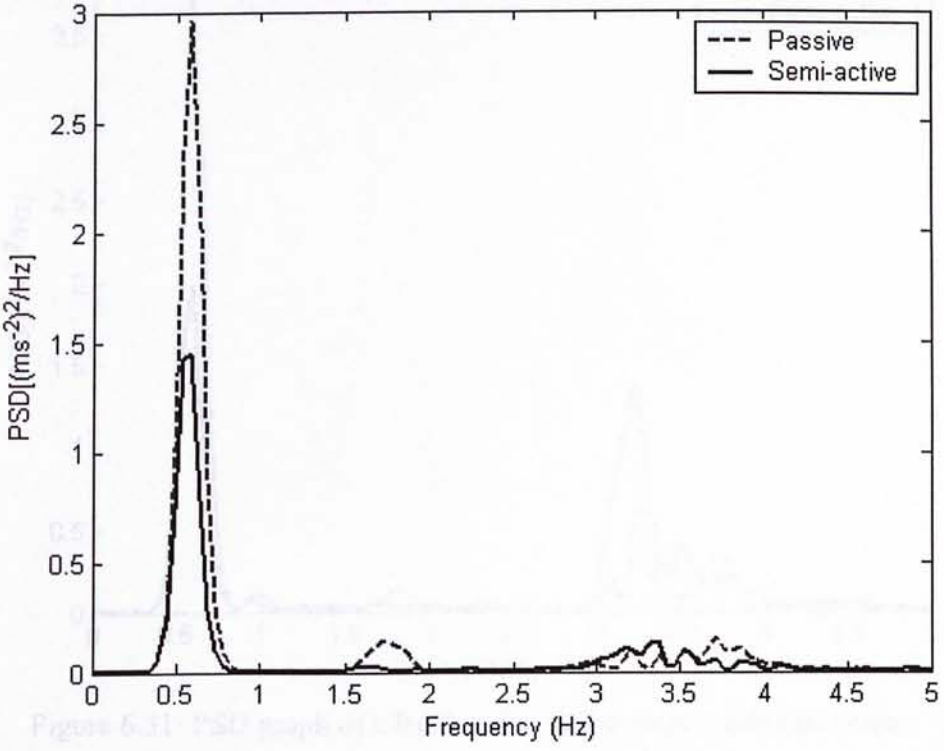

Figure 6.29: PSD graph of CBAC under mixed sway mode excitation.

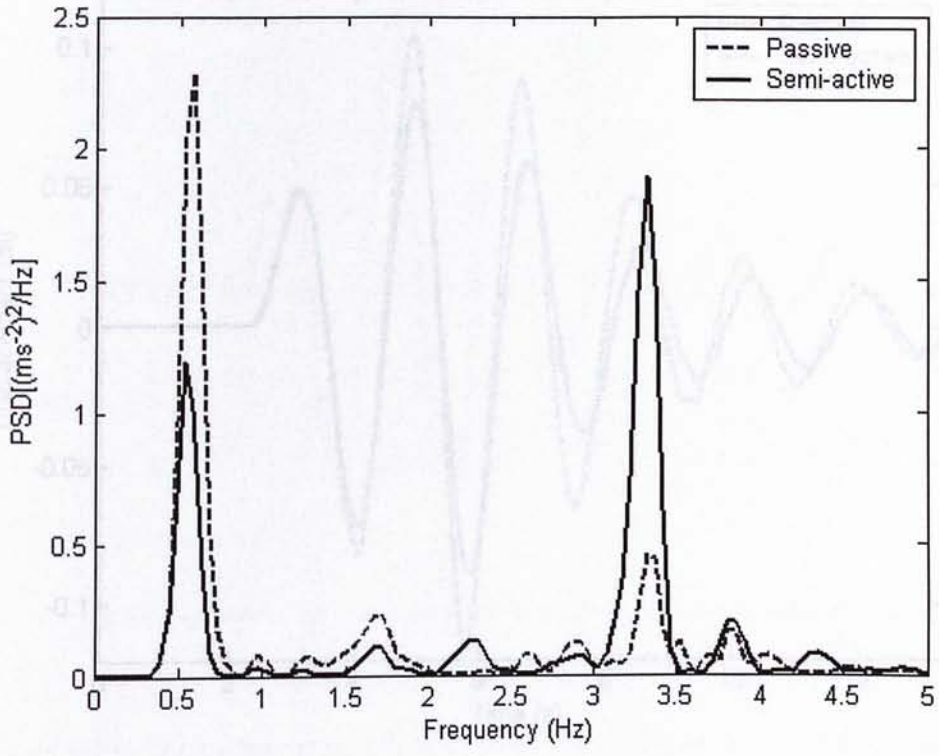

Figure 6.30: PSD graph of CBAL under mixed sway mode excitation.

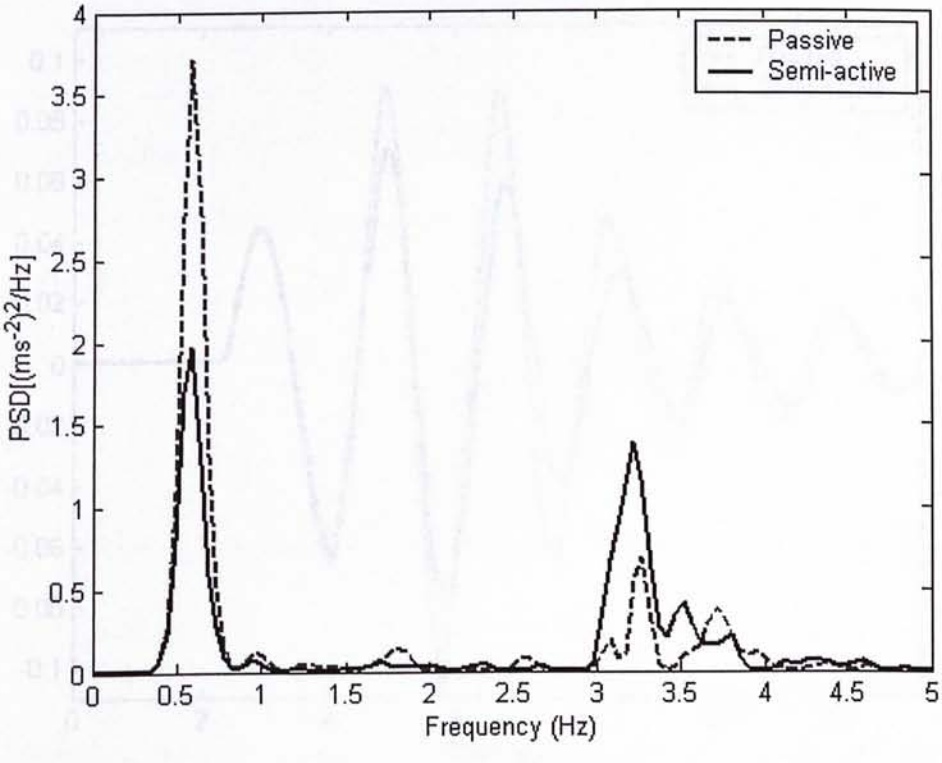

Figure 6.31: PSD graph of CBAT under mixed sway mode excitation.

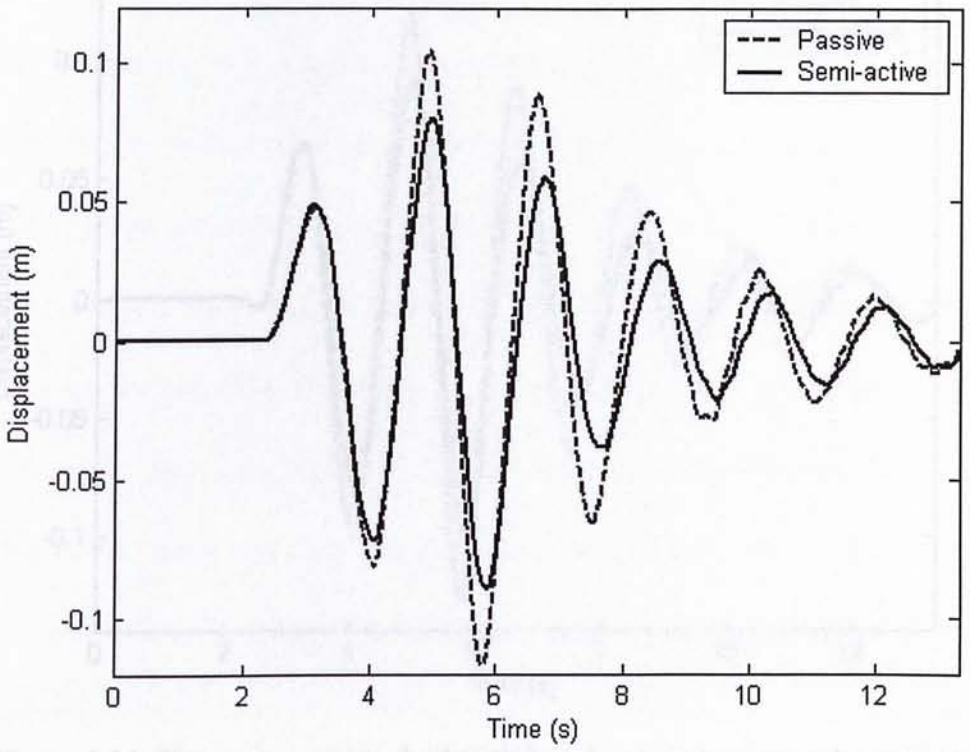

Figure 6.32: Time response graph of CBDC under mixed sway mode excitation.

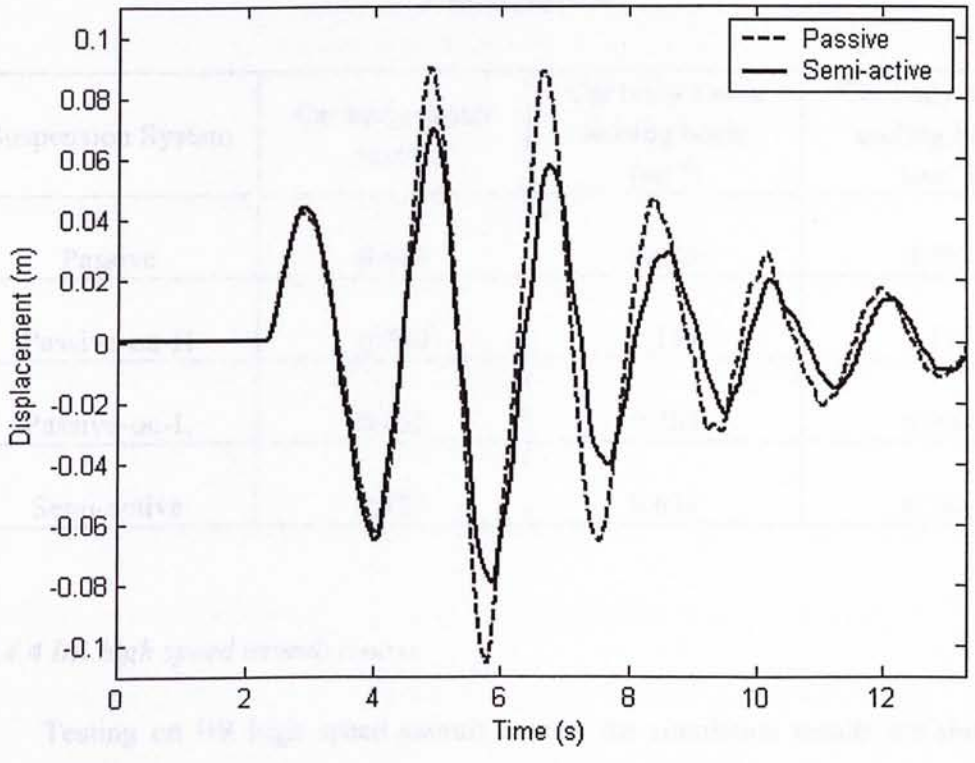

Figure 6.33: Time response graph of CBDL under mixed sway mode excitation.

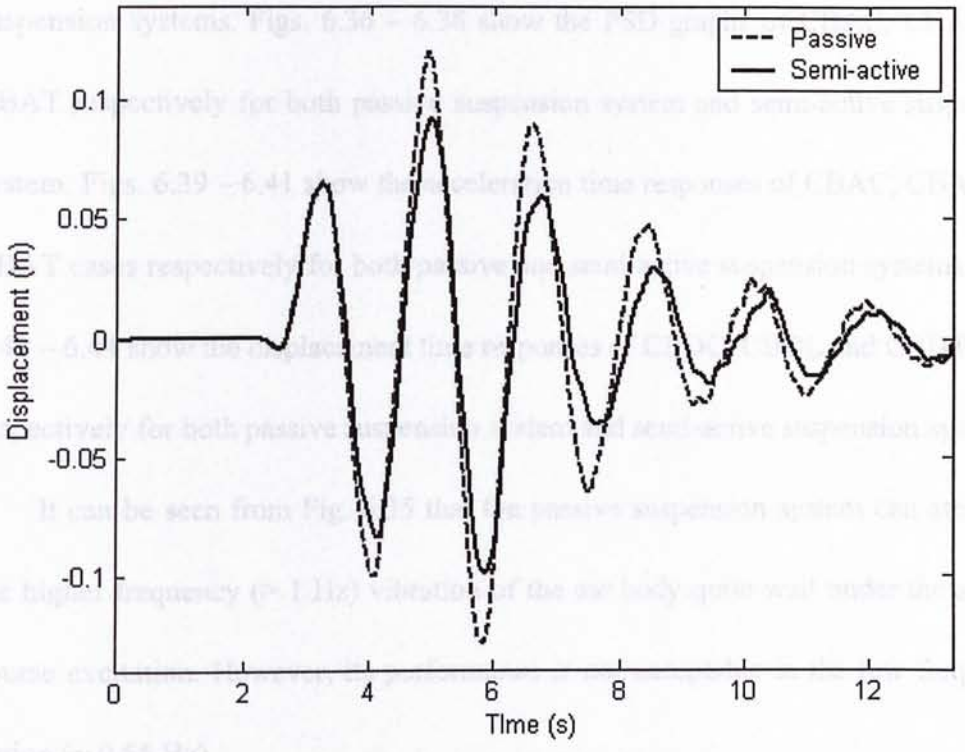

Figure 6.34: Time response graph of CBDT under mixed sway mode excitation.

TABLE 9: LATERAL RMS ACCELERATION UNDER THE MIXED MODE EXCITATION.

Suspension System	Car body center (ms^{-2})	Car body above leading bogie (ms^{-2})	Car body above trailing bogie (ms^{-2})
Passive	0.609	0.635	0.782
Passive-on-H	0.730	1.110	1.171
Passive-on-L	0.692	0.705	0.843
Semi-active	0.477	0.638	0.742

6.4.4 BR high speed assault course

Testing on BR high speed assault course, the simulation results are shown in Figs. 6.35 – 6.44. Fig. 6.35 shows the PSD graph of CBAC case with four different

suspension systems. Figs. 6.36 – 6.38 show the PSD graphs of CBAC, CBAL and CBAT respectively for both passive suspension system and semi-active suspension system. Figs. 6.39 – 6.41 show the acceleration time responses of CBAC, CBAL and CBAT cases respectively for both passive and semi-active suspension systems. Figs. 6.42 – 6.44 show the displacement time responses of CBDC, CBDL and CBDT cases respectively for both passive suspension system and semi-active suspension system.

It can be seen from Fig. 6.35 that the passive suspension system can attenuate the higher frequency (> 1 Hz) vibration of the car body quite well under the assault course excitation. However, its performance is not acceptable in the low frequency region (~ 0.55 Hz).

On the other hand, the passive-on-H and passive-on-L cases have two extreme attenuation abilities for the low frequency region (~ 0.55 Hz) and high frequency region (> 2.5 Hz) vibrations. The passive-on-H suspension system has satisfactory attenuation ability in the low frequency region and the passive-on-L case has satisfactory performance in the high frequency region. However, the passive-on-H suspension system fails to attenuate the higher frequency (> 2.5 Hz) vibration and the passive-on-L suspension system fails to attenuate the low frequency vibration (~ 0.55 Hz).

For the semi-active suspension, it possesses the vibration attenuation ability of both the passive-on-H and passive-on-L suspension systems. Semi-active suspension has better performance than the passive-on-H suspension in high frequency region (> 2.5 Hz) and low frequency region (~ 0.55 Hz). On the other hand, the semi-active

suspension has better performance than the passive-on-L case in low frequency region and it highly resembles the vibration attenuation ability of the passive-on-L suspension system in the high frequency region (> 2.5 Hz)

As shown in Figs. 6.36 and 6.38, the semi-active suspension system has better attenuation ability for CBAC and CBAT cases than the passive suspension system for almost the whole frequency range shown. For the CBAL case as shown in Fig. 6.37, the semi-active suspension system has better attenuation ability than the passive system in frequency region below 3 Hz, but it has bigger vibration amplitude at around 3.5 Hz than the passive suspension system for the CBAL case.

On the other hand, from the acceleration time responses of CBAC, CBAL and CBAT cases in Figs. 6.39 – 6.41, it can be seen that the semi-active suspension system always yields smaller acceleration amplitude than the passive system in time domain. At the same time, from the displacement time responses of CBAC, CBAL and CBAT as shown in Figs. 6.42 – 6.44, it can be seen that the semi-active suspension system yields smaller displacement amplitude than the passive system all the time for those CBDC, CBDL and CBDT cases. As mentioned in Sections 6.4.1 and 6.4.3, the semi-active suspension has better performance for displacement reduction than the passive system with the trade-off that it leads to a higher acceleration rate than the passive system in higher frequency region.

When R.M.S values as shown in Table 10 are considered, it should be noted that the semi-active suspension system has the best performance for the CBAC, CBAT and CBAL cases compared to the passive, passive-on-H and passive-on-L

suspension systems. For the passive-on-H and passive-on-L cases, although they have satisfactory performances for some frequencies, but they posses the worse R.M.S. values than the passive and semi-active systems, which means they cannot adapt to the changing needs of the vibration attenuation in general.

TABLE 10: LATERAL RMS ACCELERATION UNDER THE ASSAULT COURSE EXCITATION.

Suspension System	Car body center (ms^{-2})	Car body above leading bogie (ms^{-2})	Car body above trailing bogie (ms^{-2})
Passive	0.617	1.094	1.223
Passive-on-H	0.579	1.169	1.251
Passive-on-L	0.780	1.556	1.522
Semi-active	0.458	0.668	0.868

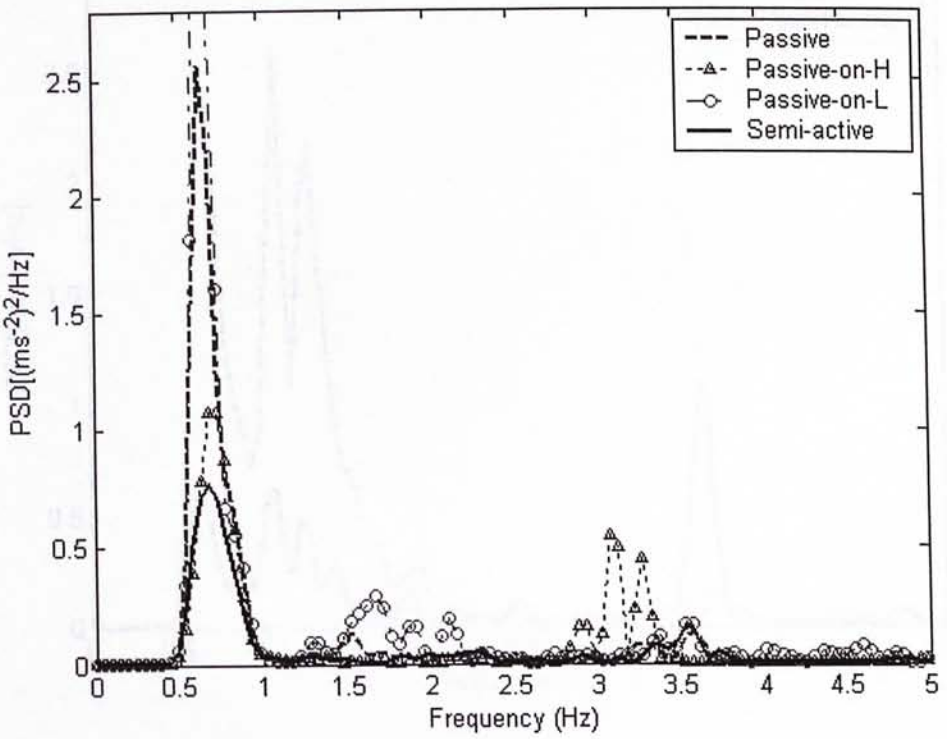

Figure 6.35: PSD graph of CBAC under assault course excitation.

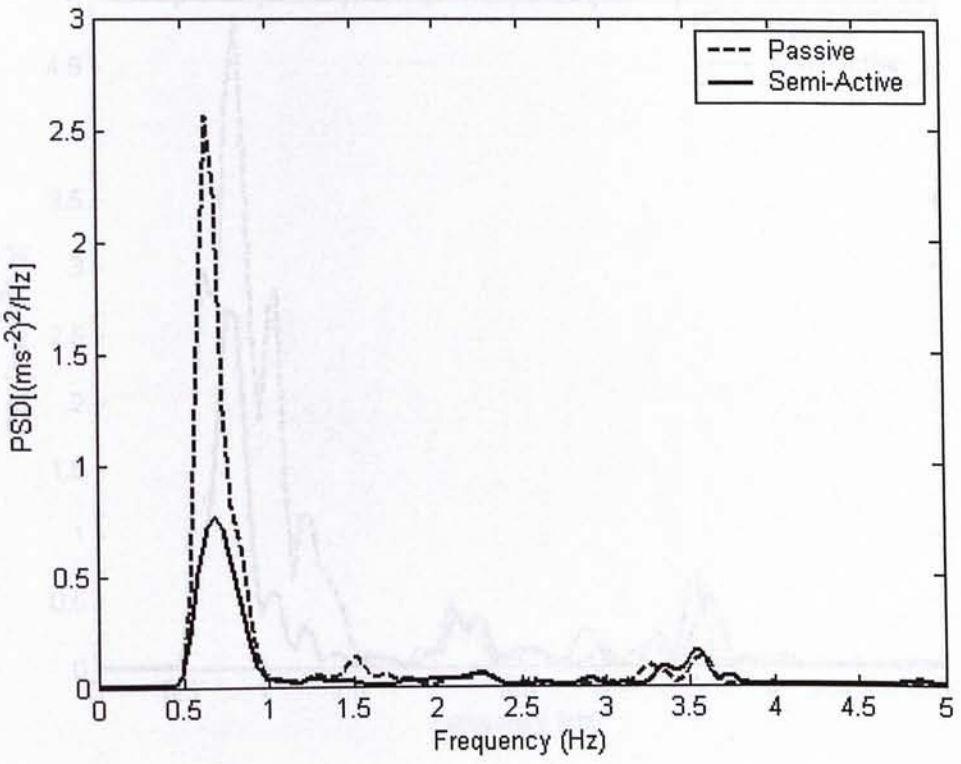

Figure 6.36: PSD graph of CBAC under assault course excitation.

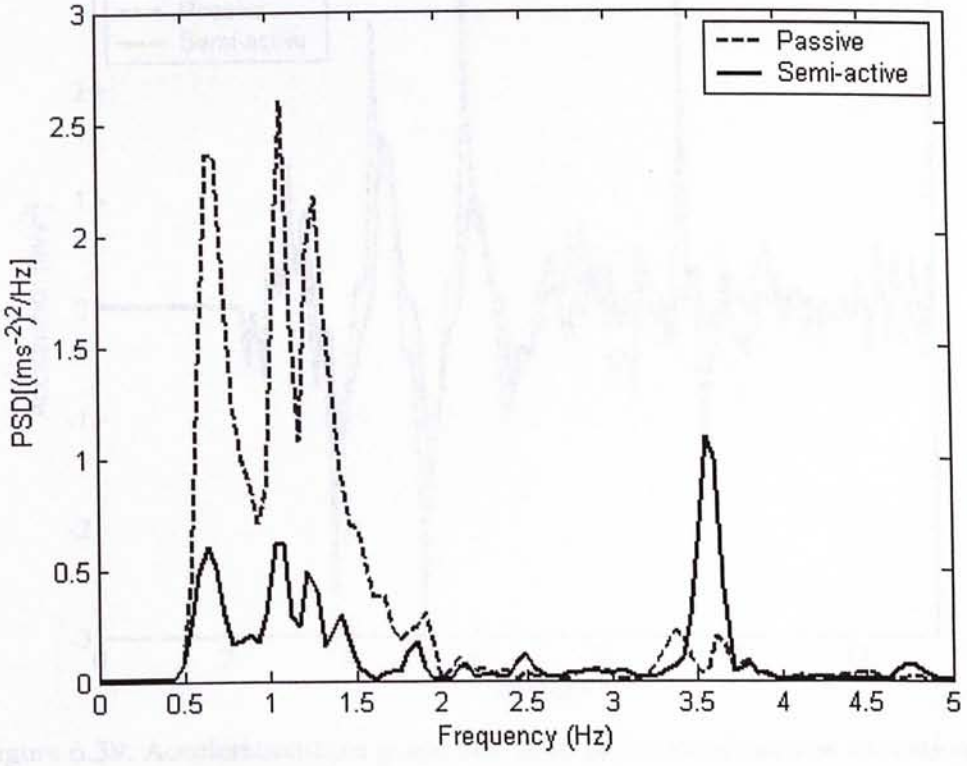

Figure 6.37: PSD graph of CBAL under assault course excitation.

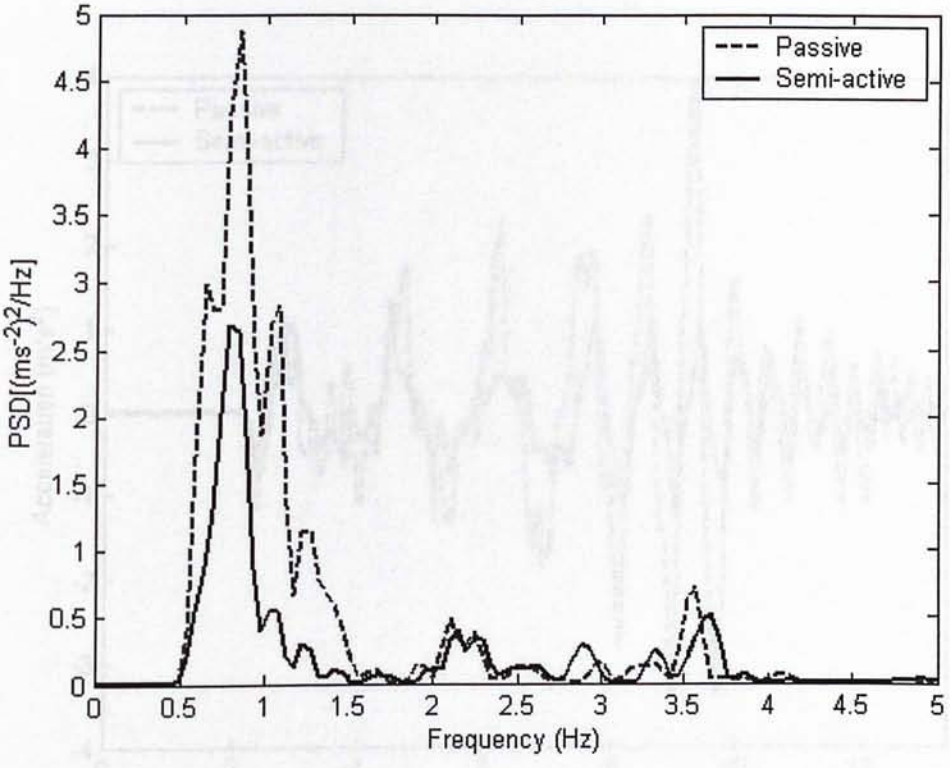

Figure 6.38: PSD graph of CBAT under assault course excitation.

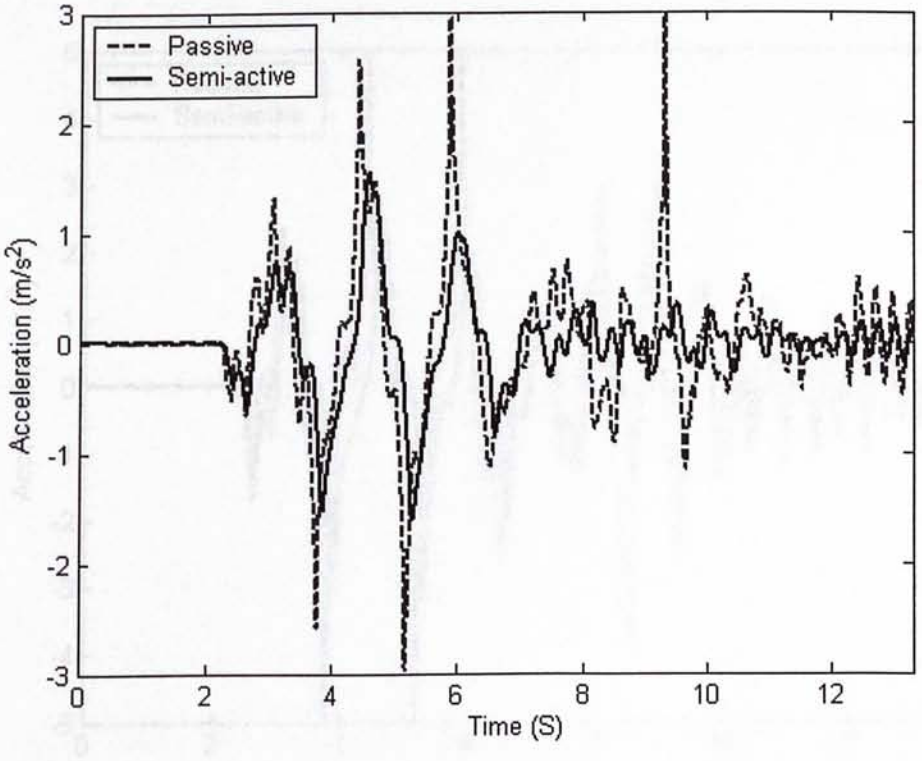

Figure 6.39: Acceleration-time graph of CBAC under assault course excitation.

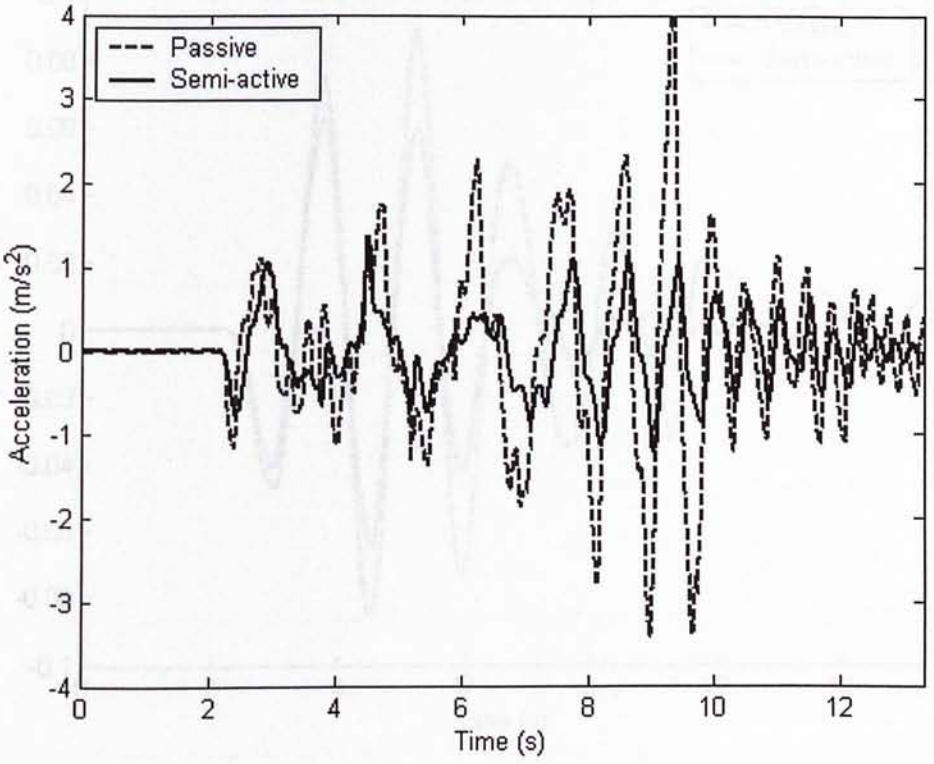

Figure 6.40: Acceleration-time graph of CBAL under assault course excitation.

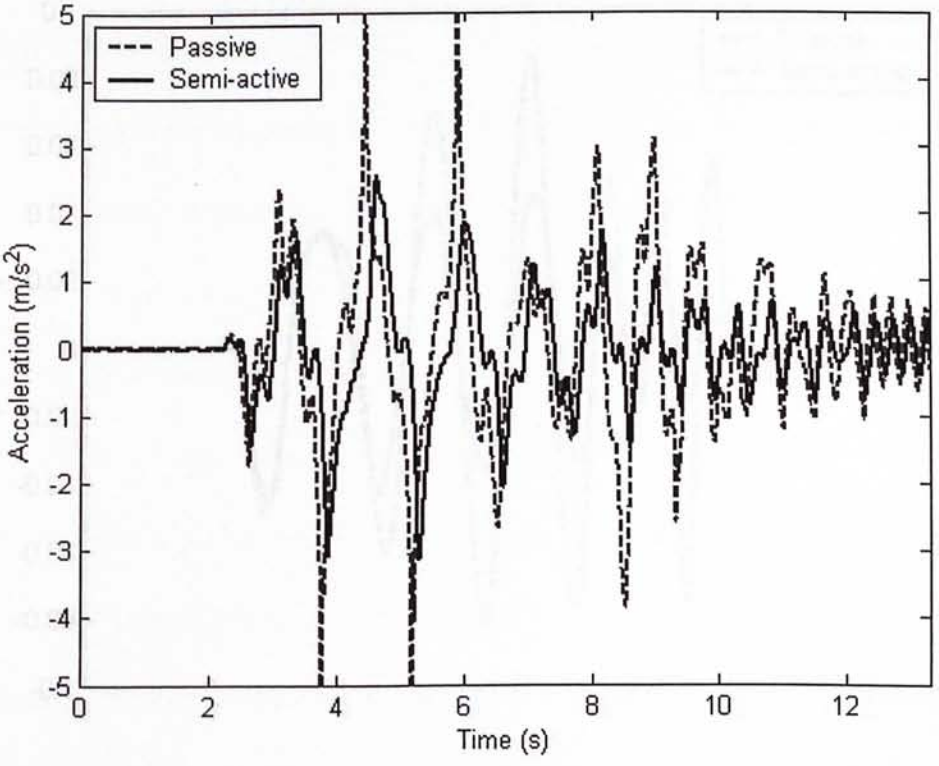

Figure 6.41: Acceleration-time graph of CBAT under assault course excitation.

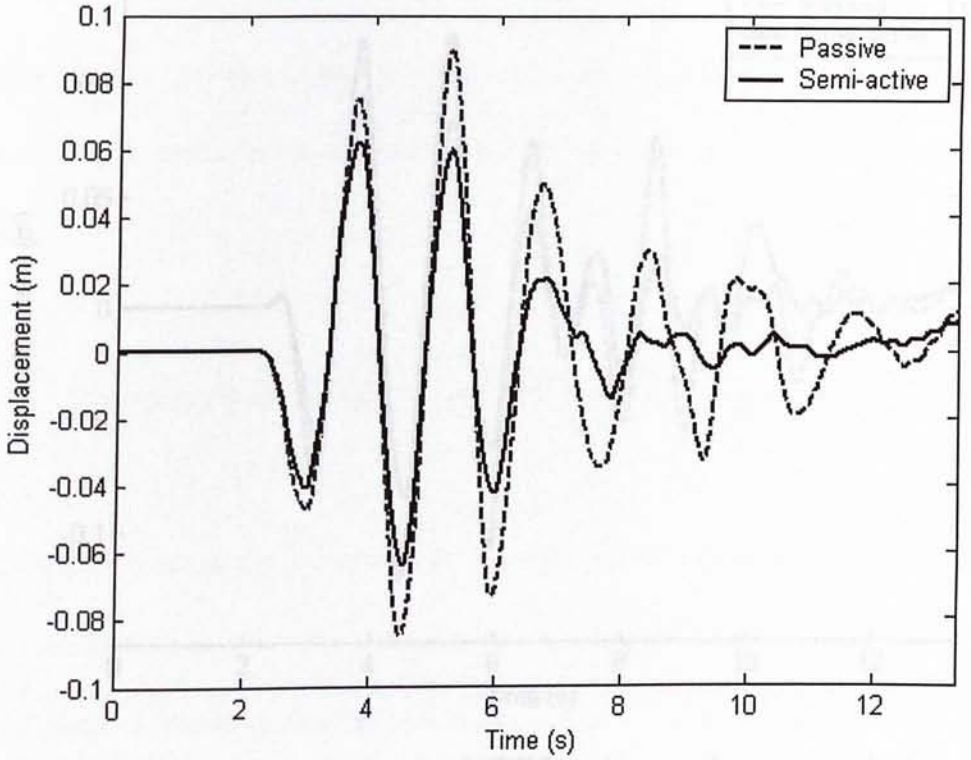

Figure 6.42: Time response graph of CBDC under assault course excitation.

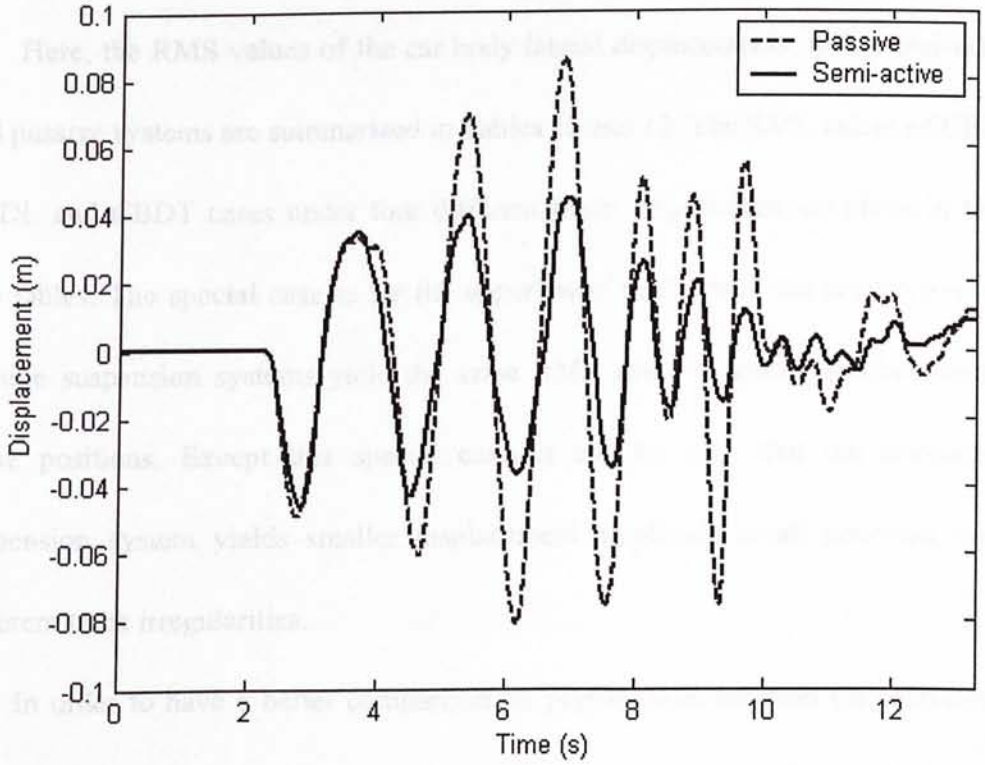

Figure 6.43: Time response graph of CBDL under assault course excitation.

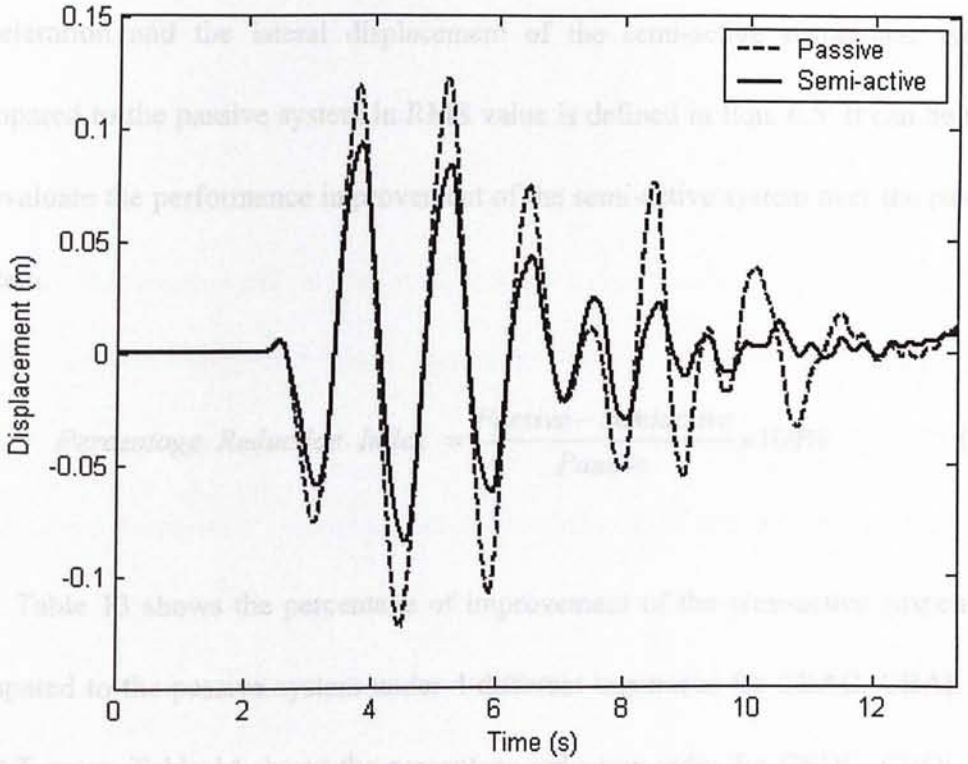

Figure 6.44: Time response graph of CBDT under assault course excitation.

6.4.5 Discussions

Here, the RMS values of the car body lateral displacements of the semi-active and passive systems are summarized in Tables 11 and 12. The RMS values of CBDC, CBDL and CBDT cases under four different track irregularities are given in these two tables. The special case is for the upper sway mode, both the semi-active and passive suspension systems yield the same RMS value of lateral displacement at those positions. Except this special case, it can be seen that the semi-active suspension system yields smaller displacement amplitude at all positions under different track irregularities.

In order to have a better comparison on performance between the semi-active suspension system and the passive system, a percentage reduction index (PRI) for the

acceleration and the lateral displacement of the semi-active suspension system compared to the passive system in RMS value is defined in Eqn. 6.5. It can be used to evaluate the performance improvement of the semi-active system over the passive system.

$$Percentage\ Reduction\ Index = \frac{Passive - Semiactive}{Passive} \times 100\% \quad (6.5)$$

Table 13 shows the percentage of improvement of the semi-active suspension compared to the passive system under 4 different test tracks for CBAC, CBAL and CBAT cases. Table 14 shows the percentage reduction index for CBDC, CBDL and CBDT cases. As shown in Table 13, the semi-active suspension has better acceleration attenuation ability than the passive system almost for all cases except the CBAL case under the mixed mode excitation, which has a PRI of – 0.4 %. It can be seen that the semi-active suspension system has about 20 – 35 % of improvement for those CBAC cases; 10 – 39 % for those CBAL cases except the CBAL cases under the mixed mode excitation, and 5 -29 % of improvement for those CBAT cases. On the other hand, as shown in Table 14, the semi-active suspension has better displacement attenuation ability than the passive system almost for all cases except the case under the upper sway mode excitation, which has the same value. It can be seen that the semi-active system has about 20 – 30 % of improvement for those CBDC cases; 20 – 40 % of improvement for those CBDL cases, and 20 -30 % of improvement for those CBAT cases.

In conclusion, it is found that the semi-active suspension system can have better performance in the acceleration as well as displacement attenuation for almost all cases. Since the assault course case can represent the general track irregularities with different frequencies and amplitudes, the semi-active suspension yields exceptional performance for the assault course case, which possesses nearly 30 % improvement in both displacement and acceleration at all positions. So it can be concluded that the semi-active suspension system has the overwhelming adaptability to the changing environment of the track irregularities for which the passive system can not attain.

However, it is still vague to evaluate the improvement of the semi-active suspension over the passive suspension by just checking the percentage of improvement of values of acceleration and displacement. Therefore, the human sensation and feel to ride comfort will be discussed in Section 6.5 to provide a more in-depth look to the improvement of the semi-active suspension.

TABLE 11: SUMMARY OF LATERAL RMS DISPLACEMENT OF PASSIVE SUSPENSION.

	Car body center (m)	Car body above leading bogie (m)	Car body above trailing bogie (m)
Lower sway mode	0.065	0.060	0.071
Upper sway mode	0.002	0.002	0.002
Mixed mode	0.040	0.036	0.044
Assault course	0.031	0.033	0.044

TABLE 12: SUMMARY OF LATERAL RMS DISPLACEMENT OF SEMI-ACTIVE SUSPENSION.

	Car body center (m)	Car body above leading bogie (m)	Car body above trailing bogie (m)
Lower sway mode	0.047	0.042	0.053
Upper sway mode	0.002	0.002	0.002
Mixed mode	0.031	0.029	0.035
Assault course	0.021	0.019	0.030

TABLE 13: PERCENTAGE IMPROVEMENT OF ACCELERATION ATTENUNTATION OF SEMI-ACTIVE SYSTEM TO PASSIVE SYSTEM.

	Car body center (ms^{-2})	Car body above leading bogie (ms^{-2})	Car body above trailing bogie (ms^{-2})
Lower sway mode	19.6 %	10 %	10.8 %
Upper sway mode	36 %	28.6 %	22.5 %
Mixed mode	35.6 %	-0.4 %	5 %
Assault course	25 %	38.9 %	29 %

TABLE 14: PERCENTAGE IMPROVEMENT OF DISPLACEMENT ATTENUNTATION OF SEMI-ACTIVE SYSTEM TO PASSIVE SYSTEM.

	Car body center (ms^{-2})	Car body above leading bogie (ms^{-2})	Car body above trailing bogie (ms^{-2})
Lower sway mode	27.6 %	30 %	25.3 %
Upper sway mode	0 %	0 %	0 %
Mixed mode	22.5 %	19.4 %	20.4 %
Assault course	32.3 %	42.4 %	31.8 %

6.5 Effects of Vibration on Ride Comfort

The ride comfort of seated persons occurs in all six axes on the seat pan (three translational: x, y and z; and three rotational: r_x, r_y, and r_z). It also happens to the three translational axes (x, y and z) at the seat-back and feet of seated persons (see Fig. 6.45). The comfort of a standing person occurs in the three translational (x, y and z) axes on the principal surface supporting the body vibration. In this study, we will focus on the lateral direction (y-direction) of the vibration, which is sensible for railway applications.

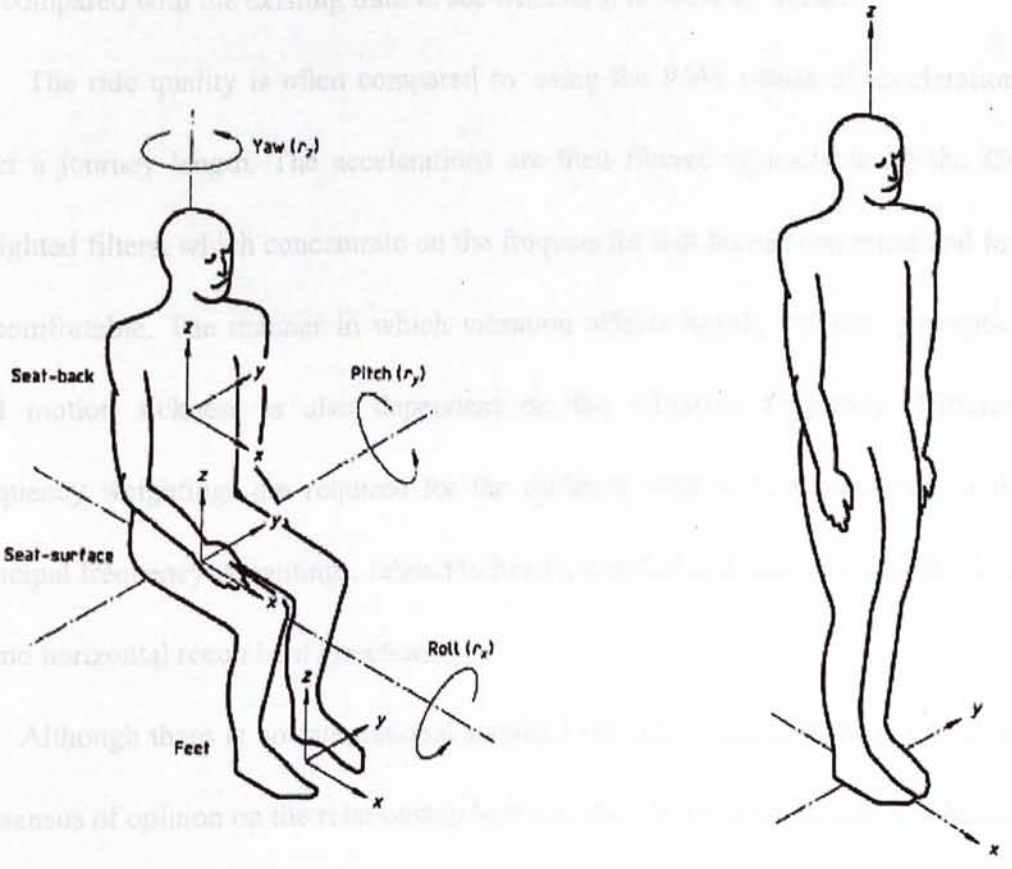

Figure 6.45: Basicentric axes of human body [45].

According to the *ISO* 2631-1 [45], the perception (definition and reaction of ride comfort) is highly dependent on the passenger expectation with regards to trip duration and the type of activities passengers expect to accomplish (e.g. reading, eating, writing, napping, etc.) and many other factors (acoustic noise, temperature, etc.). Therefore, the ride quality is usually specified by the customer taking the train and it may be "as good as" or "better than" an existing train. In such cases, accelerometers can be used to measure the accelerations of a train on a specific length of track or journey at a constant speed. Then the measured accelerations can be compared with the existing train to see whether it is better or worse.

The ride quality is often compared by using the RMS values of accelerations over a journey length. The accelerations are then filtered typically using the *ISO* weighted filters, which concentrate on the frequencies that human can sense and feel uncomfortable. The manner in which vibration affects health, comfort, perception and motion sickness is also dependent on the vibration frequency. Different frequency weightings are required for the different axes of vibration. One of the principal frequency weightings, related to health, comfort and perception, is W_d for x, y, and horizontal recumbent direction.

Although there is no international standard for ride comfort, there is still some consensus of opinion on the relationship between the vibration magnitude and human comfort. Table 15 gives the approximate indications of human's likely reactions to various magnitudes of vibration (frequency weighted RMS values in either the vertical, lateral and longitudinal directions) in public transport. In order to have a

better comparison to those sensation of ride comfort, notations from A – F are used to label the comfort level, "A" represents "Not uncomfortable" to the descending order that "F" represents "Extremely uncomfortable". Then the overlapped state of ride comfort level is represented as B-C, C-D or D-C, etc. Fig. 6.46 shows the histogram of the values of human reaction toward ride comfort and the corresponding comfort levels assigned. The corresponding results and comparisons of the performances between the semi-active suspension and passive suspension are shown in Tables 16 – 20.

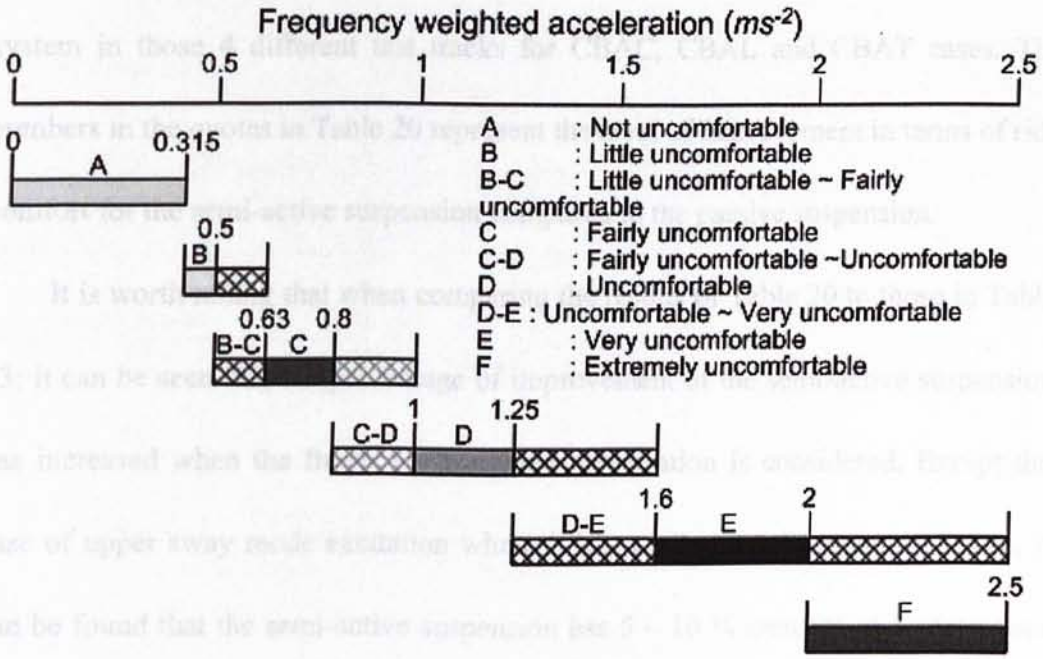

Figure 6.46: The histogram of human reaction to acceleration [45].

TABLE 15: APPROXIMATE INDICATIONS OF LIKELY REACTIONS TO VARIOUS MAGNITUDES OF VIBRATION IN PUBLIC TRANSPORT

Less than 0.315 ms^{-2}	not uncomfortable (A)
0.315 ms^{-2} to 0.63 ms^{-2}	a little uncomfortable (B)
0.5 ms^{-2} to 1 ms^{-2}	fairly uncomfortable (C)
0.8 ms^{-2} to 1.6 ms^{-2}	Uncomfortable (D)
1.25 ms^{-2} to 2.5 ms^{-2}	very uncomfortable (E)
Greater than 2 ms^{-2}	extremely uncomfortable (F)

Tables 16 and 17 show the frequency weighted (ISO W_d) RMS values of the car body lateral acceleration of the passive and semi-active suspensions in 4 different test tracks for CBAC, CBAL and CBAT cases respectively. Besides, Tables 18 and 19 shows the corresponding comfort level of the passive and semi-active suspensions in those 4 different test tracks according to the frequency weighted (ISO W_d) RMS values of the car body lateral acceleration in Tables 16 and 17. Finally, Table 20 shows the percentage improvement of the frequency weighted (ISO W_d) lateral acceleration attenuation of the semi-active suspension compared to the passive system in those 4 different test tracks for CBAC, CBAL and CBAT cases. The numbers in the quotes in Table 20 represent the level of improvement in terms of ride comfort for the semi-active suspension compared to the passive suspension.

It is worth noting that when comparing the results of Table 20 to those in Table 13; it can be seen that the percentage of improvement of the semi-active suspension has increased when the frequency weighted acceleration is considered. Except the case of upper sway mode excitation where it has similar improvement as before, it can be found that the semi-active suspension has 5 – 10 % increase of performance compared to the passive suspension for those CBAC, CBAL and CBAT cases when the frequency weighted acceleration is considered. This leads to the conclusion that when the human sensation to ride comfort is considered, the semi-active suspension system has even more significant improvement than the passive suspension system.

On the other hand, except for the case of upper sway mode excitation, the semi-active suspension has one to two levels of improvement when the comparison

is made by considering the ride comfort level as shown in Table 20. This means that the semi-active suspension can improve the grade of passenger's ride comfort, where the passenger can feel; it is not just a reduction of meaningless numerical value.

TABLE 16: FREQUENCY WEIGHTED (ISO W_d) LATERAL RMS ACCELERATION OF PASSIVE SUSPENSION.

	Car body center (ms^{-2})	Car body above leading bogie (ms^{-2})	Car body above trailing bogie (ms^{-2})
Lower sway mode	0.817	0.818	0.919
Upper sway mode	0.192	0.209	0.260
Mixed mode	0.506	0.501	0.624
Assault course	0.564	1.036	1.152

TABLE 17: FREQUENCY WEIGHTED (ISO W_d) LATERAL RMS ACCELERATION OF SEMI-ACTIVE SUSPENSION.

	Car body center (ms^{-2})	Car body above leading bogie (ms^{-2})	Car body above trailing bogie (ms^{-2})
Lower sway mode	0.591	0.619	0.733
Upper sway mode	0.122	0.152	0.203
Mixed mode	0.376	0.439	0.537
Assault course	0.394	0.536	0.764

TABLE 18: FREQUENCY WEIGHTED (ISO W_d) COMFORT LEVEL OF PASSIVE SUSPENSION.

	Car body center	Car body above leading bogie	Car body above trailing bogie
Lower sway mode	(C-D)	(C-D)	(C-D)
Upper sway mode	(A)	(A)	(A)
Mixed mode	(B-C)	(B-C)	(B-C)
Assault course	(B-C)	(D)	(D)

TABLE 19: FREQUENCY WEIGHTED (ISO W_d) COMFORT LEVEL OF SEMI-ACTIVE SUSPENSION.

	Car body center	Car body above leading bogie	Car body above trailing bogie
Lower sway mode	(B-C)	(B-C)	(C)
Upper sway mode	(A)	(A)	(A)
Mixed mode	(B)	(B)	(B-C)
Assault course	(B)	(B-C)	(C)

TABLE 20: PERCENTAGE IMPROVEMENT OF FREQUENCY WEIGHTED (ISO W_d) VIBRATION ATTENUNTATION OF SEMI-ACTIVE SUSPENSION TO PASSIVE SUSPENSION.

	Car body center	Car body above leading bogie	Car body above trailing bogie
Lower sway mode	27.7 % (2)	24.3 % (2)	20.2 % (1)
Upper sway mode	36.4 % (0)	27.3 % (0)	21.9 % (0)
Mixed mode	25.7 % (1)	12.4 % (1)	13.9 % (0)
Assault course	30.1 % (1)	48.2 % (3)	33.7 % (2)

CHAPTER 7

CONCLUSIONS

In this thesis, the primary objective is to develop a semi-active train suspension system using MR dampers that can improve the current passive suspension system in railway vehicle, so that the ride comfort of the passenger can be improved. To achieve this, the other objective is to develop and fabricate a custom-made MR damper, which is suitable for railway vehicle suspension. A fundamental understanding of the behavior of the MR damper has been developed through the design, experiments, and mathematical modeling of the MR damper.

First of all, different designs and structures of current MR dampers have been studied to find out a suitable type of MR damper for this research. The double-ended type MR damper is chosen because it is best fit to the requirement. Then the MR damper geometry design and the basic magnetic circuit concerning double-ended MR damper have been studied.

After design parameters have been determined, the custom-made MR damper is fabricated. Additional practical considerations of MR damper design including modification process, sealing and wire wrapping have been investigated.

The fabricated MR damper has been tested under various conditions in order to investigate its behaviors. Then, the MR damper I has encountered the force-lag problem, which deteriorates the damper performance. The reasons for the force-lag phenomenon have been investigated so that the special MR fluid filling setup is used to increase the internal pressure of the MR damper. Besides, MR damper II is fabricated with more precise dimensions.

Finally, simulation of the semi-active train suspension using MR dampers has been done. The MR damper is mathematically modeled in SIMULINK with experimental validation and then integrated with the railway vehicle model in the railway dynamic software VAMPIRE©. The passive, passive-on-H, passive-on-L and semi-active suspension systems are tested with four different test tracks including the lower sway mode, upper sway mode, mixed sway mode and BR high speed assault course. An on-off semi-active control strategy based on the measurement of the absolute lateral velocity of the car body is adopted for the semi-active suspension system. The performance of the semi-active train suspension system using MR dampers is evaluated by comparing with the passive, passive-on-H and passive-on-L suspension systems. The results indicate that the semi-active suspension with the developed MR dampers outperforms those passive suspension systems and it can improve the ride quality of the passenger substantially.

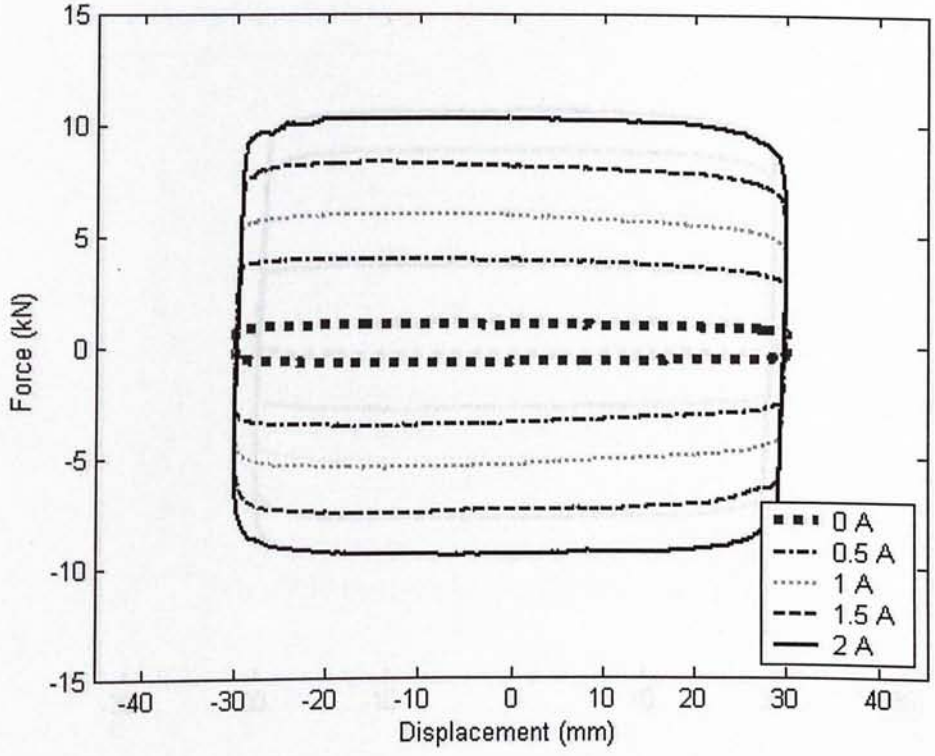

Figure A.1: Force-displacement graph under 30 mm, 0.05 Hz sinusoidal displacement excitation.

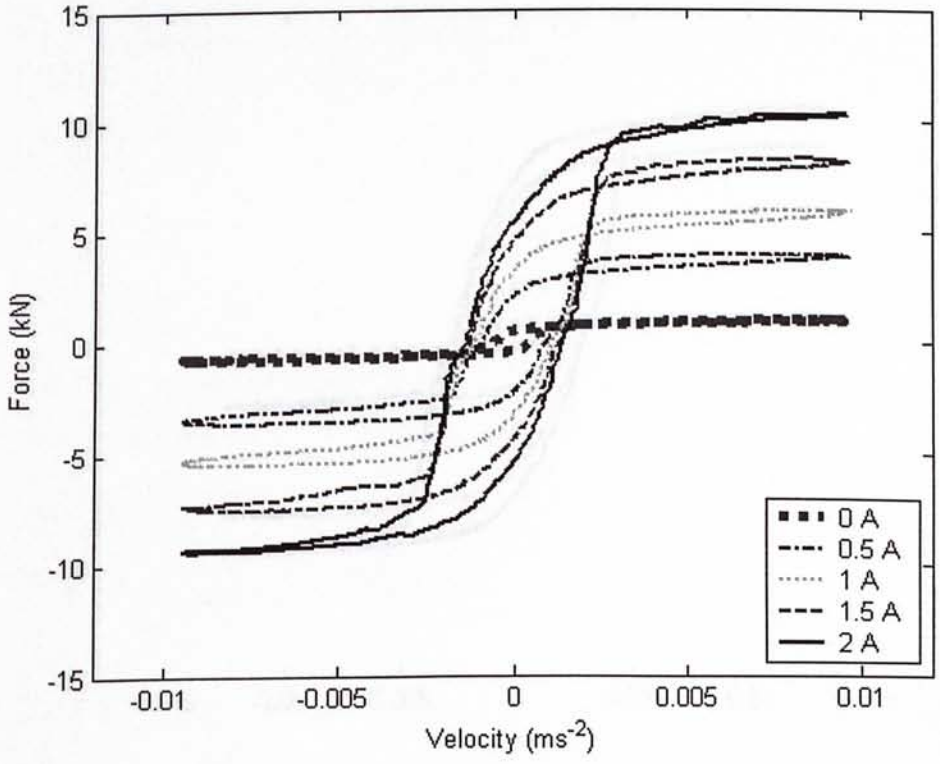

Figure A.2: Velocity-displacement graph under 30 mm, 0.05 Hz sinusoidal displacement excitation.

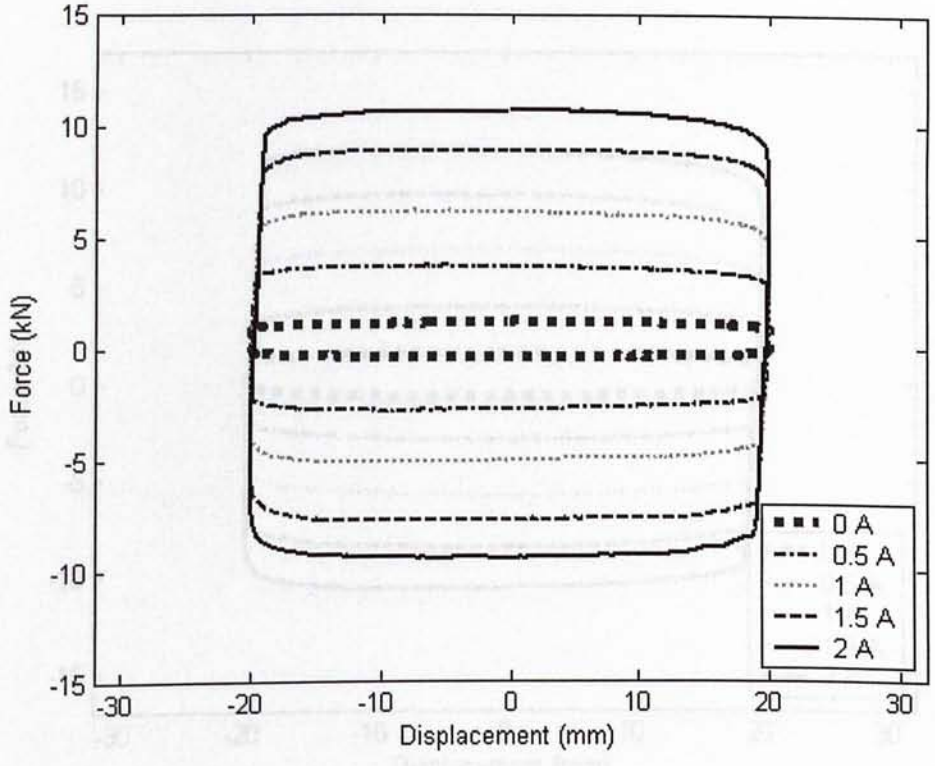

Figure A.3: Force-displacement graph under 20 mm, 0.1 Hz sinusoidal displacement excitation.

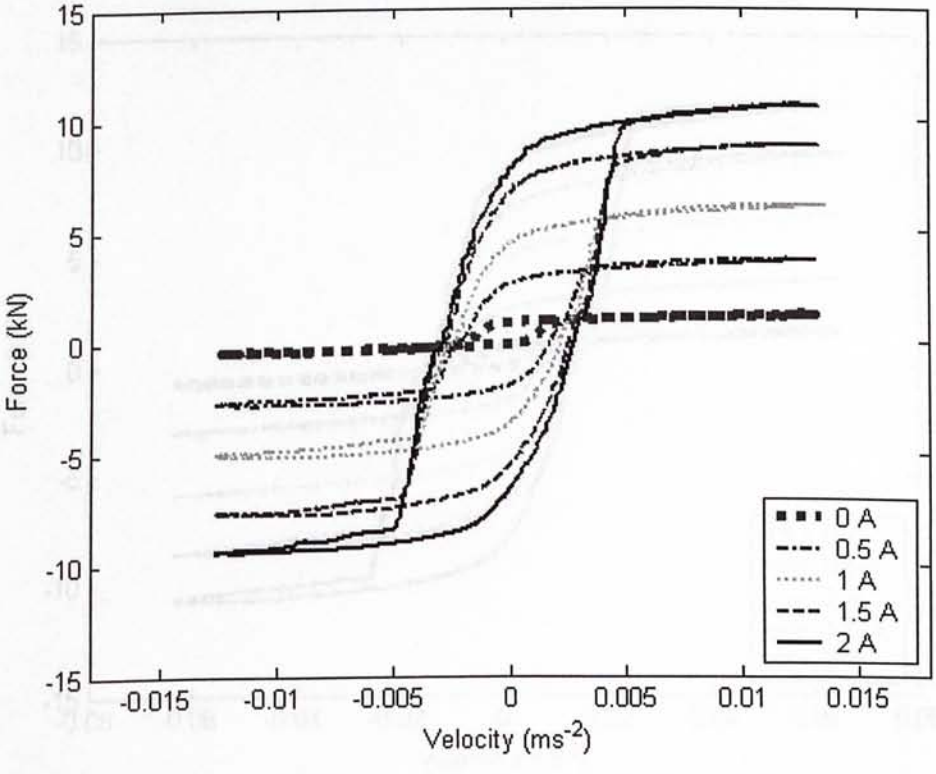

Figure A.4: Velocity-displacement graph under 20 mm, 0.1 Hz sinusoidal displacement excitation.

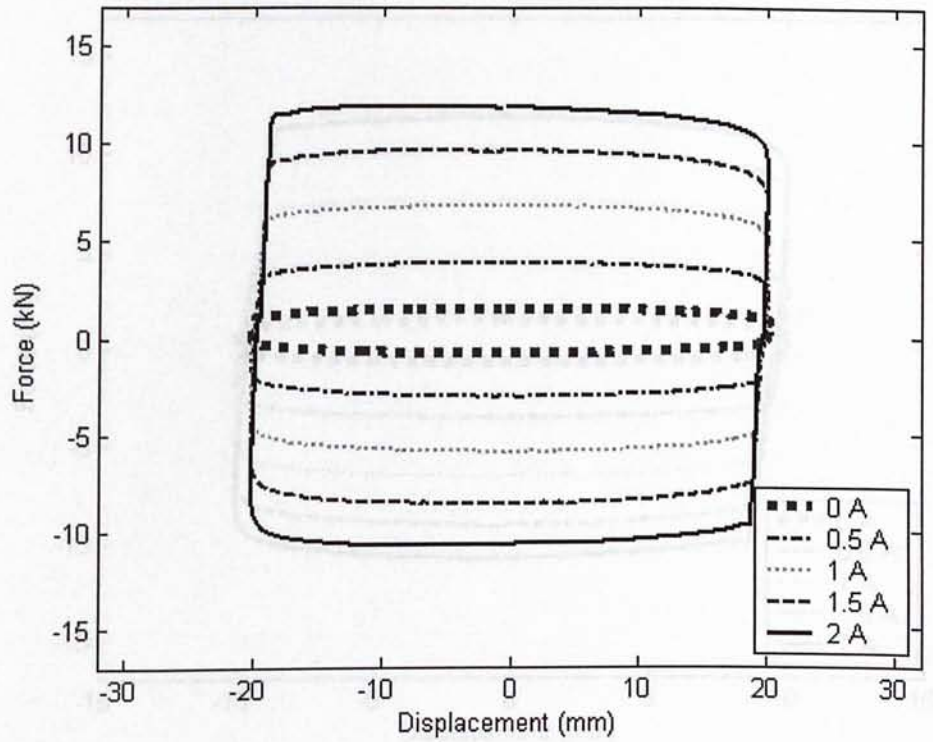

Figure A.5: Force-displacement graph under 20 mm, 0.5 Hz sinusoidal displacement excitation

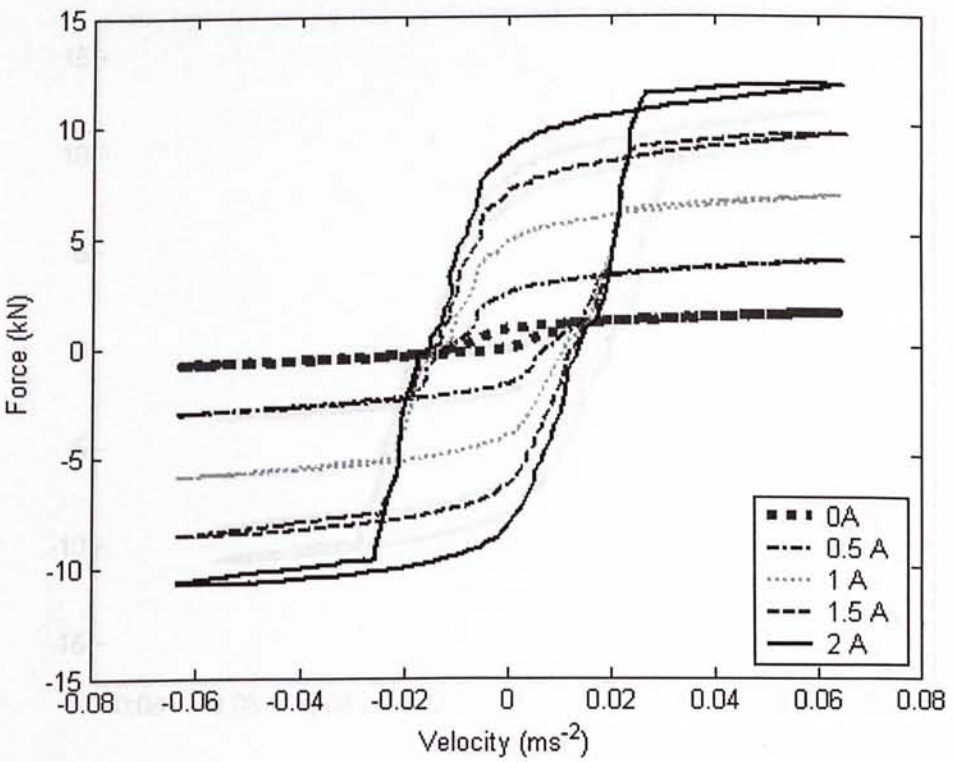

Figure A.6: Force-velocity graph under 20 mm, 0.5 Hz sinusoidal displacement excitation

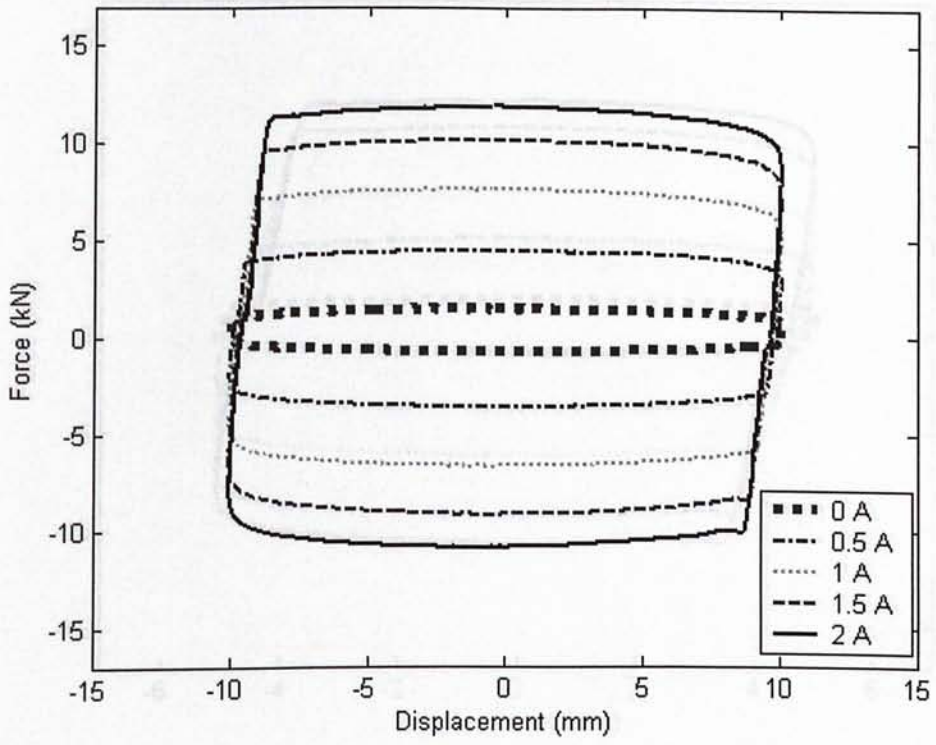

Figure A.7: Force-displacement graph under 10 mm, 1 Hz sinusoidal displacement excitation.

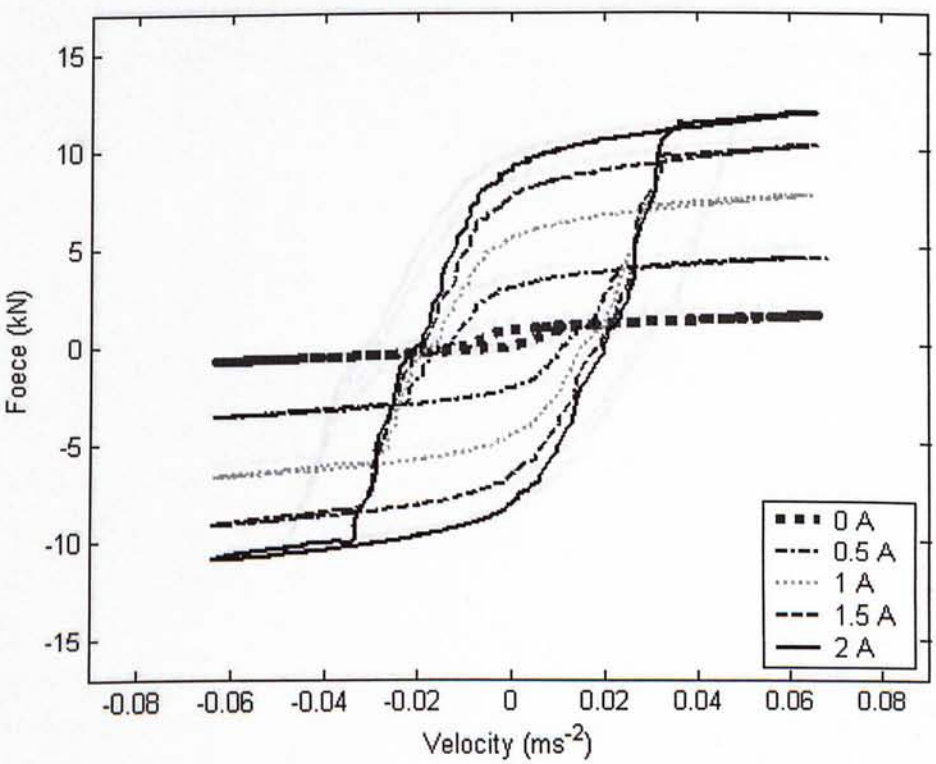

Figure A.8: Force-velocity graph under 10 mm, 1 Hz sinusoidal displacement excitation.

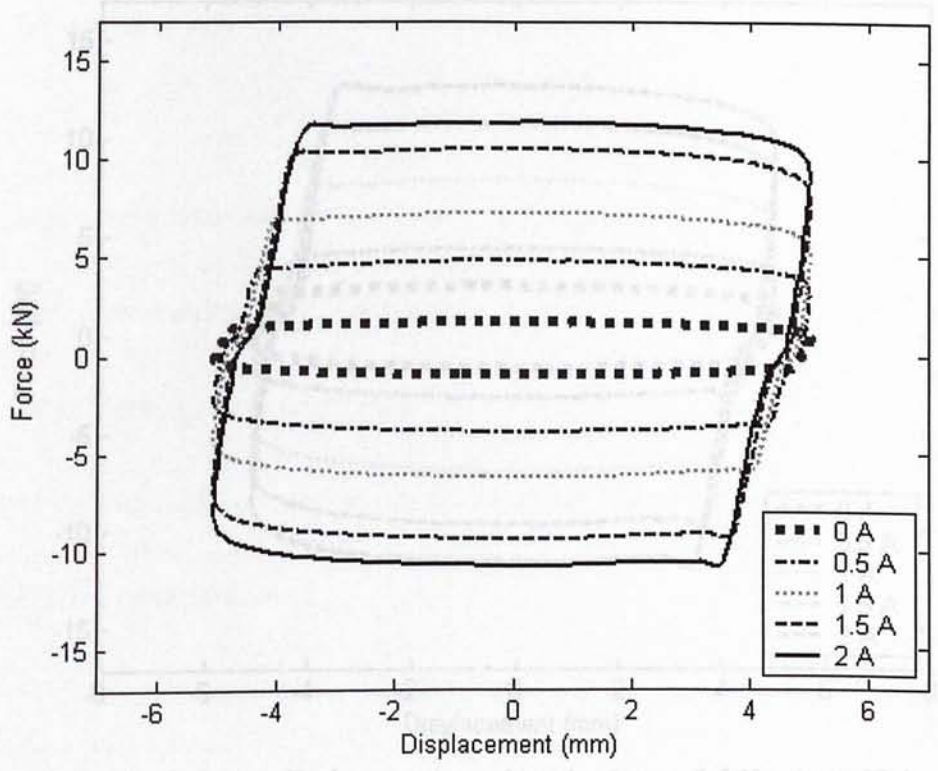

Figure A.9: Force-displacement graph under 5 mm, 2 Hz sinusoidal displacement excitation.

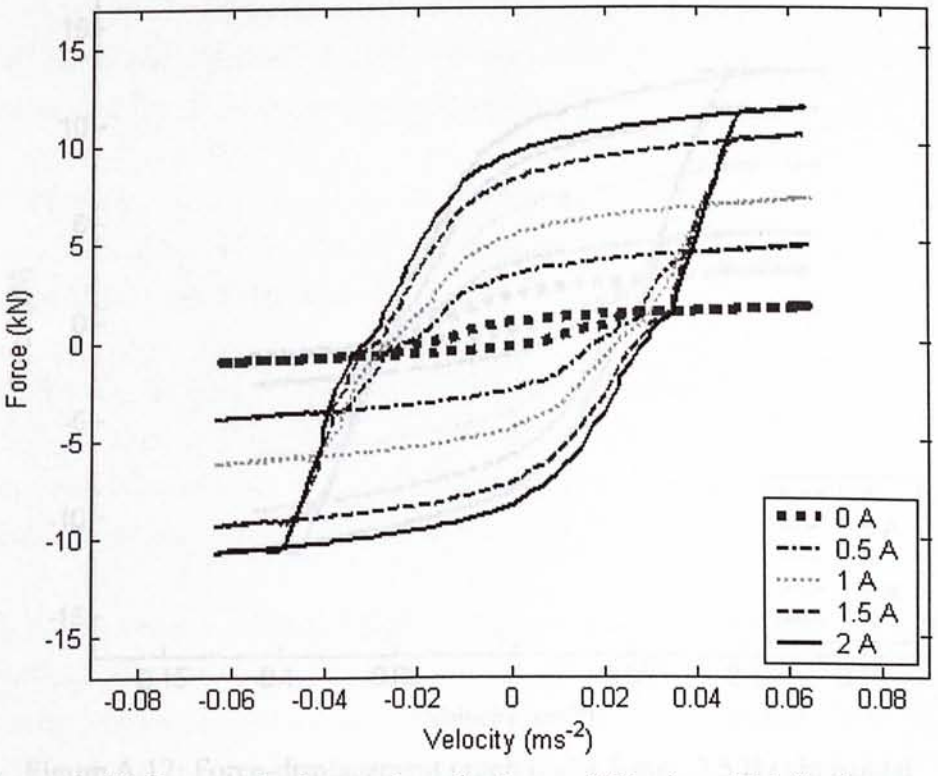

Figure A.10: Force-velocity graph under 5 mm, 2 Hz sinusoidal displacement excitation.

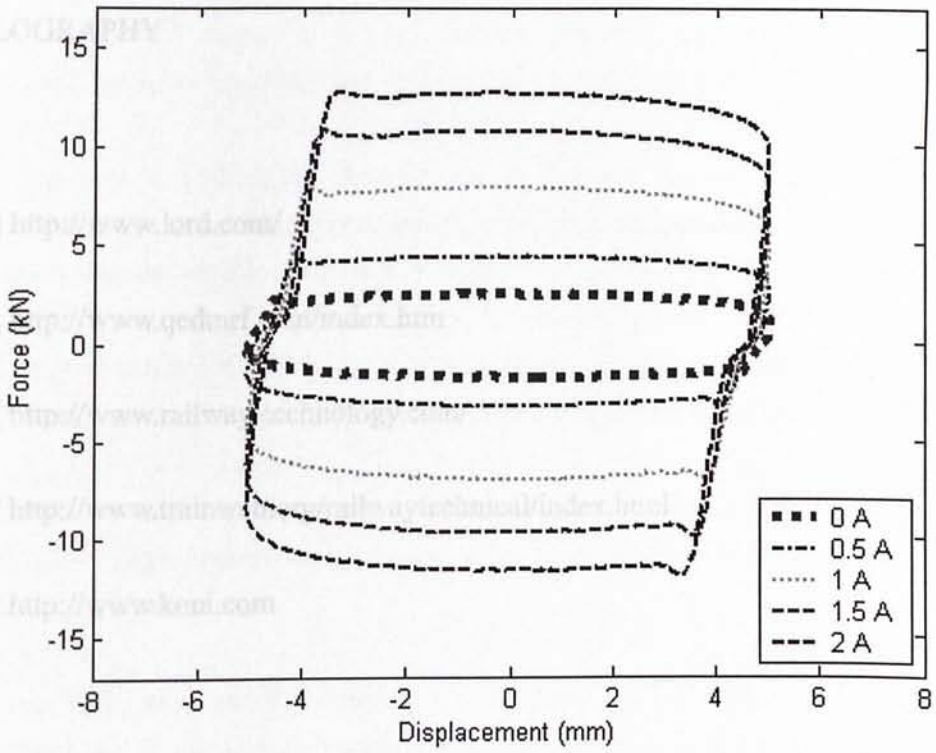

Figure A.11: Force-displacement graph under 5 mm, 3.5 Hz sinusoidal displacement excitation

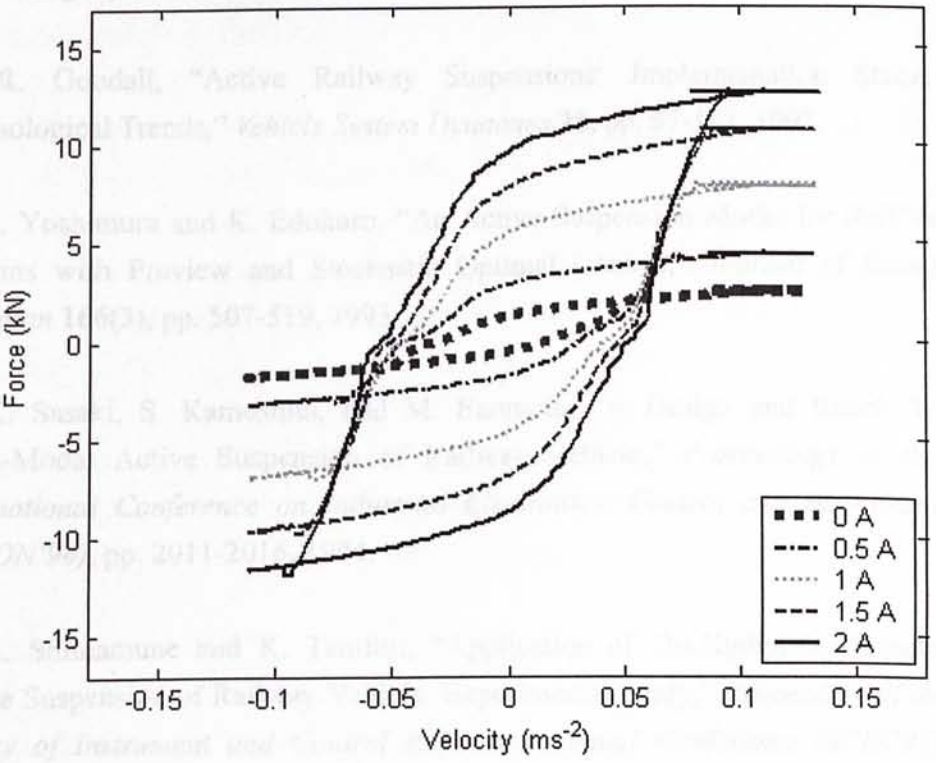

Figure A.12: Force-displacement graph under 5 mm, 3.5 Hz sinusoidal displacement excitation

BIBLOGRAPHY

[W1] http://www.lord.com/

[W2] http://www.qedmrf.com/index.htm

[W3] http://www.railway-technology.com/

[W4] http://www.trainweb.org/railwaytechnical/index.html

[W5] http://www.koni.com

[1] V. S. Atray and P. N. Roschke, "Design, Fabrication, Testing, and Fuzzy Modeling of a Large Magnetorheological Damper for Vibration Control in a Railcar," *Proceedings of the 2003 IEEE/ASME Joint Rail Conference*, pp. 223-229, 2003.

[2] R. Goodall, "Active Railway Suspensions: Implementation Status and Technological Trends," *Vehicle System Dynamics* **28**, pp. 87-117, 1997.

[3] T. Yoshimura and K. Edokoro, "An Active Suspension Model for Rail/Vehicle Systems with Preview and Stochastic Optimal Control," *Journal of Sound and Vibration* **166(3)**, pp. 507-519, 1993.

[4] K. Sasaki, S. Kamoshita, and M. Enomoto, "A Design and Bench Test of Multi-Modal Active Suspension of Railway Vehicle," *Proceedings of the 20th International Conference on Industrial Electronics, Control and Instrumentation (IECON'94)*, pp. 2011-2016, 1994.

[5] R. Shimamune and K. Tanifuji, "Application of Oil-Hydraulic Actuator for Active Suspension of Railway Vehicle: Experimental Study," *Proceeding of the 34th society of Instrument and Control Engineers Annual Conference (SCIE'95)*, pp. 1335-1340, 1995.

[6] M. Nagai and R. Shinano, "Study on Active Vibration Control for High Speed Railway Vehicles Using a Full-Vehicle Model," *Proceedings of the 5th International Symposium on Advanced Vehicle Control (AVEC 2000)*, pp. 645-652, 2000.

[7] L. Jezequel, V. Roberti, B. Ouyahia, and Y. Toutain, "Improvement of Very High Speed Trains Comfort with Preview Semi-Active Suspensions," *Vehicle System Dynamics Supplement* **23**, pp. 299-313, 1993.

[8] H. R. O'Neill and G. D. Wale, "Semi-Active Suspension Improves Rail Vehicle Ride," *Computing & Control Engineering Journal* **5(4)**, pp. 183-188, 1994.

[9] H. Fujimoto and M. Miyamoto, "Measures to Reduce the Lateral Vibration of the Tail Car in a High Speed Train," *Proceedings of Institute of Mechanical Engineers*, Vol. 210, pp. 87-93, 1996.

[10] A. Stribersky, A. Kienberger, G. Wagner, and H. Muller, "Design and Evaluation of a Semi-Active Damping for Rail Vehicles," *Vehicle System Dynamics Supplement* **28**, pp. 669-681, 1998.

[11] H. S. Tzou and G. L. Anderson, "Intelligent Structural Systems," *Kluwer Academic Publishers*, 1992.

[12] J. D. Carlson and K. D. Weiss, "A Growing Attraction to Magnetic Fluids," *Machine Design*, pp. 61-64, August 1994.

[13] N. D. Sims, R. Stanway, and A. R. Johnson, "Vibration Control Using Smart Fluids: A State-of-the-Art Review," *The Shock and Vibration Digest*, Vol. 31, No. 3, pp. 195-203, 1999.

[14] J. D. Carlson and B. F. Spencer Jr., "Magneto-Rheological Fluid Dampers for Semi-Active Seismic Control," *Proceedings of the 3rd International Conference on Motion and Vibration Control*, Vol. III, pp. 35-40, 1996.

[15] W. H. Liao and D. H. Wang, "Semiactive Vibration Control of Train Suspension Systems via Magnetorheological Dampers," *Journal of Intelligent Material Systems and Structures*, Vol. 14, No. 3, pp. 161-172, 2003.

[16] D. H. Wang and W. H. Liao, "Ride Quality Improvement Ability of Semi-Active, Active and Passive Suspension Systems for Railway Vehicles," *Proceedings of SPIE Conference on Smart Structures and Materials*, SPIE Vol. 5056, pp. 201-212, 2003.

[17] O. Ashour, D. Kinder, and V. Giurgiutiu and C. Rogers, "Manufacturing and Characterization of Magnetorheological Fluids," *Proceedings of SPIE Conference on Smart Structures and Materials: Smart Materials Technologies*, SPIE Vol. 3040, pp. 174-184, 1997.

[18] J. D. Carlson and B. F. Spencer Jr., "Magneto-rheological Fluid Dampers: Scalability Band Design Issues for Application to Dynamic Hazard Mitigation," *Proc. 2nd Workshop on Structural Control: Next Generation of Intelligent Structures*, Hong Kong. China, pp. 99-109, 1996.

[19] G. Yang, "Large-scale Magnetorheological Fluid Damper for Vibration Mitigation: Modeling, Testing and Control," *P.H.D. dissertation*, University of Notre Dame, December 2001.

[20] G. M. Kamath, and N. M. Wereley, "A Nonlinear Viscoelastic-plastic Model for Electrorheological Fluids," *Smart Material and Structures*, 6, 351, 1997.

[21] M. R. Jolly, J. W. Bender and J. D. Carlson, "Properties and Applications of Commercial Magnetoeheological Fluids," *SPIE 5th Annual International Symposium on Smart Structures and Materials*, San Diego, CA, March 15, 1998.

[22] M. Muriuki and W. W. Clark, "Design Issues in Magnetorheological Fluid Actuators," *Proc. Smart Structures and Materials: Passive Damping and Isolation*, SPIE Vol. 3672, pp. 55-64, 1999.

[23] "MR Brake – MRB-2107-3 Product Bulletin," *Lord Corporation Product Bulletin.*

[24] "Vibration and Seat Design," *Lord Corporation*, March, 2001.

[25] "MR 180 KN Damper," *Lord Corporation Product Bulletin.*

[26] I. Okamoto, "Railway Technology Today 5 - How Bogies Work," *Japan*

Railway & Transport Review No. 18, pp. 52–61, 1998.

[27] J. D. Carlson, "What Makes a Good Fluids?," *8th International Conference on ER Fluids and MR Fluids Suspensions*, Nice, July 9-13, 2001.

[28] S. J. Dyke, B. F. Spencer, Jr., M. K. Sain and J. D. Carlson, "Modeling and Control of Magnetorheological Dampers for Seismic Response Reduction," *Smart Materials and Structures*, Vol. 5, pp. 565-575, 1996.

[29] L. Pang, G. M. Kamath, N. M. Wereley, "Dynamic Characterization and Analysis of Magnetorheological Damper Behavior," *Proceedings of SPIE Conference on Smart Structures and Materials: Passive Damping and Isolation*, SPIE Vol. 3327, pp. 284-302, 1998.

[30] B. F. Spencer, Jr., G. Yang, J. D. Carlson, and M. K. Sain, "Smart Dampers for Seismimc Protection of Structures: A Full-scale Study," *Proceedings of the Second World Conference on Structural Control (2WCSC)*, Kyoto, Japan, Vol. 1, pp. 417-426, June 28 - July 1, 1998.

[31] K. Sunakoda, H. Sodeyama, N. Iwata, H. Fujitani, S. Soda, "Dynamic Characteristics of Magneto-rheological Fluid Damper," *Proceedings of SPIE's 7th Annual International Symposium on Smart Structures and Materials*, No. 3989-20, 2000.

[32] G. Yang, H. J. Jung, and B. F. Spencer, Jr. "Dynamic Modeling of Full-scale MR Dampers for Civil Engineering Applications," *Proc. US-Japan Workshop on Smart Structures for Improved Seismic Performance in Urban Region,* Seattle, WA, August 14–16, 2001.

[33] S. P. Kelso, "Experimental Characterization of Commercially Practical Magnetorheological Fluid Damper Technology," *Proc. Smart Structures and Materials: Industrial and Commercial Applications of Smart Structures Technologies*, SPIE Vol. 4332, pp. 292-299, 2001.

[34] H. Gavin, J. Hoagg and M. Dobossy, "Optimal Design of MR Dampers," *Proc. U.S.-Japan Workshop on Smart Structures for Improved Seismic Performance in Urban Regions*, pp. 225-236, August 14, 2001.

[35] J. C. Poynor, "Innovative Designs for Magneto-Rheological Dampers," *Master of Science Thesis*, Virginia Polytechnic Institute and State University, Department of Mechanical Engineering, August 2001.

[36] B. F. Spencer, Jr., S. J. Dyke, M. K. Sain and J. D. Carlson, "Phenomenological Model of a Magnetorheological Damper," *J.Engineering. Mech.*, ASCE, 123:230-238, 1997.

[37] G. Yang, B. F. Spencer, Jr., J. D. Carlson, and M. K. Sain, "Large-Scale MR Fluid Dampers: Modeling and Dynamic Performance Considerations," *Engineering Structures,* 24(3), pp. 309-323, 2002

[38] N. D. Sims, N. J. Holmes and R. Stanway, "A Unified Modelling and Model Updating Procedure for Electrorheological and Magnetorheological Vibration Dampers," *Smart Materials and Structures*, Volume 13, Number 1, pp. 100-121, Feb. 2004.

[39] H. U. Oh and J. Onoda, "An Experimental Study of a Semiactive Magneto-rheological Fluid Variable Damper for Vibration Suppression of Truss Structures," *Smart Material and Structures*, 11, pp. 156-162, 2002.

[40] "Magneto-Rheological Fluid/Material Compatibility Data Sheet," Lord Corporation Engineering Note.

[41] "Magnetic Circuit Design," Lord Corporation Engineering Note.

[42] "Hydrocarbon-Based MR Fluid MRF-132AD Product Bulletin," *Lord Corporation.*

[43] *VAMPIRE® Version 4.30 User Manual*, AEA Technology.

[44] B. Gilbert, "Vampire® - Opportunities for Fast, Optimised, Railway Simulations," *16th European ADAMS User Conference 2001*, November 14-15, Berchtesgaden, Germany, 2001.

[45] "Mechanical Vibration and Shock – Evaluation of Human Exposure to Whole-Body Vibration – Part 1: General Requirements," *ISO International Standard*, ISO 2631-1, 1997.